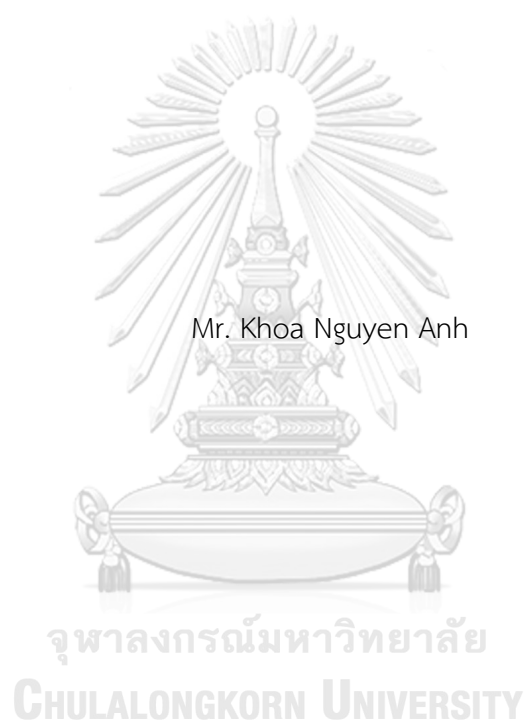


α -GLUCOSIDASE INHIBITORS FROM THE STEMS OF *Thunbergia laurifolia*



A Thesis Submitted in Partial Fulfillment of the Requirements

for the Degree of Master of Science in Chemistry

Department of Chemistry

FACULTY OF SCIENCE

Chulalongkorn University

Academic Year 2021

Copyright of Chulalongkorn University

ตัวยับยั้งแอลฟาไกลูโคซิเดสจากลำต้นรางจืด *Thunbergia laurifolia*



วิทยานิพนธ์นี้เป็นส่วนหนึ่งของการศึกษาตามหลักสูตรปริญญาวิทยาศาสตรมหาบัณฑิต

สาขาวิชาเคมี ภาควิชาเคมี

คณะวิทยาศาสตร์ จุฬาลงกรณ์มหาวิทยาลัย

ปีการศึกษา 2564

ลิขสิทธิ์ของจุฬาลงกรณ์มหาวิทยาลัย

Thesis Title **α**-GLUCOSIDASE INHIBITORS FROM THE STEMS
 OF *Thunbergia laurifolia*

By Mr. Khoa Nguyen Anh

Field of Study Chemistry

Thesis Advisor Professor PREECHA PHUWAPRAISIRISAN, Ph.D.

Accepted by the FACULTY OF SCIENCE, Chulalongkorn University in Partial Fulfillment of the Requirement for the Master of Science

..... Dean of the FACULTY OF SCIENCE
(Professor POLKIT SANGVANICH, Ph.D.)

THESIS COMMITTEE

..... Chairman
(Professor SUMRIT WACHARASINDHU, Ph.D.)

..... Thesis Advisor
(Professor PREECHA PHUWAPRAISIRISAN, Ph.D.)

..... Examiner
(Professor KHANITHA PUDHOM, Ph.D.)

..... External Examiner
(Assistant Professor Kanok-on Rayanil, Ph.D.)

เกาเหวียน อานท์ : ตัวยับยั้งแอลฟาไกลูโคซิเดสจากลำต้นรางจืด *Thunbergia laurifolia*. (α -GLUCOSIDASE INHIBITORS FROM THE STEMS OF *Thunbergia laurifolia*) อ.ที่ปรึกษาหลัก : ศ. ดร.ปรีชา ภูวไพริศาล

การแยกสารจากลำต้นรางจืด (*Thunbergia laurifolia* L.) โดยใช้การชี้นำด้วยการยับยั้งอัลฟาไกลูโคซิเดส ได้สารใหม่ 1 ชนิด คือ 5-acetoxymuranaphthoquinone (1) พร้อมทั้งสารที่เคยมีรายงานมาแล้วอีก 19 สาร (2-20) โครงสร้างของสารที่แยกได้ทั้งหมดพิสูจน์ทราบด้วยข้อมูลทางสเปกโตรสโกปีรวมทั้งการเปรียบเทียบกับข้อมูลที่เคยมีรายงานมาแล้ว สารที่แยกได้ทั้งหมดได้รับการทดสอบฤทธิ์ยับยั้งอัลฟาไกลูโคซิเดส Syringaresinol (6) rosmarinic acid (11) 1,2,8-trihydroxyxanthone (17) และ isojacareubin (18) แสดงฤทธิ์ยับยั้งสูงที่สุดในบรรดาสารที่แยกได้ การศึกษาทางจลนศาสตร์เคมีบ่งชี้ว่า syringaresinol (6) 1,2,8-trihydroxyxanthone (17) และ isojacareubin (18) ยับยั้งการทำงานของมอลเตสและซูเครส ด้วยกลไกแบบ non-competitive ส่วน rosmarinic acid (11) ยับยั้งมอลเตสด้วยกลไกแบบ non-competitive และยับยั้งซูเครสด้วยกลไกแบบผสม (mixed inhibition)

จุฬาลงกรณ์มหาวิทยาลัย
CHULALONGKORN UNIVERSITY

สาขาวิชา เคมี
ปีการศึกษา 2564

ลายมือชื่อนิสิต

ลายมือชื่อ อ.ที่ปรึกษาหลัก

6272002023 : MAJOR CHEMISTRY

KEYWORD: Acanthaceae *Thunbergia naphthoquinone* α -glucosidase diabete

Khoa Nguyen Anh : α -GLUCOSIDASE INHIBITORS FROM THE STEMS OF *Thunbergia laurifolia*. Advisor: Prof. PREECHA PHUWAPRAISIRISAN, Ph.D.

Alpha-glucosidase inhibitory assay-guided isolation of *Thunbergia laurifolia* L. stems yielded a new compound named 5-acetoxymethoxy-1,4-naphthoquinone (1) along with nineteen known compounds (2-20). The structure of the isolated compounds was elucidated by the analysis of multiple spectroscopic data as well as by comparison with the previous reports. The isolated compounds were evaluated for α -glucosidase inhibition. Syringaresinol (6), rosmarinic acid (11), 1,2,8-trihydroxyxanthone (17), and isojacareubin (18) showed the most potent inhibitory activity among isolated compounds. Kinetic study indicated that syringaresinol (6), 1,2,8-trihydroxyxanthone (17), and isojacareubin (18) could inhibit the maltase and sucrase function by non-competitive, and rosmarinic acid (11) was identified as a non-competitive inhibitor against maltase and a mixed manner inhibitor against sucrase.



Field of Study: Chemistry

Student's Signature

Academic Year: 2021

Advisor's Signature

ACKNOWLEDGEMENTS

I wish to express my endless thanks and gratefulness to my advisor Professor Dr. Preecha Phuwapraisirisan. His kindly support and continuous advice go through the process of completion of my thesis. His encouragement and comments had significantly enriched and improved my work.

I would like to thank the Chairman: Professor Dr. Sumrit Wacharasindhu, Department of Chemistry, Faculty of Science, Chulalongkorn University; the thesis examiners: Professor Dr. Khanitha Pudhom, Department of Chemistry, Faculty of Science, Chulalongkorn University, and Assistant Professor Dr. Kanok-on Rayanil, Department of Chemistry, Faculty of Science, Silapakorn University, Nakorn Pathom for their great discussion and suggestion.

I wish to thank Chulalongkorn University for the H.M. the King Bhumibhol Adulyadej's 72nd Birthday Anniversary Scholarship and Center of Excellence in Natural Products for financial support on research assistance.

Special thanks to Ms. Titiruetai Dounwichitrkul, Dr. Wisuttaya Worawalai, and Ms. Thita Yodsawat for the guidance of α -glucosidase inhibitory assay as well as the support in my study.

Finally, I want to express my special gratitude to my family and friends for their love, support, and encouragement.

Khoa Nguyen Anh

TABLE OF CONTENTS

	Page
.....	iii
ABSTRACT (THAI).....	iii
.....	iv
ABSTRACT (ENGLISH).....	iv
ACKNOWLEDGEMENTS	v
TABLE OF CONTENTS.....	vi
LIST OF FIGURES	ix
LIST OF SCHEMES	xv
LIST OF ABBREVIATIONS	xvii
Chapter 1.....	1
1.1 Diabetes and α -glucosidase inhibition.....	1
1.1.1 Diabetes mellitus.....	1
1.1.2 α -glucosidase inhibition.....	2
1.2 Botanical aspect, traditional claim, and pharmacology activities of <i>Thunbergia laurifolia</i>	4
1.3 Pharmacology activities of <i>Thunbergia laurifolia</i>	5
1.3.1 Detoxifying effects	5
1.3.2 Antioxidant effects	6
1.3.3 Anti-inflammatory effects.....	7
1.3.4 Antidiabetic activity of <i>Thunbergia laurifolia</i>	7
1.4 Phytochemical study of <i>Thunbergia laurifolia</i> and related species	8

1.5 Scope of research and expected beneficial outcomes.....	10
1.5.1 Scope of research.....	10
1.5.2 Expected beneficial outcomes from the thesis	10
Chapter 2.....	11
2.1. General experimental procedures.....	11
2.2. Plant material and extraction.....	11
2.3. Isolation and purification of ethyl acetate extract.....	12
2.4. Isolation and purification of aqueous methanol layer.....	15
2.5. Rat intestinal α -Glucosidase inhibition assay.....	18
2.6. Kinetic study of α -glucosidase inhibition.....	19
Chapter 3.....	21
3.1. α -Glucosidase inhibition screening of crude extracts and sub-fractions.....	21
3.2. Chemical constituents from the stem of <i>Thunbergia laurifolia</i>	22
3.2.1 Structural elucidation of new compound (1)	23
3.2.2 Structural elucidation of compounds 2-5	25
3.2.3 Structural elucidation of compounds 6-7	27
3.2.4 Structural elucidation of compounds 8-11	31
3.2.5 Structural elucidation of compounds 12-14	33
3.2.6 Structural elucidation of compounds 15-17	36
3.2.7 Structural elucidation of compounds 18.....	40
3.2.8 Structural elucidation of compounds 19.....	42
3.2.9 Structural elucidation of compounds 20.....	43
3.3. Rat intestine α -glucosidase inhibition of isolated compounds.....	45

3.4. Kinetic study of syringaresinol (6) and rosmarinic acid (11), 1,2,8-trihydroxyxanthone (17), and isojacareubin (18)	48
Chapter 4.....	56
APPENDIX.....	60
REFERENCES	102
VITA.....	107



LIST OF FIGURES

Figure 1.1 The difference between diabetes type 1 and type 2.....	1
Figure 1.2 Carbohydrate metabolism catalyzed by α -glucosidase and function of the inhibitor [5].....	3
Figure 1.3 Chemical structures of Acarbose, Voglibose, and Miglitol [6]	3
Figure 1.4 (a) Botanical aspect of <i>Thunbergia laurifolia</i> (b) dried stems (c) dried leaves.....	5
Figure 1.5 Chemical constituents from <i>Thunbergia</i> genus.....	9
Figure 2.6 The structures of isolated compounds from the stem of <i>Thunbergia laurifolia</i>	17
Figure 3.1 The percentage of inhibition of crude extracts against maltase and sucrase at 1 mg/mL	21
Figure 3.2 The percentage of inhibition of sub-fractions from ethyl acetate extract against maltase at 1 mg/mL.....	21
Figure 3.3 The percentage of inhibition of sub-fractions from ethyl acetate extract against sucrase at 1 mg/mL.....	22
Figure 3.4 The HMBC and COSY correlations of compound (1).....	25
Figure 3.5 The HMBC correlations of compound (7).....	29
Figure 3.6 The structures of compounds (12, 13, 14).....	34
Figure 3.7 The HMBC correlations of compound (15).....	37
Figure 3.8 The HMBC correlations of compounds (16, 17).....	39
Figure 3.9 The HMBC correlations of compound (18).....	41
Figure 3.10 The HMBC correlations of compounds (19).....	42
Figure 3.11 The HMBC correlations of compound (20)	44
Figure 3.12 Schemetic diagram presenting inhibition trend of isolated compounds..	48

Figure 3.13 Lineweaver-Burk plots for inhibitory activity of syringaresinol (6).....	49
Figure 3.14 Secondary replot of slope vs. $[I]$ from a primary Lineweaver-Burk plot for the determination of K_i of (6).....	49
Figure 3.15 Lineweaver-Burk plots for inhibitory activity of rosmarinic acid (11).....	50
Figure 3.16 Secondary replot of slope vs. $[I]$ from a primary Lineweaver-Burk plot for the determination of K_i of (11).....	50
Figure 3.17 Secondary replot of intercept vs. $[I]$ from a primary Lineweaver-Burk plot for the determination of K_i' of (11).....	51
Figure 3.18 Lineweaver-Burk plots for inhibitory activity of 1,2,8-trihydroxyxanthone (17) against A3 (maltase) and B3 (sucrase)	51
Figure 3.19 Secondary replot of slope vs. $[I]$ from a primary Lineweaver-Burk plot for the determination of K_i of (17).....	52
Figure 3.20 Lineweaver-Burk plots for inhibitory activity of isojacareubin (18).....	52
Figure 3.21 Secondary replot of slope vs. $[I]$ from a primary Lineweaver-Burk plot for the determination of K_i of (18).....	53
Figure 3.22 Putative mechanism pathway of syringaresinol (6) for non-competitive inhibition (A1, B1) against maltase and sucrase	54
Figure 3.23 Putative mechanism pathway of rosmarinic acid (11) for non-competitive (A2) and mixed (B2) inhibition against maltase and sucrase	54
Figure 3.24 Putative mechanism pathway of 1,2,8-trihydroxyxanthone (17) for non-competitive inhibition (A3, B3) against maltase and sucrase	55
Figure 3.25 Putative mechanism pathway of isojacareubin (18) for non-competitive inhibition (A4, B4) against maltase and sucrase	55
Figure S1 HR-ESI-MS spectrum of furanonaphthoquinone (1).....	60
Figure S2 The $^1\text{H-NMR}$ spectrum of furanonaphthoquinone (1) in Chloroform- <i>d</i>	60
Figure S3 The $^{13}\text{C-NMR}$ spectrum of furanonaphthoquinone (1) in Chloroform- <i>d</i>	61

Figure S4	The COSY spectrum of furanonaphthoquinone (1) in Chloroform- <i>d</i>	61
Figure S5	The HSQC spectrum of furanonaphthoquinone (1) in Chloroform- <i>d</i>	62
Figure S6	The HMBC spectrum of furanonaphthoquinone (1) in Chloroform- <i>d</i>	62
Figure S7	The ¹ H-NMR spectrum of compound (2) in Chloroform- <i>d</i>	63
Figure S8	The ¹³ C-NMR spectrum of compound (2) in Chloroform- <i>d</i>	63
Figure S9	The COSY spectrum of compound (2) in Chloroform- <i>d</i>	64
Figure S10	The HSQC spectrum of compound (2) in Chloroform- <i>d</i>	64
Figure S11	The HMBC spectrum of compound (2) in Chloroform- <i>d</i>	65
Figure S12	The ¹ H-NMR spectrum of compound (3) in Chloroform- <i>d</i>	65
Figure S13	The ¹³ C-NMR spectrum of compound (3) in Chloroform- <i>d</i>	66
Figure S14	The COSY spectrum of compound (3) in Chloroform- <i>d</i>	66
Figure S15	The HSQC spectrum of compound (3) in Chloroform- <i>d</i>	67
Figure S16	The HMBC spectrum of compound (3) in Chloroform- <i>d</i>	67
Figure S17	The ¹ H-NMR spectrum of compound (4) in Chloroform- <i>d</i>	68
Figure S18	The ¹³ C-NMR spectrum of compound (4) in Chloroform- <i>d</i>	68
Figure S19	The COSY spectrum of compound (4) in Chloroform- <i>d</i>	69
Figure S20	The HSQC spectrum of compound (4) in Chloroform- <i>d</i>	69
Figure S21	The HMBC spectrum of furanonaphthoquinone (4) in Chloroform- <i>d</i>	70
Figure S22	The ¹ H-NMR spectrum of compound (5) in Chloroform- <i>d</i>	70
Figure S23	The ¹³ C-NMR spectrum of compound (5) in Chloroform- <i>d</i>	71
Figure S24	The COSY spectrum of compound (5) in Chloroform- <i>d</i>	71
Figure S25	The HSQC spectrum of furanonaphthoquinone (5) in Chloroform- <i>d</i>	72
Figure S26	The HMBC spectrum of compound (5) in Chloroform- <i>d</i>	72
Figure S27	The ¹ H-NMR spectrum of compound (6) in Chloroform- <i>d</i>	73

Figure S28	The ^{13}C -NMR spectrum of compound (6) in Chloroform- <i>d</i>	73
Figure S29	The COSY spectrum of compound (6) in Chloroform- <i>d</i>	74
Figure S30	The ^1H -NMR spectrum of compound (7) in Chloroform- <i>d</i>	74
Figure S31	The ^{13}C -NMR spectrum of compound (7) in Chloroform- <i>d</i>	75
Figure S32	The COSY spectrum of compound (7) in Chloroform- <i>d</i>	75
Figure S33	The HSQC spectrum of compound (7) in Chloroform- <i>d</i>	76
Figure S34	The HMBC spectrum of compound (7) in Chloroform- <i>d</i>	76
Figure S35	The ^1H -NMR spectrum of compound (8) in Methanol- <i>d</i> ₄	77
Figure S36	The ^{13}C -NMR spectrum of compound (8) in Methanol- <i>d</i> ₄	77
Figure S37	The HSQC spectrum of compound (8) in Methanol- <i>d</i> ₄	78
Figure S38	The ^1H -NMR spectrum of compound (9) in Methanol- <i>d</i> ₄	78
Figure S39	^{13}C -NMR spectrum of compound (9) in Methanol- <i>d</i> ₄	79
Figure S40	The HSQC spectrum of compound (9) in Methanol- <i>d</i> ₄	79
Figure S41	The ^1H -NMR spectrum of compound (10) in DMSO- <i>d</i> ₆	80
Figure S42	The ^{13}C -NMR spectrum of compound (10) in DMSO- <i>d</i> ₆	80
Figure S43	The HSQC spectrum of compound (10) in DMSO- <i>d</i> ₆	81
Figure S44	The ^1H -NMR spectrum of compound (11) in Methanol- <i>d</i> ₄	81
Figure S45	The ^{13}C -NMR spectrum of compound (11) in Methanol- <i>d</i> ₄	82
Figure S46	The HSQC spectrum of compound (11) in Methanol- <i>d</i> ₄	82
Figure S47	The HMBC spectrum of compound (11) in Methanol- <i>d</i> ₄	83
Figure S48	The ^1H -NMR spectrum of compound (12) in chloroform- <i>d</i>	83
Figure S49	The ^{13}C -NMR spectrum of compound (12) in chloroform- <i>d</i>	84
Figure S50	The COSY spectrum of compound (12) in chloroform- <i>d</i>	84
Figure S51	The ^1H -NMR spectrum of compound (13) in DMSO- <i>d</i> ₆	85

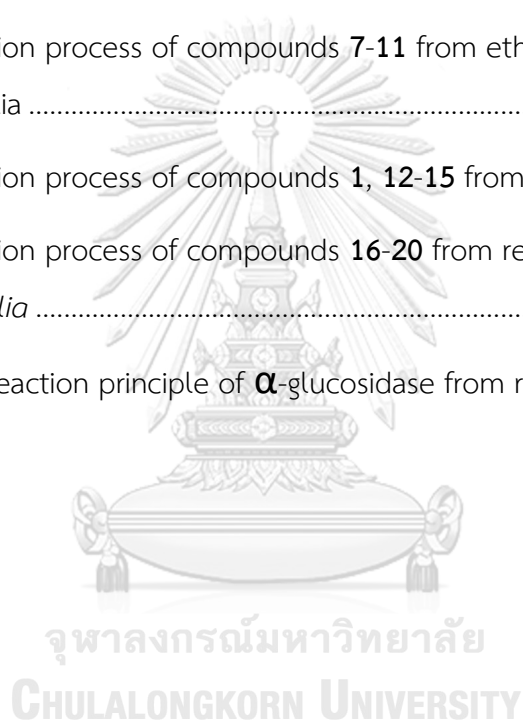
Figure S52	The ^{13}C -NMR spectrum of compound (13) in $\text{DMSO-}d_6$	85
Figure S53	The ^1H -NMR spectrum of compound (14) in $\text{DMSO-}d_6$	86
Figure S54	The ^{13}C -NMR spectrum of compound (14) in $\text{DMSO-}d_6$	86
Figure S55	The HSQC spectrum of compound (14) in $\text{DMSO-}d_6$	87
Figure S56	The ^1H -NMR spectrum of compound (15) in Chloroform- <i>d</i>	87
Figure S57	The ^{13}C -NMR spectrum of compound (15) in Chloroform- <i>d</i>	88
Figure S58	The HSQC spectrum of compound (15) in Chloroform- <i>d</i>	88
Figure S59	The HMBC spectrum of compound (15) in Chloroform- <i>d</i>	89
Figure S60	The ^1H -NMR spectrum of compound (16) in Chloroform- <i>d</i>	89
Figure S61	The ^{13}C -NMR spectrum of compound (16) in Chloroform- <i>d</i>	90
Figure S62	The COSY spectrum of compound (16) in Chloroform- <i>d</i>	90
Figure S63	The HSQC spectrum of compound (16) in Chloroform- <i>d</i>	91
Figure S64	The HMBC spectrum of compound (16) in Chloroform- <i>d</i>	91
Figure S65	The ^1H -NMR spectrum of compound (17) in $\text{DMSO-}d_6$	92
Figure S66	The ^1H -NMR spectrum of compound (17) in $\text{DMSO-}d_6$	92
Figure S67	The HSQC spectrum of compound (17) in $\text{DMSO-}d_6$	93
Figure S68	The HMBC spectrum of compound (17) in $\text{DMSO-}d_6$	93
Figure S69	The ^1H -NMR spectrum of compound (18) in $\text{DMSO-}d_6$	94
Figure S70	The ^1H -NMR spectrum of compound (18) in $\text{DMSO-}d_6$	94
Figure S71	The COSY spectrum of compound (18) in $\text{DMSO-}d_6$	95
Figure S72	The HSQC spectrum of compound (18) in $\text{DMSO-}d_6$	95
Figure S73	The HMBC spectrum of compound (18) in DMSO	96
Figure S74	The ^1H -NMR spectrum of compound (19) in Methanol- d_4	96
Figure S75	The ^{13}C -NMR spectrum of compound (19) in Methanol- d_4	97

Figure S76 The COSY spectrum of compound (19) in Methanol- d_4	97
Figure S77 The HSQC spectrum of compound (19) in Methanol- d_4	98
Figure S78 The HMBC spectrum of compound (19) in Methanol- d_4	98
Figure S79 The ^1H -NMR spectrum of compound (20) in Methanol- d_4	99
Figure S80 The ^{13}C -NMR spectrum of compound (20) in Methanol- d_4	99
Figure S81 The COSY spectrum of compound (20) in Methanol- d_4	100
Figure S82 The HSQC spectrum of compound (20) in Methanol- d_4	100
Figure S83 The HMBC spectrum of compound (20) in Methanol- d_4	101



LIST OF SCHEMES

Scheme 2.1 Extraction scheme of <i>Thunbergia laurifolia</i>	12
Scheme 2.2 Isolation process of compounds 2-5 from ethyl acetate extract of <i>Thunbergia laurifolia</i>	14
Scheme 2.3 Isolation process of compound 6 from ethyl acetate extract of <i>Thunbergia laurifolia</i>	14
Scheme 2.4 Isolation process of compounds 7-11 from ethyl acetate extract of <i>Thunbergia laurifolia</i>	15
Scheme 2.5 Isolation process of compounds 1, 12-15 from remaining water layer..	16
Scheme 2.6 Isolation process of compounds 16-20 from remaining aqueous layer of <i>Thunbergia laurifolia</i>	17
Scheme 2.7 The reaction principle of α -glucosidase from rat small intestine	19



LIST OF ABBREVIATIONS

1D	One Dimensional
$^1\text{H-NMR}$	Proton nuclear magnetic resonance
$^{13}\text{C-NMR}$	Carbon-13 nuclear magnetic resonance
2D	Two Dimensional
calcd	calculated
Chloroform- <i>d</i>	Deuterated chloroform
CH_2Cl_2	Dichloromethane
CC	Column Chromatography
COSY	Correlated Spectroscopy
d	Doublet
dd	Doublet of doublet
DDPH	2,2-Diphenyl-1-picrylhydrazyl
$\text{DMSO-}d_6$	Deuterated dimethyl sulfoxide
FCC	Flash Column Chromatography
HMBC	Heteronuclear multiple bond correlation experiment
HRESIMS	High resolution electrospray ionisation mass spectrometry

HSQC	Heteronuclear single quantum coherence spectroscopy
Hz	Hertz
IC ₅₀	Concentration that required for 50% of inhibition in invitro
J	Coupling constant
K _m	Michaelis constant
mg	Milligram
m	Multiplet
mL	Milli litter
m/z	Mass per charge
NMR	Nuclear magnetic resonance
s	singlet
TLC	Thin layer chromatography
δ_{H}	Chemical shift of proton
δ_{C}	Chemical shift of carbon
λ_{max}	Maximum wavelength
μL	Micro litter
μM	Micromolar
UV	Ultraviolet

V_{\max}

Maximum reaction rate



Chapter 1

Introduction

1.1 Diabetes and α -glucosidase inhibition

1.1.1 Diabetes mellitus

The group of diseases due to defects in insulin secretion, insulin action, or both is collectively referred to as diabetes, which is classified into three types: type-1, type-2, and gestational diabetes. Type-1 diabetes is known as insulin-dependent diabetes, which accounts for only 5–10% of those with diabetes. That is a chronic condition in which the pancreas produces little or no insulin. Type-2 diabetes is associated with insulin deficiencies, primarily a defect in insulin secretion accompanied by insulin resistance, which accounts for 90–95% of those with diabetes. It has considered as one of the most remarkable public health problems in the 21st century. Besides, gestational diabetes is a special case, occurs only during the pregnancy of women. The main reason is due to changing of endocrine hormones and lack of science in the diet [1, 2]

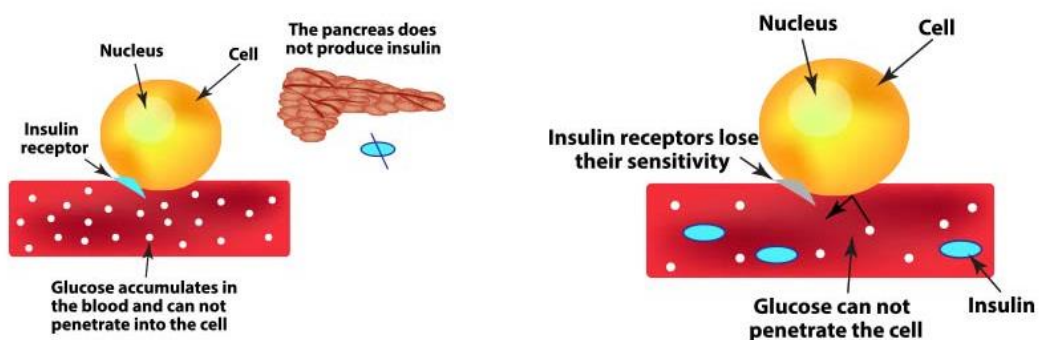


Figure 1.1 The difference between diabetes type 1 and type 2

<https://bitly.com.vn/qb6bnc>

1.1.2 α -glucosidase inhibition

A straightforward and effective approach applied to suppress type-2 diabetes is inhibiting α -glucosidase, an oligosaccharide hydrolysing enzyme located on the surface membrane of intestinal cells. Therefore, glucose liberated from oligosaccharide after the meal would be controllable and subsequently reduced blood glucose level [3]. To date, acarbose, miglitol, and other related α -glucosidase inhibitors are a few drugs approved for type-2 diabetes treatment. However, these agents cause gastrointestinal harm such as flatulence, abdominal bloating, and diarrhoea. Many researchers have studied for effective α -glucosidase inhibitors from natural sources to pave the way for alternative antidiabetic drugs that may substitute acarbose and its family [4]. Some recognized examples of α -glucosidase inhibitors from natural sources often present in the form of herbal medicines include deoxynojirimycin from *Morus alba* and kotalanol from *Salacia reticulata*.

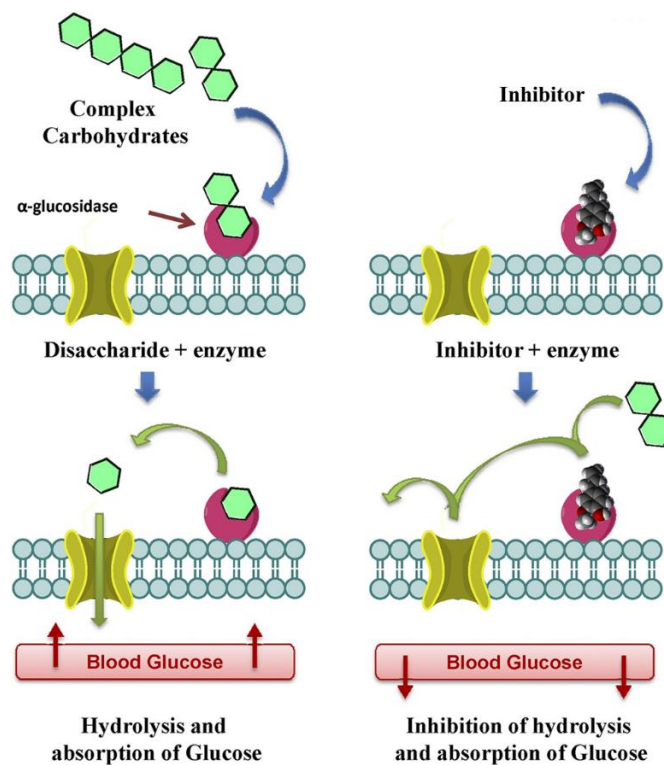


Figure 1.2 Carbohydrate metabolism catalyzed by α -glucosidase and function of the inhibitor [5]

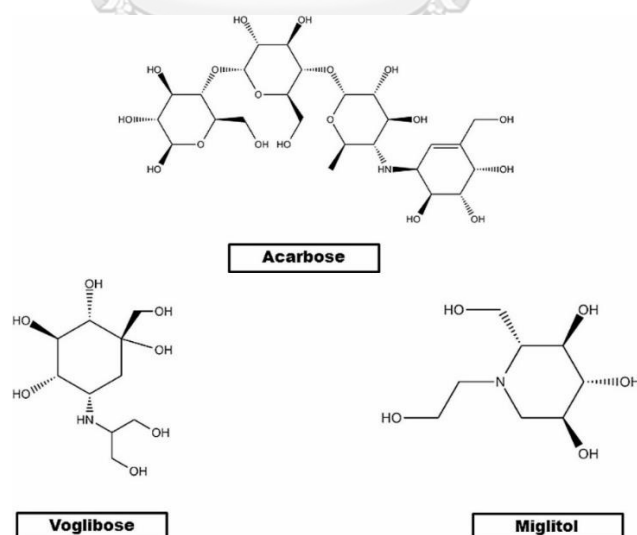


Figure 1.3 Chemical structures of Acarbose, Voglibose, and Miglitol [6]

In the search for α -glucosidase inhibitors from medicinal plants that have been evidenced for antidiabetic activity in animal models, the stem extract of *Thunbergia laurifolia* has been noted for significant inhibition against α -glucosidase in our screening. Small scale fractionation of the extract demonstrated improved inhibition found in partial purified fractions. This observation possibly links to antidiabetic activity previously found in animal models; however, the active components responsible for this inhibition remained unexplored.

1.2 Botanical aspect, traditional claim, and pharmacology activities of *Thunbergia laurifolia*

Thunbergia laurifolia, commonly known in Thai as ‘Rang-Jeud’, belongs to the family Acanthaceae. It is a climbing plant with smooth opposed leaves along the stem. The leaves have heart-shaped with serrated leaf margin and taper to a pointed tip. The hermaphrodite flower is trumpet-shaped with a short broad tube, white outside and yellowish inside. The corolla is pale blue in colour with 5–7 petals, one larger than the others. The purple flowers are trumpet-shaped and produced during November-January. The seed pod is cone-shaped, 1 cm long, with a round base. In Thailand, leaves of *T. laurifolia* are believed to have detoxifying effects. They are used as an antidote for poisons and drugs, including the treatment of drug addiction. The mixture of the root or leaf of *T.laurifolia* with water rinsed from rice can be effectively used as a detoxifying agent in Thai traditional medicine. To date, the

crushed dried leaves are commercially packed and sold as tea back to drink as a detoxifying drink [7, 8].

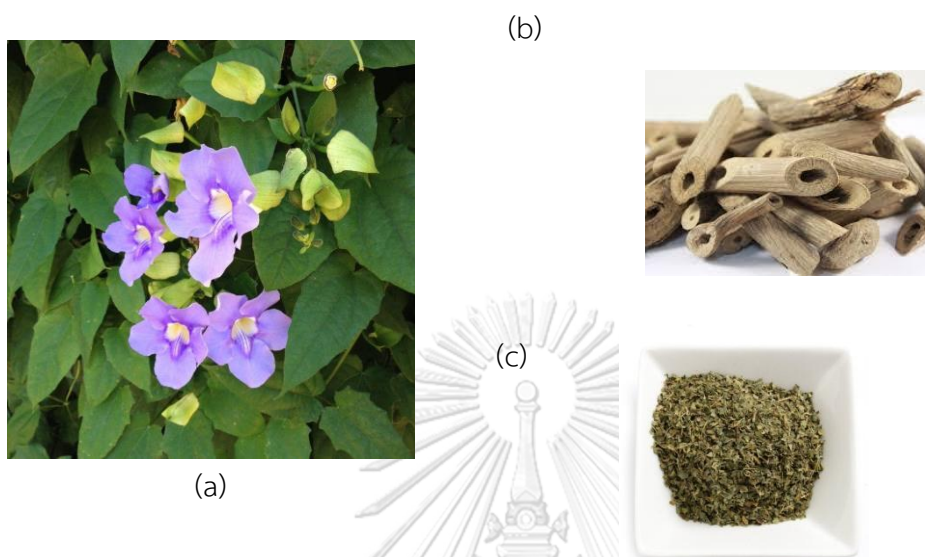


Figure 1.4 (a) Botanical aspect of *Thunbergia laurifolia* (b) dried stems (c) dried leaves

1.3 Pharmacology activities of *Thunbergia laurifolia*

1.3.1 Detoxifying effects

Detoxifying effects of the leaf extract on various animal models were recorded with several examinations such as organs, blood chemistry, hematology, and histology [7]. The effects of aqueous leaf extract of *T. laurifolia* in alleviating lead poisoning in the brain and detoxification of cadmium of mice have been studied in the research of Tangpong [9] and Morkmek [10]. Aqueous leaf extract of *T. laurifolia* showed the effect in alleviating lead poisoning in the brain of mice. The result indicated that aqueous leaf extract of *T. laurifolia* reduces neuronal cell death

and memory loss caused by lead uptake in mice. This extract was proved to regenerate the levels of caspase-3 activity, sustain antioxidant capacity and antioxidant enzymes in the brain. Furthermore, in the research of Morkmek and co-workers described that abnormal appearance and behavior were lesser in rats fed with the extract prior to cadmium exposure than in those fed with the extract after cadmium exposure [10].

In 2000, Usanawarong and co-workers has reported that the aqueous leaves extract of *T. laurifolia* was useful for detoxifying of paraquat by decreasing plasma malonaldehyde, an indicator of lipid peroxidation of paraquat-intoxicated rat [11]. Moreover, the research of Chinacarawat and co-workers showed that orally administered *T. laurifolia* capsule reduce organophosphate and carbamate insecticide poisoning with dose of 600 mg/day for 2 weeks. Especially, it has no side effect in high-risk volunteer [12].

1.3.2 Antioxidant effects

The aqueous extract also yielded the effective free radical scavenging (DPPH). In the previous report of Chan and co-workers, the developing leaves had the highest total phenolic contents of 513 mg gallic acid equivalents (GAE) in 100 g, followed by young and mature leaves with values of 407 and 298 mg GAE in 100 g, respectively. Antioxidation activity in conjunction with phenolic contents was most widely examined; however, it revealed low capacity among 13 commercial samples [7].

1.3.3 Anti-inflammatory effects

The anti-inflammatory effect of the aqueous leaves extract of *T. laurifolia* has been determined to be twofold higher than that of *Garcinia mangostanarind* rind extract with carrageenan induced paw edema model in rat in the research of Pongphasuk and co-workers [13]. In addition, *T. laurifolia* showed anti-inflammatory properties which improved liver function in hamsters treated with liver fluke infection or after administration of N-nitrosodimethylamine. The report indicated that fresh and dried aqueous extract from *T. laurifolia* leaves clearly reduced the inflammatory cells. The anti-inflammatory activity of the plant extract was well-correlated with the total antioxidant capacity [14]. Furthermore, rosmarinic acid which was isolated from an ethanolic extract of *T. laurifolia* leaves has been characterized anti-inflammatory effects against acute and chronic inflammation in the study of Suwanchaikasem [15].

1.3.4 Antidiabetic activity of *Thunbergia laurifolia*

Although *Thunbergia laurifolia* has long been claimed in Thai pharmacopeia for its antidiabetic activity, there was no scientific experiment conducted to prove this claim. Until 2004, Aritajat and co-workers examined this claim by investigating blood glucose level in alloxan-induced diabetic rats administrated with *T. laurifolia* leave aqueous extract. After 15-day treatment, blood glucose levels in diabetic rats were approximately three-time reduced. This observation was possibly associated with the protective effect of *T. laurifolia* extract on β -cell although its recovery was marginally detected. However, the active components responsible for lowering blood

glucose level have not been identified [16]. Moreover, the study of Hongsing and co-workers in 2018 showed that the extract of leaf and stem as well as their active phytochemical (rosmarinic acid) contents possess antidiabetic potent with high activity [17]. The studies have shown that *T. laurifolia* is a potential herb for the treatment of diabetes, which should be studied in-depth in terms of its phytochemistry as well as its active components. Although subsequent investigations on the biological activity of *T. laurifolia* were reported, there has been no study relevant to its antidiabetic activity.

1.4 Phytochemical study of *Thunbergia laurifolia* and related species

In addition to rosmarinic acid (1, Figure 2), the common metabolite isolated from *T. laurifolia*, iridoid glucosides have been typically reported. In 2002, two iridoid glucosides having carboxylic acid at C-8 named grandifloric acid (2) and 8-*epi*-grandifloric acid (3) together with the epoxy iridoid named 3'-O- β -glucopyranosyl stilbericoside (4) were isolated from the aerial part. Furthermore, a series of different glucosides, namely benzyl alcohol glucosides (5,6), aliphatic alcohol glucosides (7,8), and flavonoid C-glucosides (9, 10) were also identified [18]. To date, there has been no additional phytochemical study on *T. laurifolia*.

In fact, iridoid glucosides are likely to be chemotaxonomic markers for the genus *Thunbergia* because they are dominantly encountered in all species. Phytochemical study conducted by Jensen and co-workers (1989) on the fresh foliage of 4 different species, namely *Thunbergia alata*, *Thunbergia fragan*,

Thunbergia frandifolia, and *Thunbergia mysorensis*, reported the isolation of stilbericoside (**11**), 6-*epi*-stilbericoside (**12**) and thunbergioside (**13**). Iridoids **11** and **12** encompassing epoxide moiety at C-7 and C-8 while the unusual iridoid **13** incorporated chloride atom at C-7, which was possibly generated by nucleophilic (chloride ion) substitution of epoxy iridoid [19]. Subsequent investigation by Damtoft and coworkers (1994) reported two iridoid glucosides named alatoside (**14**) and thunaloside (**15**) from the fresh leaves of *T. alata* [20]. In 1996, Ismail and coworkers discovered the novel iridoid glucosides-isounedoside (**16**) along with some known iridoid glucosides [21]. Although iridoid glucosides have been recognized as chemotaxonomic markers of *T. laurifolia* and other species, the biological activity of the isolated iridoids has not been investigated.

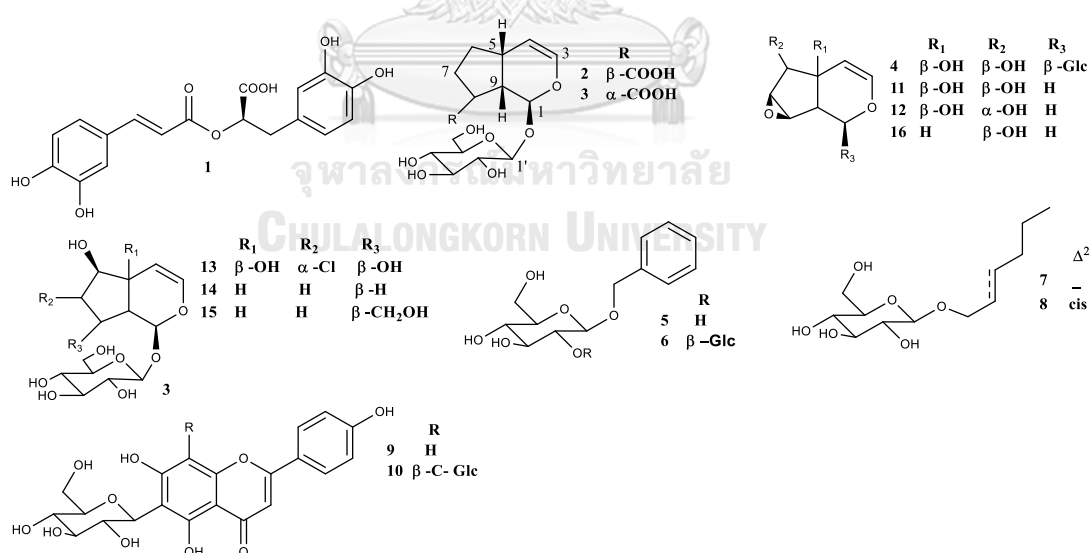


Figure 1.5 Chemical constituents from *Thunbergia* genus

1.5 Scope of research and expected beneficial outcomes

1.5.1 Scope of research

To extract, isolate, and structural elucidation of the chemical constituents from the stems of *Thunbergia laurifolia* and to evaluate the α -glucosidase inhibition of isolated compounds.

1.5.2 Expected beneficial outcomes from the thesis

α -Glucosidase inhibitors and their inhibitory mechanism will be obtained.



Chapter 2

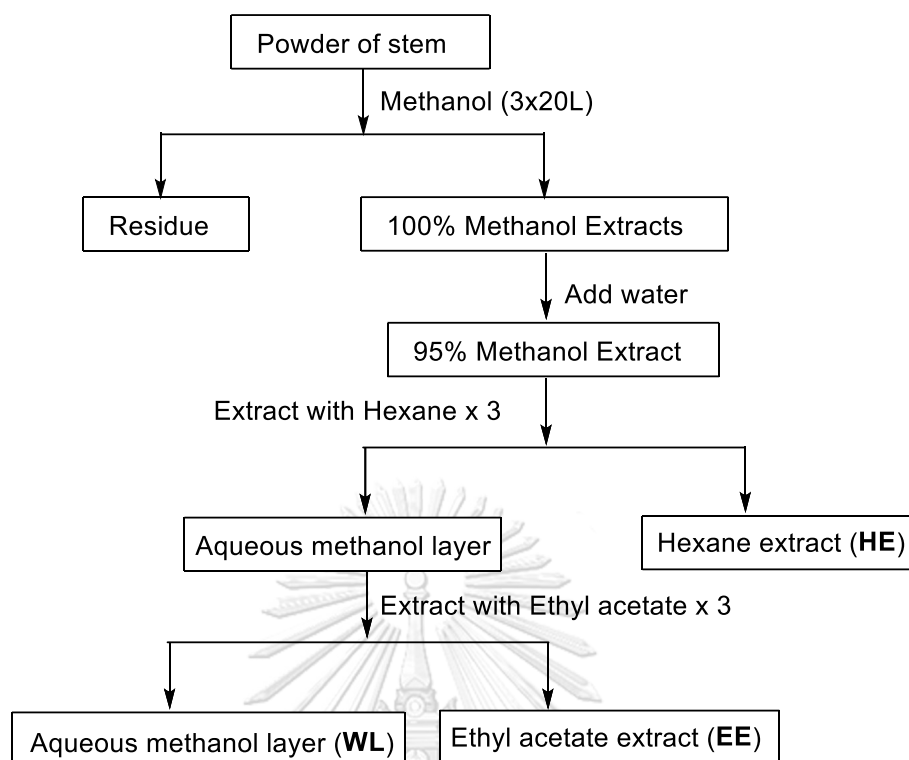
Experimental

2.1. General experimental procedures

^1H -NMR and ^{13}C -NMR spectra were recorded with JEOL JNM-ECZ500R/S1 NMR spectrometers operating at 500 MHz for ^1H or 125 MHz for ^{13}C nuclei. High-resolution mass spectra (HRMS) were recorded using electrospray ionization (ESI) with a MicroTOF Bruker mass spectrometer. Analytical thin layer chromatography (TLC) was performed with precoated Merck silica gel 60 F₂₅₄ plates (0.25 mm for thick layer) and visualized under UV light at 254 nm and dipping in anisaldehyde reagent followed by hot plate heating. Column chromatography was performed with Merck silica gel 60 (70-230 mesh).

2.2. Plant material and extraction

The stems of *T. laurifolia* were collected from Nakhonratchasima, Thailand in 2018. The specimens have been kept at Center of Excellence in Natural Products (voucher number CENP-PP-2018-003), Chulalongkorn University. The dried stems of *T. laurifolia* (5 kg) were ground and extracted by methanol (3 × 20 L) to give a methanol extract. The methanol extract was partitioned with hexane, ethyl acetate to give hexane extract (**HE**) (10 g), ethyl acetate extract (**EE**) (30 g) and the remaining aqueous layer (**WL**). The solvent was evaporated in vacuo using a rotary evaporator to obtain the crude extracts. The extraction method is summarized in Scheme 2.1



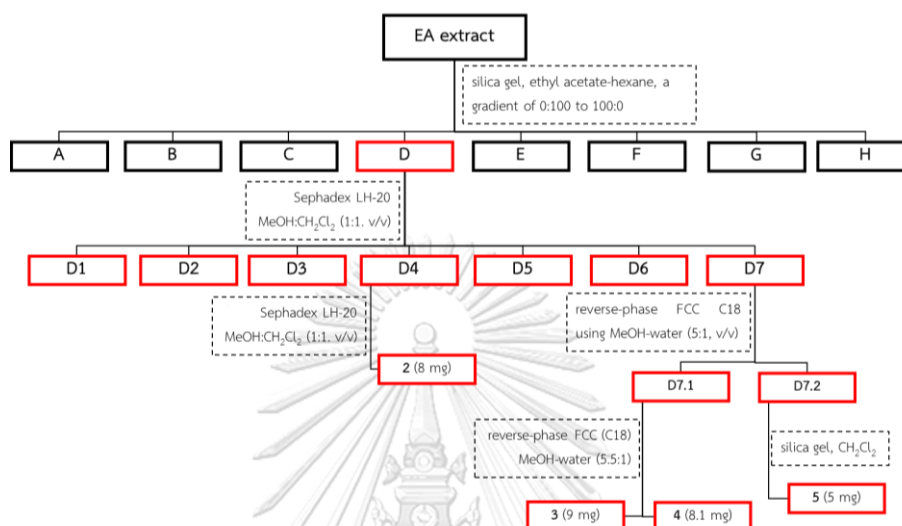
Scheme 2.1 Extraction scheme of *Thunbergia laurifolia*

2.3. Isolation and purification of ethyl acetate extract

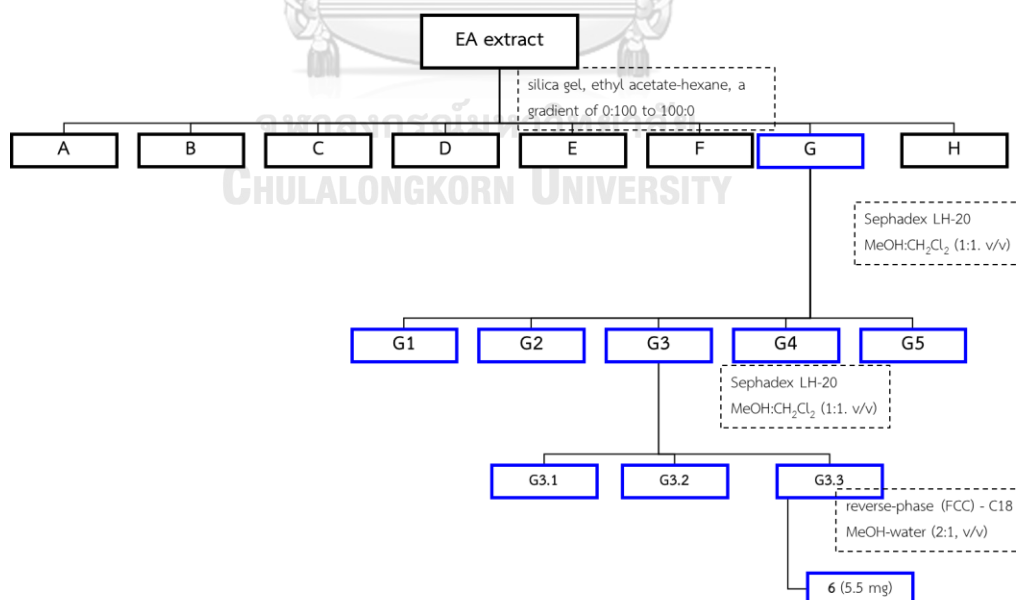
The ethyl acetate extract (30 g) was separated by column chromatography (CC) (silica gel, ethyl acetate-hexane, a gradient of 0:100 to 100:0) to give 8 fractions (A-H). Fraction **D** (4g) was fractionated by Sephadex LH-20 column eluted with MeOH-CH₂Cl₂ (1:1, v/v) to obtain seven subfractions (**D1-D7**). Fraction **D7** (300 mg) was purified by reversed-phase flash column chromatography (FCC) C18 using MeOH-water (5:1, v/v) to give 2 subfractions (**D7.1-D7.2**). Compound **2** (8 mg) was obtained from subfraction **D7.2** (110 mg) by using column chromatography (silica gel, CH₂Cl₂). From subfraction **D7.1** (160 mg), compounds **3** (9 mg) and **4** (8.1 mg) were purified by reversed-phase FCC (C18) using MeOH-water (5.5:1, v/v) as mobile phase. Subfraction **D4** (200 mg) was separated by repeating Sephadex LH-20 column using MeOH-CH₂Cl₂

(1:1, v/v) as mobile phase to afford compound **5** (5 mg). Fraction **G** (800 mg) was separated by Sephadex LH-20 column eluted with CH₂Cl₂-MeOH (1:1, v/v) to afford 5 subfractions (**G1-G5**). Subfraction **G3** (120 mg) was purified by Sephadex LH-20 CC using CH₂Cl₂-MeOH (1:1, v/v) to obtain 3 subfraction (**G3.1-G3.3**). Compound **6** (5.5 mg) was obtained from subfraction G3.3 (40 mg) by purifying on reversed-phase C18 column chromatography using MeOH-water (2:1, v/v) as mobile phase. Fraction **H** (5 g) was separated by using Sephadex LH-20 column eluted with MeOH to afford four subfractions (**H1-H4**). Subfraction **H1** (500 mg) was purified by repeated Sephadex LH-20 column using MeOH to give 3 subfrations (**H1.1-H1.3**). Compound **7** (20 mg) was obtained from subfraction **H1.1** (120 mg) by reversed-phase FCC (C18) using MeOH-water (1:1, v/v) as mobile phase. Subfraction **H2** (600 mg) was chromatographed on Sephadex LH-20 column with MeOH to obtain 3 subfractions (**H2.1-H2.3**). Compound **8** (15 mg) was obtained from subfraction **H2.2** (100 mg) by reversed-phase FCC (C18) using MeOH-water (3:2, v/v) as mobile phase. Subfraction **H3** (650 mg) was separated by reversed-phase FCC (C18) using MeOH-water (7:3, v/v) as mobile phase to yield compound **9** (20 mg). Subfraction **H4** (900 mg) was fractioned by Sephadex LH-20 column eluted with MeOH to give 4 subfractions (**H4.1-H4.4**). Compound **10** (30 mg) was obtained from fraction **H4.2** by using reversed-phase C-18 column and MeOH-water (3:2, v/v) as mobile phase. Subfraction **H4.4** (250 mg) was purified by repeating Sephadex LH-20 column using MeOH to obtain 3 subfractions (**H4.4.1-H4.4.3**). From

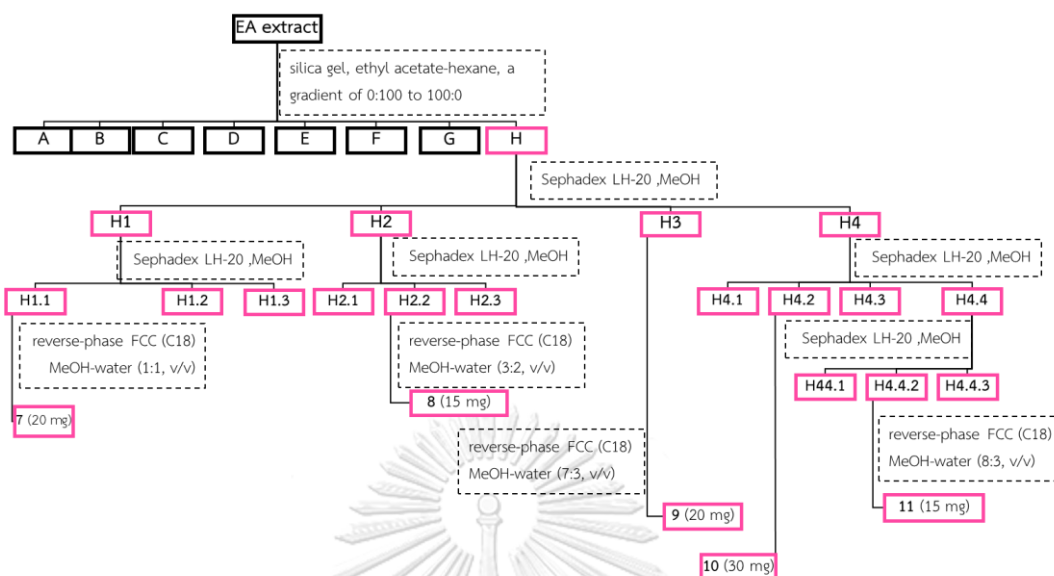
subfraction **H4.4.2** (100 mg), compound **11** (15 mg) was isolated by reversed-phase FCC (C18) using mobile phase MeOH-water (8:3, v/v).



Scheme 2.2 Isolation process of compounds **2-5** from ethyl acetate extract of *Thunbergia laurifolia*



Scheme 2.3 Isolation process of compound **6** from ethyl acetate extract of *Thunbergia laurifolia*

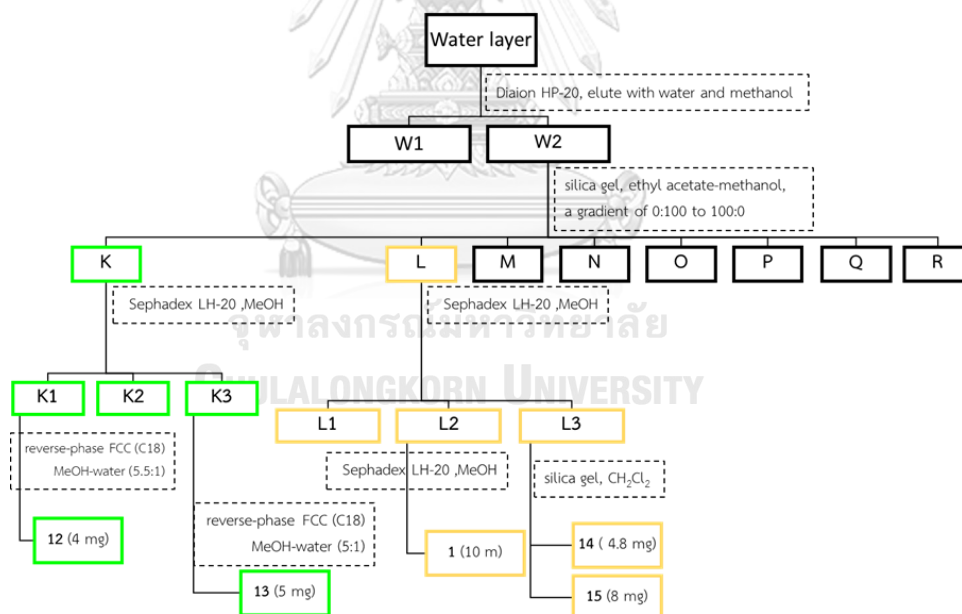


Scheme 2.4 Isolation process of compounds **7-11** from ethyl acetate extract of *Thunbergia laurifolia*

2.4. Isolation and purification of aqueous methanol layer

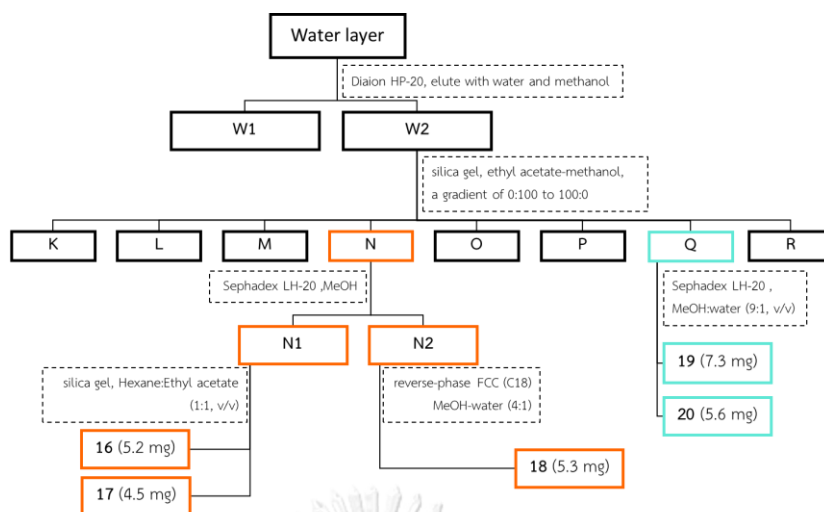
The remaining aqueous methanol layer (**WL**) was purified by Diaion HP-20 column using water and methanol as mobile phases to afford two subfractions (**W1** and **W2**). Subfraction **W2** was separated by CC (silica gel, ethyl acetate-methanol, a gradient of 0:100 to 100:0) to give 8 fractions (**K-R**). Fraction **K** (200 mg) was applied on Sephadex LH-20 column eluted with MeOH:CH₂Cl₂ (1:1, v/v) to yield three subfractions (**K1-K3**). Compound **12** (4 mg) was purified from subfraction **K1** (48 mg) by reversed-phase FCC (C18) column using MeOH:water (5:1, v/v) as mobile phase. Compound **13** (5 mg) was separated by reversed-phase FCC (C18) column from subfraction **K3** (52 mg) using MeOH:water (5:1, v/v) as mobile phase. Fraction **L** (300 mg) was separated by Sephadex LH-20 column using MeOH to give three subfractions

(L1-L3). From subfraction L2 (50 mg), compound 1 (10 mg) was purified by repeating Sephadex LH-20 column using MeOH. Subfraction L3 (36 mg) was applied CC (silica gel, CH₂Cl₂) to afford compounds 14 (4.8 mg) and 15 (8 mg). Fraction N was purified by Sephadex LH-20 column using MeOH to obtain two subfractions (N1 and N2). Subfraction N1 was separated by CC (silica gel, Hexane:Ethyl acetate (1:1, v/v)) to yield compounds 16 (5.2 mg) and 17 (4.5 mg). Compound 18 (5.3 mg) was obtained from subfraction N2 by using reversed-phase FCC (C18) and MeOH:water (4:1, v/v). Fraction Q was purified by Sephadex LH-20 column using MeOH:water (9:1) to afford compounds 19 (7.3 mg) and 20 (5.6 mg).



Scheme 2.5 Isolation process of compounds 1, 12-15 from remaining water layer

of *Thunbergia laurifolia*



Scheme 2.6 Isolation process of compounds 16-20 from remaining aqueous layer of

Thunbergia laurifolia

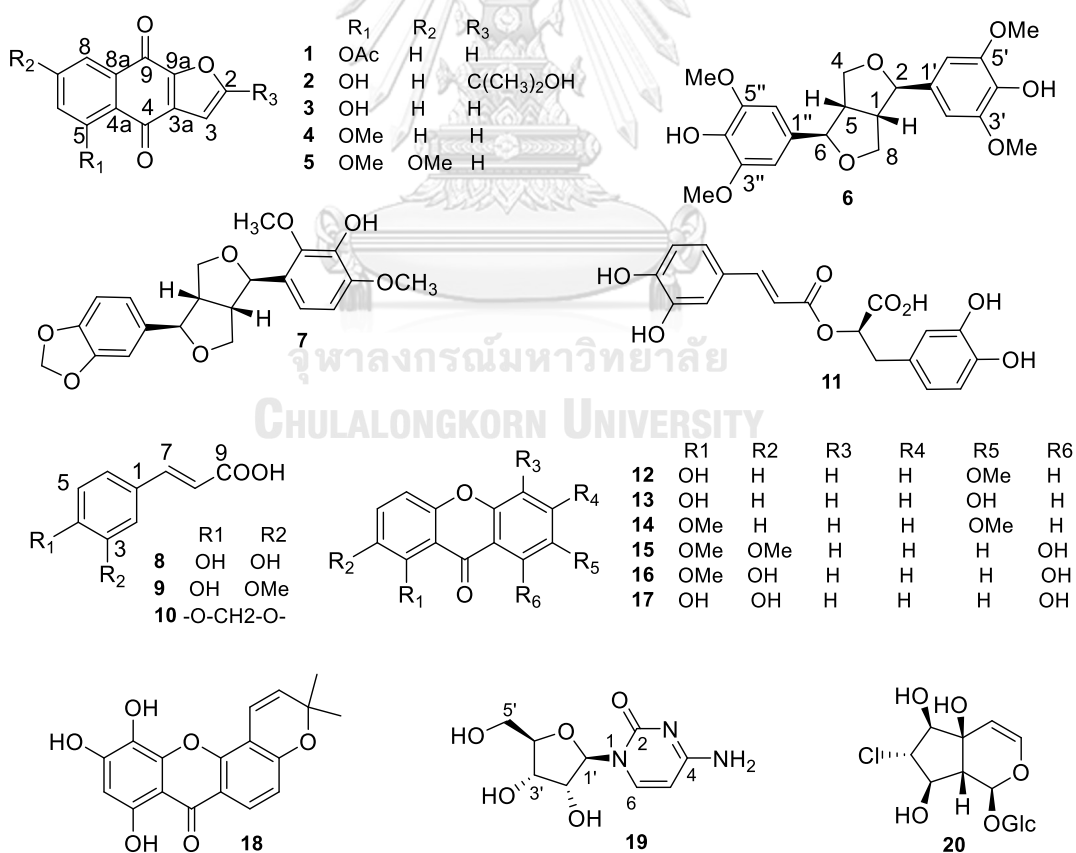
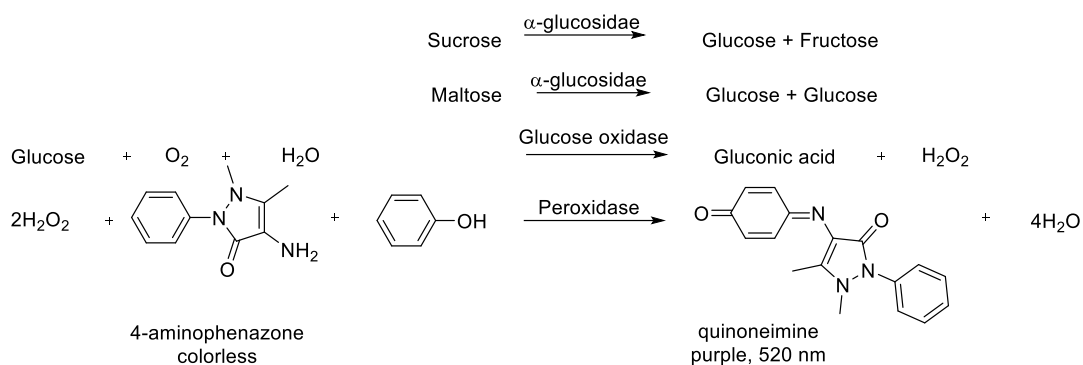


Figure 2.6 The structures of isolated compounds from the stem of *Thunbergia laurifolia*

2.5. Rat intestinal α -Glucosidase inhibition assay

α -Glucosidase inhibition was validated by colorimetric method on a BioRed microplate reader model 3550 UV. Sucrose, maltose, and rat intestine acetone powder were obtained from Sigma-Aldrich (St.Louis, MO, USA). Glucose assay kit was obtained from Human Gesellschaft für Biochemica und Diagnostica mbH (Germany). Acarbose was obtained from Bayer (Germany).

α -Glucosidase inhibition against rat intestinal maltase and sucrase was evaluated using the method previously described [22]. The enzyme solution prepared from rat intestinal acetone powder (Sigma, St. Louis) was used as a source of maltase and sucrase. The isolated compounds were added with the phosphate buffer solution (pH 6.9, 30 μ L), substrate solution (maltose: 10 mM, sucrose: 100 mM each 20 μ L) in the phosphate buffer solution, glucose assay kit (SU-GLLQ2, Human, 80 μ L), and enzyme solution (20 μ L). Then, the mixture was incubated at 37°C for 10 minutes (maltose) and 40 minutes (sucrose). The quantity of glucose is thus proportional to quinoneimine and can be determined by absorption at 500 nm using Bio-Rad 3550 microplate reader. The percentage of inhibition was calculated by $[(A_0 - A_1)/A_0] \times 100$, with A_1 and A_0 are respectively the absorbance with and without the samples.



Scheme 2.7 The reaction principle of α -glucosidase from rat small intestine

2.6. Kinetic study of α -glucosidase inhibition

Enzyme kinetic study was performed according to the previous report [20]. The type of inhibition was investigated by constructing Lineweaver Burk plot parameters which were determined by varying the concentration of the substrates (maltose and sucrose) and rat intestinal α -glucosidase in the absence and presence of tested compounds. The active compounds (10 μL) were added to phosphate buffer (pH 6.9, 30 μL) with increased concentration of maltose (2-10 mM) and sucrose (20-100 mM). The mixture was added enzyme solution (20 μL) and incubated at 37°C for 10 minutes (maltose) and 40 minutes (sucrose). α -Glucosidase activity was recorded at 500 nm using microplate reader. Data from kinetic study provide the insights into the mechanism of inhibition [22].

The Lineweaver Burk plot equation in double reciprocal form can be written as:

$$\frac{1}{v_o} = \frac{K_m}{V_{max}} \frac{1}{[S]} + \frac{1}{V_{max}}$$

Secondary plots can be constructed from:

$$\text{Slope} = \frac{K_m}{V_{max}} + \frac{K_m[I]}{V_{max}K_i}$$
$$Y - \text{intercept} = \frac{1}{V_{max}} + \frac{[I]}{\alpha K_i' V_{max}}$$

v_0 : initial velocity of an enzyme inhibited reaction, V_{max} : maximum reaction rate, K_m : Michaelis constant, K_i : the dissociation constant for the enzyme-inhibitor complex, K_i' : the dissociation constant for the enzyme substrate-inhibitor complex, S : concentration of substrate.



Chapter 3

Results and Discussion

3.1. α -Glucosidase inhibition screening of crude extracts and sub-fractions

The glucosidase inhibition (Figure 3.1) indicated that ethyl acetate extract (EE) shows the highest activity over hexane (HE) extract and aqueous-methanol layer (WL). Based on the screening, the EE and WL from the stem of *Thunbergia laurifolia* were further fractionated and purified.

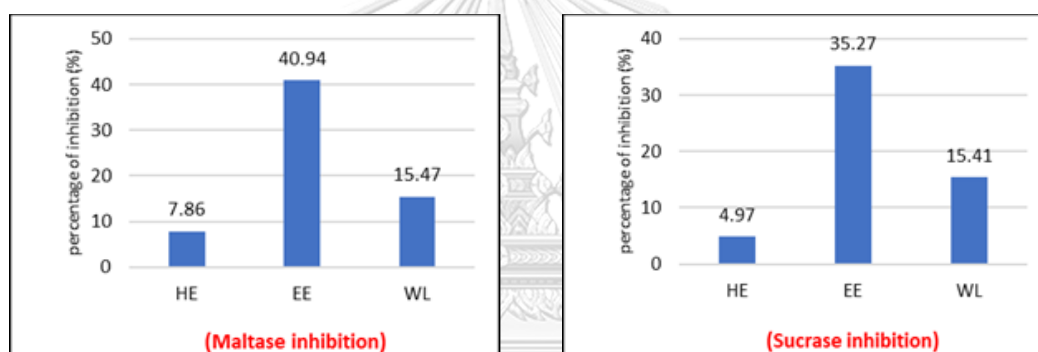


Figure 3.1 The percentage of inhibition of crude extracts against maltase and sucrase at 1 mg/mL

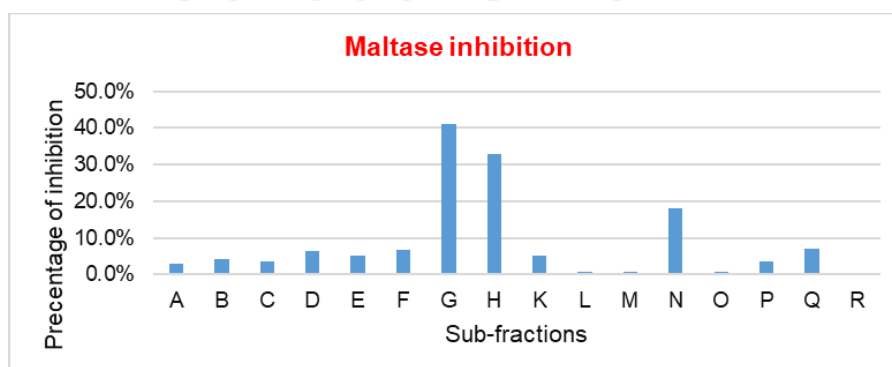


Figure 3.2 The percentage of inhibition of sub-fractions from ethyl acetate extract against maltase at 1 mg/mL

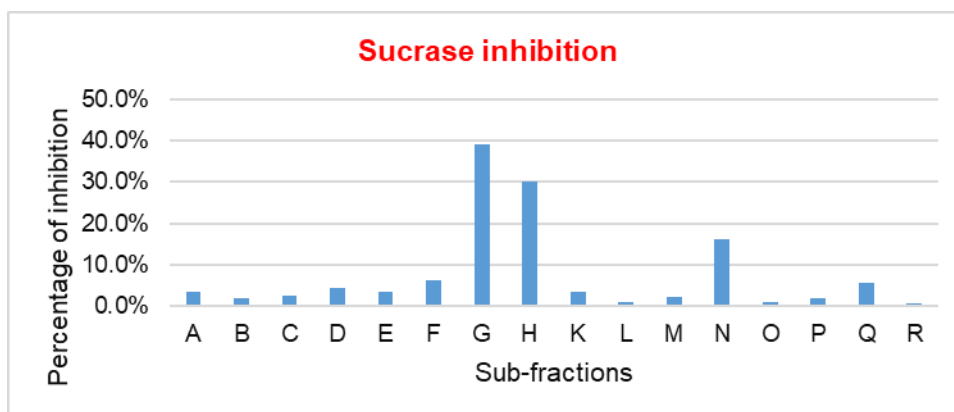


Figure 3.3 The percentage of inhibition of sub-fractions from ethyl acetate extract against sucrase at 1 mg/mL

3.2. Chemical constituents from the stem of *Thunbergia laurifolia*

Bioactive-guided isolation of *Thunbergia laurifolia* L. stems yielded one new compound named 5-acetoxynaphthoquinone (**1**), together with nineteen known compounds, 5-hydroxyisopropyl naphtho[2,3-b]furan-4,9quinone (**2**) [23], 5-hydroxynaphtho[2,3-b]furan-4,9quinone (**3**) [23], 5-methoxynaphtho[2,3-b]furan-4,9quinone (**4**) [24], 5,7-dimethoxynaphtho[2,3-b]furan-4,9quinone (**5**) [23], syringaresinol (**6**) [25], lignan α -7a (**7**) [26], caffeic acid (**8**) [27], ferulic acid (**9**) [27], 3',4'-methylenedioxycinnamic acid (**10**) [28], rosmarinic acid (**11**) [29], 1-hydroxy-7-methoxyxanthone (**12**) [30], euxanthone (**13**) [30], 1,7-dimethoxyxanthone (**14**) [31], 1,2-dimethoxy-8-hydroxyxanthone (**15**) [32], 2,8-dihydroxy-1-methoxyxanthone (**16**) [33], 1,2,8-trihydroxyxanthone (**17**) [34], cytidine (**19**) [35, 36], isojacareubin (**18**) [37], thunbergioside (**20**) [19, 38]

Structure elucidation of new compound was fully performed based on spectroscopic data such as NMR and HRMS. The identity of known compounds was

characterized mainly on NMR data compared with previous reports. Comparison with authentic samples was also carried out if available, and 2D NMR was performed in case the published data gave no clear information. In addition, characterization of known compounds in the same group was described collectively.

3.2.1 Structural elucidation of new compound (1)

Compound **1** was obtained as a light-yellow amorphous powder. The pseudomolecular ion observed in HRESIMS at m/z 279.0262 (calcd. for $C_{14}H_8O_5Na^+$, 279.0269) indicated that the molecular formula was $C_{14}H_8O_5$. The UV absorption bands showed at 246, 283, and 346 nm. The 1H -NMR and HSQC spectrum of **1** described signals of trisubstituted benzene ring [δ_H 7.38 (1H, dd, $J = 8.0, 1.3$ Hz), δ_H 7.76 (1H, dd, $J = 8.0, 7.8$ Hz), δ_H 8.20 (1H, dd, $J = 7.8, 1.3$ Hz)], two methine protons of furan ring [δ_H 7.75 (1H, d, $J = 1.9$ Hz), δ_H 6.93 (1H, d, $J = 1.9$ Hz)], one methyl group δ_H 2.47 (3H, s). The ^{13}C -NMR spectrum of **1** revealed the signals of 14 carbons, including five methine carbons, one methyl carbon, and eight non-protonated carbons with the presence of three ketone carbons at 179.6, 172.7, and 169.7 ppm.

The combined data from 1H -NMR, ^{13}C -NMR, and HSQC indicated that the core structure of **1** is furanonaphthoquinone [23, 24]. The COSY cross peaks (Figure 3.2) of H-6 (δ_H 7.38), H-7 (δ_H 7.76), and H-8 (δ_H 8.20) supported the connection of C-6/C-7/C-8. The HMBC correlations from H-6 (δ_H 7.38) to C-5 (δ_C 150.5) and C-4a (δ_C 124.4) supported the connection of C-6/C-5/C-4a. In addition, the HMBC correlations of H-7

(δ_{H} 7.76) with C-5 (δ_{C} 150.5) and C-8a (δ_{C} 134.56) together with the correlations of H-8 (δ_{H} 8.20) with C-6 (δ_{C} 130.3), C-4a (δ_{C} 124.4) and C-9 (δ_{C} 172.7) indicated the connection of C-7/C-8/C-8a/C-9. Proton H-2 (δ_{H} 7.75) showed the correlations with C-3 (δ_{C} 108.9) and C-3a (δ_{C} 131.5) and proton H-3 (δ_{H} 6.93) illustrated the correlation with C-2 (δ_{C} 149.1), C-3a (δ_{C} 131.5), and C-9a (δ_{C} 151.6) indicating the presence of furan ring and supporting the connection of C-2/C-3/C-3a/C-9a. Furthermore, the correlation of H-8 (δ_{H} 8.20) with C-9 (δ_{C} 172.7) and the comparison of NMR data with compound **3** [23] allowed to assign the acetoxy group (-OAc) at C-5 (δ_{C} 169.7). From the above spectroscopic evidence, the structure of **1** was completely identified and named as 5-acetoxynaphthoquinone.

NMR data of compounds **1**

$^1\text{H-NMR}$ (500 MHz, Chloroform-*d*) δ (ppm) 7.78 (1H, d, J = 1.9 Hz, H-2), 6.93 (1H, d, J = 1.9 Hz, H-3), 7.38 (1H, dd, J = 8.5, 1.3 Hz, H-6), 7.76 (1H, dd, J = 8.0, 7.8 Hz, H-7), 8.20 (1H, dd, J = 7.8, 1.3 Hz, H-8); $^{13}\text{C-NMR}$ (125 MHz, Chloroform-*d*) 149.1 (C-2), 108.9 (C-3), 131.5 (C-3a), 179.6 (C-4), 124.4 (C-4a), 150.5 (C-5), 130.3 (C-6), 135.0 (C-7), 125.7 (C-8), 134.6 (C-8a), 151.6 (C-9a), 172.7 (C-9), 169.7 (C-10), 21.2 (C-11).

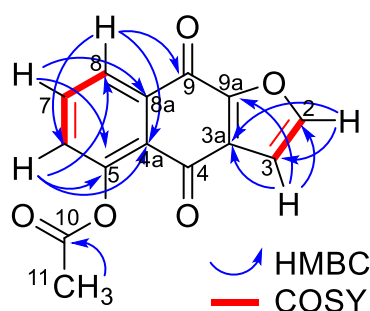


Figure 3.4 The HMBC and COSY correlations of compound (1)

3.2.2 Structural elucidation of compounds 2-5

Compound **2** was obtained as amorphous yellow powder. The $^1\text{H-NMR}$ and HSQC spectrum of **2** described three signals of trisubstituted benzene ring [δ_{H} 7.23 (1H, d, $J=8.1$ Hz, H-6), δ_{H} 7.62 (1H, dd, $J=8.1, 7.8$ Hz, H-7), δ_{H} 7.74 (1H, d, $J = 7.8$ Hz, H-8)], methine protons of furan ring δ_{H} 6.79 (1H, s, H-3), two methyl group δ_{H} 1.76 (6H, s, H-11, H-12). The $^{13}\text{C-NMR}$ spectrum of **2** revealed the signals of 15 carbons, including four methine carbons, two methyl carbon, and nine non-protonated carbons with the presence of two ketone carbons at 186.8 ppm and 172.8 ppm. These two carbonyl carbons indicated the characteristic feature of naphthoquinone. In addition, the $^{13}\text{C-NMR}$ data were compared with the previous report which identified the structural skeleton belonging to the furanonaphthoquinone [23]. From the above NMR data, compound **2** was identified as 5-hydroxyisopropylnaptho[2,3-b]furan-4,9quinone.

Compound **3** showed NMR data essentially similar to those of compounds **1** and **2**. The $^1\text{H-NMR}$ revealed three signals of trisubstituted benzene ring [δ_{H} 7.29 (1H, d, $J = 8.5$ Hz, H-6), [δ_{H} 7.62 (1H, dd, $J = 8.5, 7.3$ Hz, H-7), [δ_{H} 7.77 (1H, d, $J = 7.3$ Hz, H-8)], two methine protons of furan ring δ_{H} 7.78 (1H, d, $J = 2.0$ Hz, H-2) and δ_{H} 6.99 (1H, d, $J = 2.0$ Hz, H-3). Furthermore, the $^1\text{H-NMR}$ showed the presence of a hydrogen bond signal at 12.17 ppm which illustrated the connection of the hydroxy group with carbonyl carbon. On the other hand, the $^{13}\text{C-NMR}$ presented two carbonyl carbons at

186.6 and 173.0 ppm together with ten olefinic carbons. The structure of compound **3** was identified as 5-hydroxynaphtho[2,3-b]furan-4,9quinone.

Compounds **4** and **5** were obtained as orange amorphous powder. The ^{13}C -NMR of **4** and **5** were compared with that of compound **3** which showed the same feature with two carbonyl carbons (compound **4** at 186.6, 179.3 ppm; compound **5** at 179.3, 173.0 ppm). However, compound **4** showed the presence of one methoxy group at 56.7 ppm and lacks a hydrogen bond signal in ^1H -NMR. From the above data, compound **4** was indicated as 5-methoxynaphtho[2,3-b]furan-4,9quinone. The ^1H -NMR of **5** lacked hydrogen bond and one olefinic proton signal. In addition, the ^1H -NMR and ^{13}C -NMR showed more two methoxy signals at δ_{H} 3.99 (3H, s)- δ_{C} 56.7 (MeO-5) and δ_{H} 3.97 (3H, s)- δ_{C} 56.17 (MeO-7). From these evidence, the structure of compound **5** was identified as 5,7-dimethoxynaphtho[2,3-b]furan-4,9quinone.

NMR data of compounds 2-5

5-Hydroxyisopropyl naphtho[2,3-b]furan-4,9quinone (**2**): yellow powder; ^1H -NMR (500 MHz, chloroform-*d*) δ (ppm) 6.79 (1H, s, H-3), 7.23 (1H, d, $J=8.1$ Hz, H-6), 7.62 (1H, dd, $J=8.1, 7.8$ Hz, H-7), 7.74 (1H, d, $J = 7.8$ Hz, H-8), 1.76 (6H, s, H-11, H-12); ^{13}C -NMR (125 MHz, Chloroform-*d*) 168.4 (C-2), 102.4 (C-3), 131.2 (C-3a), 186.8 (C-4), 115.4 (C-4a), 163.5 (C-5), 125.4 (C-6), 136.4 (C-7), 120.1 (C-8), 132.9 (C-8a), 172.8 (C-9), 152.1 (C-9a), 69.6 (C-10), 28.9 (C-11, C-12) [23].

5-Hydroxynaphtho[2,3-b]furan-4,9quinone (**3**): yellow powder; $^1\text{H-NMR}$ (500 MHz, chloroform-*d*) δ (ppm) 7.78 (1H, d, J = 2.0 Hz, H-2), 6.99 (1H, d, J = 2.0 Hz, H-3), 7.29 (1H, d, J = 8.5 Hz, H-6), 7.62 (1H, dd, J = 8.5, 7.3 Hz, H-7), 7.77 (1H, d, J = 7.3 Hz, H-8); $^{13}\text{C-NMR}$ (125 MHz, Chloroform-*d*) 149.0 (C-2), 108.5 (C-3), 130.4 (C-3a), 186.6 (C-4), 115.5 (C-4a), 162.6 (C-5), 125.5 (C-6), 136.5 (C-7), 120.2 (C-8), 132.8 (C-8a), 173.0 (C-9a), 153.0 (C-9) [23].

5-Methoxynaphtho[2,3-b]furan-4,9quinone (**4**): yellow powder; $^1\text{H-NMR}$ (500 MHz, chloroform-*d*) δ (ppm) 7.73 (1H, d, J = 1.4 Hz, H-2), 6.97 (1H, d, J =1.4 Hz, H-3), 7.33 (1H, d, J = 8.4 Hz, H-6), 7.69 (1H, dd, J = 8.4, 7.6 Hz, H-7), 7.91 (1H, d, J = 7.6 Hz, H-8), 4.02 (3H, s, MeO-5); $^{13}\text{C-NMR}$ (125 MHz, Chloroform-*d*) 148.9 (C-2), 109.2 (C-3), 132.2 (C-3a), 186.6 (C-4), 120.7 (C-4a), 160.7 (C-5), 118.8 (C-6), 135.2 (C-7), 120.1 (C-8), 134.2 (C-8a), 173.4 (C-9), 151.2 (C-9a), 56.7 (MeO-5) [24].

5,7-Dimethoxynaphtho[2,3-b]furan-4,9quinone (**5**): yellow powder; $^1\text{H-NMR}$ (500 MHz, chloroform-*d*) δ (ppm) 7.71 (1H, d, J = 1.8 Hz, H-2), 6.97 (1H, d, J = 1.8 Hz, H-3), 6.74 (1H, d, J = 2.4 Hz, H-6), 7.41 (1H, d, J =2.4 Hz, H-8), 3.99 (3H, s, MeO-5), 3.97 (3H, s, MeO-7); $^{13}\text{C-NMR}$ (125 MHz, Chloroform-*d*) 148.9 (C-2), 109.4 (C-3), 132.6 (C-3a), 179.3 (C-4), 115.1 (C-4a), 162.9 (C-5), 104.4 (C-6), 164.9 (C-7), 104.7 (C-8), 137.2 (C-8a), 173.0 (C-9), 151.0 (C-9a), 56.7 (MeO-5), 56.17 (MeO-7) [23].

3.2.3 Structural elucidation of compounds 6-7

The $^1\text{H-NMR}$ spectrum of **6** indicated the presence of two pairs of equivalent aromatic protons, a singlet signal for phenolic protons δ_{H} 6.58 (4H, s, H-2', H-6', H-

2'', H-6''), four aromatic methoxy groups (δ_{H} 3.90 (12H, s, MeO-3', MeO-5', MeO-3'', MeO-5''). In addition, the $^1\text{H-NMR}$ also showed the signals belonging to bis-tetrahydrofuran ring which revealed symmetrical feature containing methine protons at 3.09 (2H, br, H-1, H-5), two oxygenated methylene protons at 4.28 (4H, dd, $J = 9.0, 6.8$ Hz, H-4a, H-8a), two oxygenated methylene protons at δ_{H} 3.91 (m, Hb-4, Hb-8), along with two oxygenated methine signals at δ_{H} 4.73 (2H, d, $J = 4.1$ Hz, H-2, H-6). The bis-tetrahydrofuran was characterized as *cis*-configuration of two tetrahydrofuran rings fused in naturally occurring [39]. The $^1\text{H-NMR}$ data of H-1, H-5, H-4, and H-8 were compared with the previous reports which help to reconfirm the configuration of bis-tetrahydrofuran ring.

The $^{13}\text{C-NMR}$ spectrum showed twenty-two carbon signals, including four methoxy carbons at (δ_{C} 56.5 (3'-OCH₃, 5'-OCH₃, 3''-OCH₃, 5''-OCH₃), eight quaternary carbons at δ_{C} 146.3 (C-3', C-5', C-3'', C-5''), 132.2 (C-1', C-1''), 134.4 (C-4', C-4'') two oxygenated methylene carbons at δ_{C} 71.9 (C-4, C-8), six methine carbons were at δ_{C} 102.8 (C-2', C-6', C-2'', C-6''), 54.5 (C-1, C-5) and two oxygenated methines at δ_{C} 86.2 (C-2, C-6). From the above NMR data, compound **6** was identified as syringaresinol.

The $^1\text{H-NMR}$ data of compound **7** indicated the characteristic structure of furofuran lignan like compound **6** with the presence of bis-tetrahydrofuran ring. The $^1\text{H-NMR}$ and HSQC spectra of **7** described five olefinic proton at δ_{H} 6.86 (1H, d, $J = 1.4$ Hz, H-2''), 6.77 (1H, d, $J = 8.0$ Hz, H-5''), 6.81 (1H, dd, $J = 8.0, 1.5$ Hz, H-6''), 6.62 (1H,

d, $J = 8.5$ Hz, H-5'), 6.84 (1H, d, $J = 8.5$ Hz, H-6'), one signal dioxymethylene group at δ_{H} 5.94 (2H, s, O-CH₂-O), and two methoxy groups at δ_{H} 3.92 (3H, s, MeO-2') and 3.88 (3H, s, MeO-4'). The olefinic proton at δ_{H} 6.86 (1H, d, $J = 1.4$ Hz) showed the meta-coupling with proton at δ_{H} 6.81 (1H, dd, $J = 8.0, 1.5$ Hz). The dioxymethylene proton and methine proton at δ_{H} 6.81 (1H, dd, $J = 8.0, 1.5$ Hz) showed the HMBC correlation with carbon at 147.3 (C-4'') which help to determine the skeleton of ring A containing the dioxymethylene group. In ring B, proton at 6.62 (1H, d, $J = 8.5$ Hz, H-5') and 6.84 (1H, d, $J = 8.5$ Hz, H-6') showed the ortho-coupling. Proton at 6.84 (1H, d, $J = 8.5$ Hz, H-6') showed the HMBC correlations with two carbons at 144.5 (C-2') and 147.2 (C-4'). Proton at 6.62 (1H, d, $J = 8.5$ Hz, H-5') showed the correlations with carbon at 128.1 (C-1') and 138.6 (C-3'). Based on the HMBC correlations of protons H-5' and H-6', the positions of all substituted group in ring B were determined as Figure 3.3.

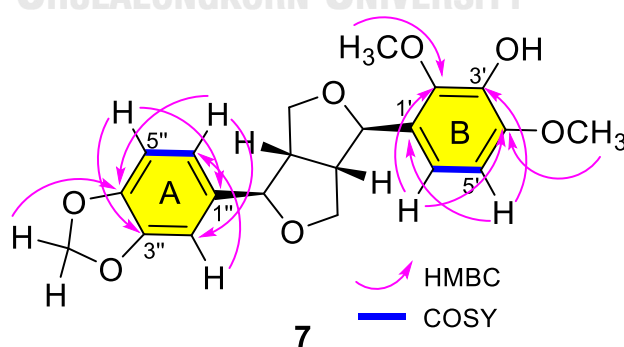


Figure 3.5 The HMBC correlations of compound (7)

NMR data of compounds 6 and 7

Syringaresinol (**6**): white powder; $^1\text{H-NMR}$ (500 MHz, chloroform-*d*) δ (ppm) 6.58 (4H, s, H-2', H-6', H-2'', H-6''), 4.73 (2H, d, $J = 4.1$ Hz, H-2, H-6), 4.28 (4H, dd, $J = 9.0, 6.8$ Hz, H-4a, H-8a), 3.91 (4H, m, H-4b, H-8b), 3.09 (2H, s, H-1, H-5), 3.90 (12H, s, MeO-3', MeO-5', MeO-3'', MeO-5''); $^{13}\text{C-NMR}$ (125 MHz, chloroform-*d*) 54.5 (C-1), 86.2 (C-2), 71.9 (C-4), 54.5 (C-5), 86.2 (C-6), 71.9 (C-8), 132.2 (C-1'), 102.8 (C-2'), 146.3 (C-3'), 134.4 (C-4'), 146.3 (C-5'), 102.8 (C-6'), 132.2 (C-1''), 102.8 (C-2''), 146.3 (C-3''), 134.4 (C-4''), 146.3 (C-5''), 102.8 (C-6''), 56.5 (MeO-3''), 56.5 (MeO-5''), 56.5 (MeO-3'''), 56.5 (MeO-5''') [25].

Lignan α -7a (**7**): white powder; $^1\text{H-NMR}$ (500 MHz, chloroform-*d*) δ (ppm) 6.86 (1H, d, $J = 1.4$ Hz, H-2''), 6.77 (1H, d, $J = 8.0$ Hz, H-5''), 6.81 (1H, dd, $J = 8.0, 1.5$ Hz, H-6''). 6.62 (1H, d, $J = 8.5$ Hz, H-5'), 6.84 (1H, d, $J = 8.5$ Hz, H-6'), 5.94 (2H, s, O-CH₂-O), 3.05 (1H, m, H1), 5.05 (1H, d, $J = 4.8$ Hz, H-2), 4.31 (1H, dd, $J = 9.1, 7.4$ Hz, H-4a), 4.21 (1H, dd, $J = 9.1, 6.6$ Hz, H-4), 4.68 (1H, d, $J = 5.8$ Hz, H-6), 2.97 (1H, m, H-5), 4.01 (1H, dd, $J = 9.2, 4.7$ Hz, H-8a), 3.90 (1H, dd, $J = 9.2, 4.7$ Hz, H-8), 3.92 (3H, s, MeO-2'), 3.88 (3H, s, MeO-4'); $^{13}\text{C-NMR}$ (125MHz, chloroform-*d*) 54.1 (C-1), 82.3 (C-2), 73.1 (C-4), 54.7 (C-5), 85.5 (C-6), 73.1 (C-8), 128.1 (C-1'), 144.5 (C-2'), 138.6 (C-3'), 147.2 (C-4'), 105.9 (C-5'), 115.8 (C-6'), 135.3 (C-1''), 106.7 (C-2''), 148.0 (C-3''), 147.3 (C-4''), 108.3 (C-5''), 119.6 (C-6''), 60.5 (MeO-2'), 56.3 (MeO-4'), 101.1 (O-CH₂-O) [26].

3.2.4 Structural elucidation of compounds 8-11

The $^1\text{H-NMR}$ data of compound **8** showed five olefinic methine protons containing three aromatic protons at δ_{H} 6.97 (1H, br, H-2), 6.71 (1H, d, $J = 8.2$ Hz, H-5), 6.86 (1H, d, $J = 8.2$ Hz, H-6) and two trans-olefinic methine protons at δ_{H} 7.46 (1H, d, $J = 15.9$ Hz, H-7), 6.16 (1H, d, $J = 15.9$ Hz, H-8). The $^{13}\text{C-NMR}$ spectrum showed seven signals containing three olefinic carbons at δ_{C} 113.8 (C-2), 115.2 (C-5), 121.5 (C-6), three quaternary carbons at δ_{C} 126.5 (C-1), 148.1 (C-3), 145.5 (C-4), and one carbonyl carbon belonging to carboxylic group at δ_{C} 169.9 (C-9). The above NMR data were consistent with those of caffeic acid [27]. Therefore, compound **8** was identified as caffeic acid.

Compounds **9** and **10** illustrated NMR spectra similar to those of compound **8**. However, compound **9** showed one more methoxy group in the $^1\text{H-NMR}$ and $^{13}\text{C-NMR}$. Then, the NMR data of compound **9** was considered together with the published report which identified the structure of **9** as ferullic acid. On the other hand, compound **10** showed the presence of dioxymethylene group at δ_{H} 5.84 (2H, s, O-CH₂-O) and δ_{C} 102.1 (O-CH₂-O). This observation supported to assign the structure of compound **10** as 3',4'-methylenedioxycinnamic acid [27, 28].

The $^1\text{H-NMR}$ and HSQC spectra of compound **11** showed eight olefinic protons including six aromatic proton at δ_{H} 6.74 (1H, d, $J = 2.0$ Hz, H-2), 6.65 (1H, d, $J = 8.0$ Hz, H-5), 6.60 (1H, dd, $J = 8.0, 2.0$ Hz, H-6), 7.0 (1H, d, $J = 2.0$ Hz, H-2'), 6.75 (1H,

d, $J = 8.2$ Hz, H-5'), and 6.89 (1H, dd, $J = 8.2, 2.0$ Hz, H-6') and two *trans*-olefinic methine proton at δ_{H} 7.49 (1H, d, $J = 15.9$ Hz, H-7') and 6.24 (1H, d, $J = 15.9$ Hz, H-8'), one oxygenated-proton at δ_{H} 5.06 (1H, d, $J = 9.3$ Hz, H-8), and two methylene protons at δ_{H} 3.06 (1H, m, H-7a), 2.91 (1H, m, H-7b). By comparing the ^1H -NMR and ^{13}C -NMR data of **11** with the previous report [29], compound **11** was determined as rosmarinic acid.

NMR data of compounds 8-11

Caffeic acid (**8**): white amorphous powder; ^1H -NMR (500 MHz, methanol- d_4) δ (ppm) 6.97 (1H, br, H-2), 6.71 (1H, d, $J = 8.2$ Hz, H-5), 6.86 (1H, d, $J = 8.2$ Hz, H-6), 7.46 (1H, d, $J = 15.9$ Hz, H-7), 6.16 (1H, d, $J = 15.9$ Hz, H-8); ^{13}C -NMR (125 MHz, methanol- d_4) 126.5 (C-1), 113.8 (C-2), 148.1 (C-3), 145.5 (C-4), 115.2 (C-5), 121.5 (C-6), 145.5 (C-7), 114.5 (C-8), 169.9 (C-9) [27].

Ferullic acid (**9**): white amorphous powder; ^1H -NMR (500 MHz, Methanol- d_4) δ (ppm) 7.13 (1H, brs, H-2), 6.8 (1H, d, $J = 8.2$ Hz, H-5), 7.02 (1H, $J = 8.2$ Hz, H-6), 7.6 (1H, d, $J = 15.9$ Hz, H-7), 6.27 (1H, d, $J = 15.9$ Hz, H-8), 3.85 (3H, s, MeO-3); ^{13}C -NMR (125 MHz, Methanol- d_4) 126.5 (C-1), 110.3 (C-2), 149.2 (C-3), 148.0 (C-4), 115.1 (C-5), 122.7 (C-6), 145.6 (C-7), 114.6 (C-8), 169.0 (C-9), 55.1 (MeO-3) [27].

3,4-Methylenedioxybenzoic acid (**10**): white amorphous powder; ^1H -NMR (500 MHz, Methanol- d_4) δ (ppm) 7.13 (1H, brs, H-2), 6.72 (1H, d, $J = 8.0$ Hz, H-5), 6.93 (1H, d, $J = 8.0$ Hz, H-6), 7.27 (1H, d, $J = 15.9$ Hz, H-7), 6.16 (1H, d, $J = 15.9$ Hz, H-8), 5.84 (2H,

s, O-CH₂-O); ¹³C-NMR (125 MHz, Methanol-*d*₄) 129.2 (C-1), 107.2 (C-2), 148.6 (C-3), 149.7 (C-4), 109.6 (C-5), 125.2 (C-6), 144.4 (C-7), 117.6 (C-8), 168.4 (C-9), 102.1 (O-CH₂-O) [28].

Rosmarinic acid (**11**): yellow amorphous powder; ¹H-NMR (500 MHz, Methanol-*d*₄) δ (ppm) 6.74 (1H, brs, H-2), 6.65 (1H, d, *J*=8.0 Hz, H-5), 6.60 (1H, d, *J*=8.0 Hz, H-6), 7.0 (1H, d, *J*= 2.0 Hz, H-2'), 6.75 (1H, d, *J*= 8.2 Hz, H-5'), 6.89 (1H, d, *J*= 8.2 Hz, H-6'), 7.49 (1H, d, *J*= 15.9 Hz, H-7'), 6.24 (1H, d, *J*= 15.9 Hz, H-8'), 5.06 (1H, d, *J*= 9.3 Hz, H-8), 3.06 (1H, m, H-7a), 2.91 (1H, m, H-7b); ¹³C-NMR (125 MHz, Methanol-*d*₄) 130.8 (C-1), 117.5 (C-2), 146.7 (C-3), 144.9 (C-4), 116.2 (C-5), 121.7 (C-6), 38.6 (C-7), 77.3 (C-8), 127.9 (C-1'), 115.1 (C-2'), 146.9 (C-3'), 149.4 (C-4'), 116.4 (C-5'), 123.0 (C-6'), 146.7 (C-7'), 115.4 (C-8'), 169.0 (C-9') [29].

3.2.5 Structural elucidation of compounds 12-14

The ¹H-NMR spectrum of compound **13** showed five aromatic protons at 6.75 (1H, d, *J*=8.1 Hz, H-2), 7.66 (1H, dd, *J*= 8.3, 8.1 Hz, H-3), 6.99 (1H, d, *J*= 8.3 Hz, H-4), 7.5 (1H, d, *J*= 9.0 Hz, H-5), 7.33 (1H, dd, *J*= 9.1, 3.0 Hz, H-6), and 7.41 (1H, d, *J*= 3.0 Hz, H-8). The ¹³C-NMR of **13** showed thirteen carbons including five olefinic methine carbons, four quaternary olefinic carbons, and one carbonyl carbon were indicative of xanthone skeleton. Proton 7.66 (1H, dd, *J*= 8.3, 8.1 Hz, H-3) had the ortho-coupling with protons 6.75 (1H, d, *J*=8.1 Hz, H-2) and 6.99 (1H, d, *J*= 8.3 Hz, H-4). Proton 7.33 (1H, dd, *J*= 9.1, 3.0 Hz, H-6) has the meta-coupling with proton 7.41 (1H, d, *J*= 3.0 Hz,

H-8) and ortho-coupling with proton 7.5 (1H, d, $J= 9.0$ Hz, H-5). These observations indicated that ring A and B were the tri-substituted aromatic rings. The ^{13}C -NMR of **13** showed the signal at 169.1 ppm, which was featured for the connection of hydroxy group at C1. Based on splitting pattern and coupling constant analysis, the structure of **13** was possibly either 1,7-dihydroxyxanthone or 1,6-dihydroxyxanthone. Compared with the NMR data of the previous reports, compound **13** was determined as 1,7-dihydroxyxanthone (euxanthone) [30, 40].

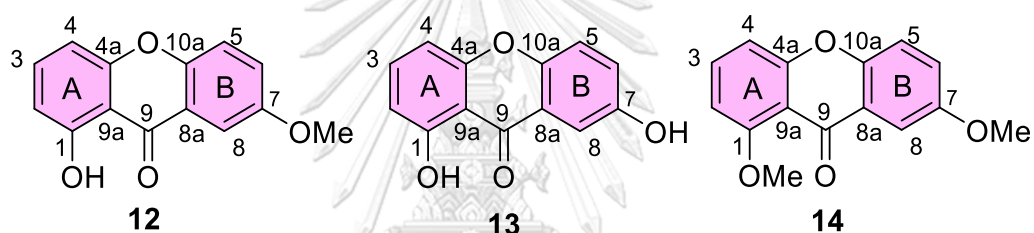


Figure 3.6 The structures of compounds (**12**, **13**, **14**)

Compounds **12** and **14** showed the similar pattern in the ^1H -NMR and ^{13}C -NMR spectra with compound **13**. However, in the ^{13}C -NMR, compound **12** showed one signal of methoxy group at 56.1 (7-OMe) whereas compound **14** showed two signals of methoxy groups at 56.4 (1-OMe), 55.8 (7-OMe). Based on comparison of ^1H -NMR and ^{13}C -NMR data with those of previous reports [28-29, 37], the structures of **12** and **14** were identified as 1-hydroxy-7-methoxyxanthone and 1,7-dimethoxyxanthone, respectively [30, 31, 40].

NMR data of compounds 12-14

1-Hydroxy-7-methoxyxanthone (**12**) yellow amorphous powder; $^1\text{H-NMR}$ (500 MHz, Chloroform-*d*) δ (ppm) 6.77 (1H, d, $J=8.3, 1.0$ Hz, H-2), 7.57 (1H, dd, $J= 8.3, 8.5$ Hz, H-3), 6.9 (1H, dd, $J= 8.5, 1.0$ Hz, H-4), 7.39 (1H, d, $J= 9.1$ Hz, H-5), 7.33 (1H, dd, $J= 9.1, 3.0$ Hz, H-6), 7.59 (1H, d, $J= 3.0$ Hz, H-8), 3.9 (3H, s, 1-OMe); $^{13}\text{C-NMR}$ (125 MHz, Chloroform-*d*) 169.1 (C-1), 110.2 (C-2), 136.7 (C-3), 107.1 (C-4), 156.2 (C-4a), 119.4 (C-5), 125.9 (C-6), 156.4 (C-7), 105.1 (C-8), 120.9 (C-8a), 182.2 (C-9), 108.8 (C-9a), 151.1 (C-10a), 56.1 (7-OMe) [30].

Euxanthone (**13**) yellow amorphous powder; $^1\text{H-NMR}$ (500 MHz, DMSO-*d*₆) δ (ppm) 6.75 (1H, d, $J=8.1$ Hz, H-2), 7.66 (1H, dd, $J= 8.3, 8.1$ Hz, H-3), 6.99 (1H, d, $J= 8.3$ Hz, H-4), 7.5 (1H, d, $J= 9.0$ Hz, H-5), 7.33 (1H, dd, $J= 9.1, 3.0$ Hz, H-6), 7.41 (1H, d, $J= 3.0$ Hz, H-8); $^{13}\text{C-NMR}$ (125 MHz, DMSO-*d*₆) 161 (C-1), 109.7 (C-2), 137.2 (C-3), 107.2 (C-4), 155.9 (C-4a), 119.4 (C-5), 125.7 (C-6), 156.2 (C-7), 107.9 (C-8), 120.5 (C-8a), 181.6 (C-9), 107.9 (C-9a), 149.4 (C-10a) [30].

1,7-Dimethoxyxanthone (**14**) yellow amorphous powder; $^1\text{H-NMR}$ (500 MHz, DMSO-*d*₆) δ (ppm) 6.91 (1H, d, $J=8.3$ Hz, H-2), 7.66 (1H, dd, $J= 8.3, 8.4$ Hz, H-3), 7.06 (1H, d, $J= 8.4$ Hz, H-4), 7.46 (1H, d, $J= 9.0$ Hz, H-5), 7.33 (1H, dd, $J= 9.0, 3.1$ Hz, H-6), 7.40 (1H, d, $J= 3.1$ Hz, H-8), 3.84 (3H, s, 1-OMe), 3.79 (3H, s, 7-OMe); $^{13}\text{C-NMR}$ (125 MHz, DMSO-*d*₆) 160.3 (C-1), 106.2 (C-2), 135.7 (C-3), 109.8 (C-4), 157.5 (C-4a), 119.3 (C-5), 123.8 (C-6), 155.8 (C-7), 106.2 (C-8), 122.9 (C-8a), 174.8 (C-9), 111.3 (C-9a), 149.2 (C-10a), 56.4 (1-OMe), 55.8 (7-OMe) [31].

3.2.6 Structural elucidation of compounds 15-17

The $^1\text{H-NMR}$ and HSQC spectrum of compound 15 showed five aromatic protons at δ_{H} 7.39 (1H, d, $J= 9.2$ Hz, H-3), 7.22 (1H, d, $J= 9.2$ Hz, H-4), 6.84 (1H, dd, $J= 8.3, 1.0$ Hz, H-5), 7.54 (1H, dd, $J= 8.3, 8.1$ Hz, H-6), 6.76 (1H, d, $J= 8.1, 1.0$ Hz, H-7), two methoxy groups at δ_{H} 4.00 (3H, s, 1-OMe), and 3.94 (3H, s, 2-OMe). The $^{13}\text{C-NMR}$ showed fifteen signals including twelve olefinic carbons at δ_{C} 148.9 (C-1), 149.3 (C-2), 121.2 (C-3), 113.0 (C-4), 151.2 (C-4a), 106.5 (C-5), 136.6 (C-6), 110.4 (C-7), 162.3 (C-8), 109.2 (C-8a), 115.9 (C-9a), 155.8 (C-10a), one carbonyl carbon at δ_{C} 182.2 (C-9) and two methyl carbons at δ_{C} 61.9 (1-OMe), 57.3 (2-OMe), thus indicating the structural skeleton of xanthone. Proton δ_{H} 7.39 (1H, d, $J = 9.2$ Hz, H-3) showed ortho-coupling with proton 7.22 (1H, d, $J = 9.2$ Hz, H-4) in ring A. Furthermore, proton at 7.39 (1H, d, $J = 9.2$ Hz, H-3) showed the correlations with carbons at δ_{C} 113.0 (C-4), 151.2 (C-4a) and proton 7.22 (1H, d, $J = 9.2$ Hz, H-4) showed the correlations with carbons at δ_{C} 123.5 (C-3), 151.0 (C-4a), and 115.9 (C-9a), which determined the connection of C-3/C-4/C-4a/C-9a. In addition, proton at 7.39 (1H, d, $J= 9.2$ Hz, H-3) and methoxy group at 4.00 (3H, s, 1-OMe) showed the correlation with carbon at δ_{C} 148.9 (C-1) and proton at 7.22 (1H, d, $J= 9.2$ Hz, H-4) and methoxy group at δ_{H} 3.94 (3H, s, 2-OMe) showed the correlation with carbon at δ_{C} 145.6 (C-2), which identified the connections of two methoxy group at C-1 and C-2 in ring A. Proton 7.54 (1H, dd, $J= 8.3, 8.1$ Hz, H-6) showed the meta-coupling with proton 6.84 (1H, dd, $J= 8.3, 1.0$ Hz,

H-5) and 6.76 (1H, d, $J = 8.1, 1.0$ Hz, H-7), which identified ring B as trisubstituted aromatic ring. Proton 7.54 (1H, dd, $J = 8.3, 8.1$ Hz, H-6) showed the correlations with carbon 162.3 (C-8) and 155.8 (C-10a), proton 6.76 (1H, d, $J = 8.1, 1.0$ Hz, H-7) showed the correlations with carbons at δ_c 106.5 (C-5), 162.3 (C-8), and 109.2 (C-8a), which identified the connection of hydroxy group at C-8. Compared to the previous report [32], the structure of compound **15** was determined as 1,2-dimethoxy-8-hydroxyxanthone.

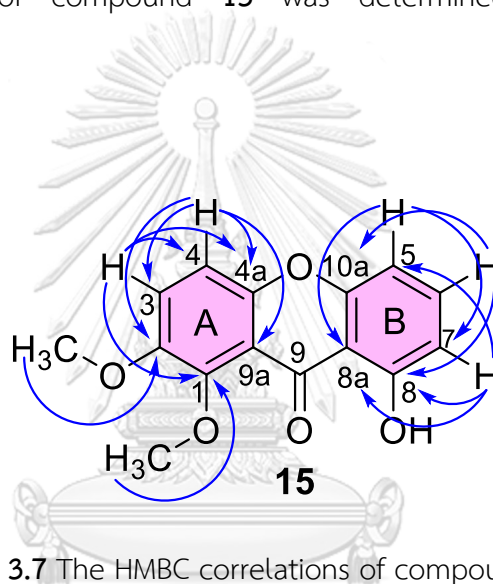


Figure 3.7 The HMBC correlations of compound (15)

Compound **16** showed the similar pattern in the $^1\text{H-NMR}$ and $^{13}\text{C-NMR}$ spectra with those of compound **15**. However, compound **16** showed only one methoxy group in the $^1\text{H-NMR}$. In the HMBC spectrum of compound **16**, proton 7.20 (1H, d, $J = 9.1$ Hz, H-4) showed the correlations with carbons at δ_c 145.6 (C-2) and 114.9 (C-9a). Proton 7.42 (1H, d, $J = 9.1$ Hz, H-3) showed the correlations with carbons at δ_c 144.3 (C-1) and 145.6 (C-2) and methoxy group showed the correlation with carbon at 144.3 (C-1), which determined the connection of methoxy group at C-1 and hydroxy group

at C-2. Compared to the published report, the structure of compound **16** was identified as 1-methoxy-2, 8-dihydroxyxanthone [33].

In the $^1\text{H-NMR}$ spectrum, compound **17** showed the similar pattern with compounds **15** and **16**. However, compound **17** did not show any signals belonging to the methoxy group. In the $^{13}\text{C-NMR}$ spectrum, compound **17** showed thirteen carbons including twelve olefinic carbons at δ_{C} 148.3 (C-1), 140.6 (C-2), 125.1 (C-3), 106.5 (C-4), 147.1 (C-4a), 107.4 (C-5), 138.1 (C-6), 110.2 (C-7), 160.5 (C-8), 107.2 (C-8a), 108.0 (C-9a), 156.2 (C-10a), and one carbonyl carbon at δ_{C} 186.0 (C-9), which were indicative of xanthone skeleton. In the HMBC spectrum of compound **17**, proton 6.95 (1H, d, $J= 8.9$ Hz, H-4) showed the correlations with carbons at δ_{C} 140.6 (C-2) and 147.1 (C-4a), and proton 7.34 (1H, d, $J= 8.9$ Hz, H-3) showed the correlations with carbons at δ_{C} 148.3 (C-1), 140.6 (C-2), and 147.1 (C-4a), thus indicating hydroxy groups at C-3 and C-4. In the ring B, proton 7.71 (1H, dd, $J= 8.4, 8.2$ Hz, H-6) showed the ortho-coupling with proton 7.00 (1H, d, $J= 8.4$ Hz, H-5), and 6.78 (1H, d, $J= 8.2$ Hz, H-7), and showed the correlations with carbons at 160.5 (C-8), 156.2 (C-10a). Proton 6.78 (1H, d, $J= 8.2$ Hz, H-7) showed the correlations with carbons at 160.5 (C-8) and 107.2 (C-8a). From these correlations, hydroxy group was determined at C-8. The structure of compound **17** was identified as 1, 2, 8-trihydroxyxanthone [34].

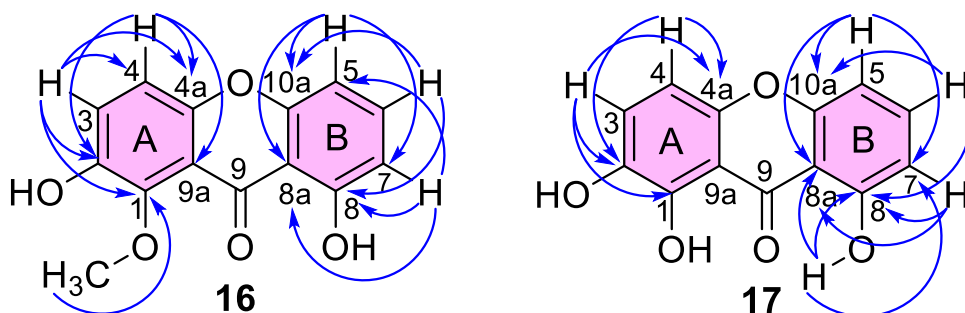


Figure 3.8 The HMBC correlations of compounds (16, 17)

NMR data of compounds 15-17

1,2-Dimethoxy-8-hydroxyxanthone (**15**) yellow amorphous powder; $^1\text{H-NMR}$ (500 MHz, Chloroform-*d*) δ (ppm) 7.39 (1H, d, $J= 9.2$ Hz, H-3), 7.22 (1H, d, $J= 9.2$ Hz, H-4), 6.84 (1H, dd, $J= 8.3, 1.0$ Hz, H-5), 7.54 (1H, dd, $J= 8.3, 8.1$ Hz, H-6), 6.76 (1H, d, $J= 8.1, 1.0$ Hz, H-7), 4.00 (3H, s, 1-OMe), 3.94 (3H, s, 2-OMe); $^{13}\text{C-NMR}$ (125 MHz, Chloroform-*d*) 148.9 (C-1), 149.3 (C-2), 121.2 (C-3), 113.0 (C-4), 151.2 (C-4a), 106.5 (C-5), 136.6 (C-6), 110.4 (C-7), 162.3 (C-8), 109.2 (C-8a), 182.8 (C-9), 115.9 (C-9a), 155.8 (C-10a), 61.9 (1-OMe), 57.3 (2-OMe) [32].

1-Methoxy-2, 8-dihydroxyxanthone (**16**) yellow amorphous powder; $^1\text{H-NMR}$ (500 MHz, Chloroform-*d*) δ (ppm) 7.42 (1H, d, $J= 9.1$ Hz, H-3), 7.20 (1H, d, $J= 9.1$ Hz, H-4), 6.86 (1H, dd, $J= 8.4, 1.0$ Hz, H-5), 7.56 (1H, dd, $J= 8.4, 8.3$ Hz, H-6), 6.76 (1H, d, $J= 8.3, 1.0$ Hz, H-7), 4.03 (3H, s, 1-OMe); $^{13}\text{C-NMR}$ (125 MHz, Chloroform-*d*) 144.3 (C-1), 145.6 (C-2), 123.5 (C-3), 114.3 (C-4), 151.0 (C-4a), 106.7 (C-5), 136.8 (C-6), 110.4 (C-7), 162.1 (C-8), 109.1 (C-8a), 182.2 (C-9), 114.9 (C-9a), 155.9 (C-10a), 62.9 (1-OMe) [33].

1, 2, 8-Trihydroxyxanthone (**17**) yellow amorphous powder; $^1\text{H-NMR}$ (500 MHz, $\text{DMSO-}d_6$) δ (ppm) 7.34 (1H, d, $J= 8.9$ Hz, H-3), 6.95 (1H, d, $J= 8.9$ Hz, H-4), 7.00 (1H, d, $J= 8.4$ Hz, H-5), 7.71 (1H, dd, $J= 8.4, 8.2$ Hz, H-6), 6.78 (1H, d, $J= 8.2$ Hz, H-7); $^{13}\text{C-NMR}$ (125 MHz, $\text{DMSO-}d_6$) 148.3 (C-1), 140.6 (C-2), 125.1 (C-3), 106.5 (C-4), 147.1 (C-4a), 107.4 (C-5), 138.1 (C-6), 110.2 (C-7), 160.5 (C-8), 107.2 (C-8a), 186.0 (C-9), 108.0 (C-9a), 156.2 (C-10a) [34].

3.2.7 Structural elucidation of compounds **18**

The $^1\text{H-NMR}$ and HSQC spectra of compound **18** showed five aromatic protons at 6.13 (1H, s, H-2), 6.92 (1H, d, $J= 8.7$ Hz, H-7), 7.49 (1H, d, $J= 8.7$ Hz, H-8), 5.73 (1H, d, $J= 10.1$ Hz, H-12), 7.03 (1H, d, $J= 10.1$ Hz, H-13), and two methyl groups at 1.4 (6H, s, H14, H-15). The $^{13}\text{C-NMR}$ spectrum of compound **18** showed eighteen signals including fourteenth olefinic carbons at δ_{C} 162.5 (C-1), 98.5 (C-2), 159.9 (C-3), 101.4 (C-4), 151.5 (C-4a), 132.7 (C-5), 152.6 (C-6), 113.5 (C-7), 116.3 (C-8), 113.1 (C-8a), 102.4 (C-9a), 146.2 (C-10a), 127.5 (C-12), 115.1 (C-13), one carbonyl carbon at δ_{C} 180.2 (C-9), one oxygenated carbon at 78.3(C-11), and two methyl carbons at δ_{C} 28.2 (C-14, C-15), which were indicative of isoprenylxanthone skeleton. Proton 5.73 (1H, d, $J= 10.1$ Hz, H-12) showed the cis coupling with proton 7.03 (1H, d, $J= 10.1$ Hz, H-13) and showed the correlation with carbon at 78.3(C-11). In the HMBC spectrum, proton 7.03 (1H, d, $J= 10.1$ Hz, H-13) showed the correlations with carbons at 159.9 (C-3), 151.5 (C-4a), 78.3(C-11), methyl group showed the correlations with carbons at 127.5 (C-12), 115.1

(C-13), which supported the presence of isoprenyl group and its connection at C4 in ring A. Furthermore, proton 6.13 (1H, s, H-2) showed the correlations with carbons at δ_c 162.5 (C-1), 101.4 (C-4), and 102.4 (C-9a), which indicated that this proton was located at C-2 as well as the presence of hydroxyl group at C-1 in ring A. In ring B, proton 7.49 (1H, d, $J= 8.7$ Hz, H-8) showed the ortho-coupling with proton 6.92 (1H, d, $J= 8.7$ Hz, H-7) and the correlations with carbons at 152.6 (C-6), 180.2 (C-9), and 146.2 (C-10a), which supported that protons 6.92 (1H, d, $J= 8.7$ Hz, H-7) and 7.49 (1H, d, $J= 8.7$ Hz, H-8) were located at C-7 and C-8, respectively. The NMR data of compound **18** were consistent with those of isojacareubin [37].

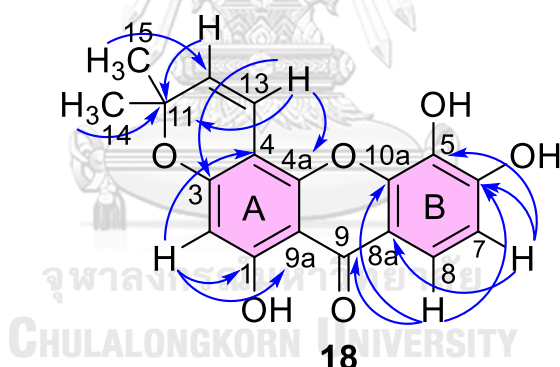


Figure 3.9 The HMBC correlations of compound (**18**)

NMR data of compound **18**

Isojacareubin(**18**) yellow amorphous powder; $^1\text{H-NMR}$ (500 MHz, $\text{DMSO-}d_6$) δ (ppm) 6.13 (1H, s, H-2), 6.92 (1H, d, $J= 8.7$ Hz, H-7), 7.49 (1H, d, $J= 8.7$ Hz, H-8), 5.73 (1H, d, $J= 10.1$ Hz, H-12), 7.03 (1H, d, $J= 10.1$ Hz, H-13), 1.4 (6H, s, H14, H-15); $^{13}\text{C-NMR}$ (125 MHz, $\text{DMSO-}d_6$) 162.5 (C-1), 98.5 (C-2), 159.9 (C-3), 101.4 (C-4), 151.5 (C-4a), 132.7

(C-5), 152.6 (C-6), 113.5 (C-7), 116.3 (C-8), 113.1 (C-8a), 180.2 (C-9), 102.4 (C-9a), 146.2 (C-10a), 78.3(C-11), 127.5 (C-12), 115.1 (C-13), 28.2 (C-14, C-15) [37].

3.2.8 Structural elucidation of compounds **19**

The $^1\text{H-NMR}$ and HSQC spectra of compound **19** showed two olefinic protons at 5.67 (1H, d, $J= 8.1$ Hz, H-5), 7.99 (1H, d, $J=8.1$ Hz, H-6), and five oxygenated protons. The $^{13}\text{C-NMR}$ of compound **19** showed two olefinic carbons at 102.7 (C-5) and 142.7 (C-6), two quaternary carbons at 152.5 (C-2) and 166.2 (C-4), and five oxygenated carbons at δ_{C} 90.6 (C-1'), 75.7 (C-2'), 71.3 (C-3'), 86.4 (C-4'), 62.3 (C-5'). In the HMBC spectrum (Figure 3.8), proton 5.67 (1H, d, $J= 8.1$ Hz, H-5) showed the correlations with carbons at 166.2 (C-4), 142.7 (C-6), proton 7.99 (1H, d, $J=8.1$ Hz, H-6) showed the correlations with carbons at δ_{C} 152.5 (C-2), 166.2 (C-4), 102.7 (C-5), 90.6 (C-1'), which indicated the structural skeleton of nucleoside connected with ribose. Compared to the NMR data of the previous report [35, 36], compound **19** was identified as cytidine.

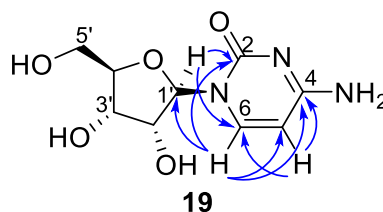


Figure 3.10 The HMBC correlations of compounds (**19**)
NMR data of compound **19**

Cytidine (**19**) white amorphous powder; $^1\text{H-NMR}$ (500 MHz, Methanol- d_4) δ (ppm) 5.67 (1H, d, $J= 8.1$ Hz, H-5), 7.99 (1H, d, $J=8.1$ Hz, H-6), 5.87 (1H, d, $J= 4.7$ Hz, H-1'), 4.11, dd, $J= 5.0, 4.7$ Hz, H-2'), 4.15, 1H, dd, $J=5.0, 4.8$ Hz, H-3'), 3.97 (1H, m, H-4'), 3.8 (1H, dd, $J= 12.3, 2.7$ Hz, H-5'a), 3.70 (1H, dd, $J= 12.3, 3.1$ Hz, H-5'b)); $^{13}\text{C-NMR}$ (125 MHz, Methanol- d_4) 152.5 (C-2), 166.2 (C-4), 102.7 (C-5), 142.7 (C-6), 90.6 (C-1'), 75.7 (C-2'), 71.3 (C-3'), 86.4 (C-4'), 62.3 (C-5').

3.2.9 Structural elucidation of compounds **20**

The $^1\text{H-NMR}$ and HSQC spectrum of compound **20** showed two olefinic protons at 6.3 (1H, d, 6.3 Hz, H-3), 5.0 (1H, d, $J=6.3$ Hz, H-4), nine methine proton at 5.53 (m, 1H, H-1), 3.61, (1H, m, H-6), 3.78 (1H, m, H-7), 3.60 (1H, m, H-8), 2.23 (1H, m, H-9), 3.19 (1H, m, H-2'), 3.36 (1H, m, H-3'), 3.28 (1H, m, H-4'), 3.27 (1H, m, H-5'), one anomeric proton at 4.56 (1H, d, $J= 8.0$ Hz, H-1'), two methylene protons at 3.84 (1H, d, $J= 12.0$ Hz, H-6'a), and 3.64 (1H, dd, $J= 12.0, 3.3$ Hz, H-6'b). The $^{13}\text{C-NMR}$ of **20** showed fourteenth carbons including two olefinic carbons at 141.9 (C-3), 109.7 (C-4), one hemiacetal carbon at 99.7 (C-1'), nine methine carbons at 93.6 (C-1), 83.1 (C-6), 69.3 (C-7), 75.3(C-8), 54.7 (C-9), 74.4 (C-2'), 77.5 (C-3'), 71.5 (C-4'), 78.2 (C-5'), one quaternary carbon at 67.8 (C-5), and one methylene carbon at 62.6 (C-6'). In the $^{13}\text{C-NMR}$ spectra, six carbon signals assignable to the β -glucopyranosyl unit, a hemiacetal carbon and proton resonances (δ_{C} 99.7 with δ_{H} 4.56), and a cis-double bond [δ_{C} 109.7 with δ_{H} 5.0 (d, $J= 6.3$ Hz) and δ_{C} 141.9 with δ_{H} 6.3 (d, $J= 6.3$ Hz)] were

observed. From this evidence, compound **20** is an iridoid glucoside. Compared to the previous report [19, 38], the NMR data of compound **20** was matched with thunbergioside. The connectivity of glucose moiety and iridoid core structure was also confirmed by HMBC spectrum (Figure 3.9).

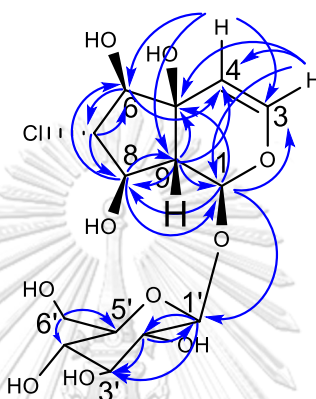


Figure 3.11 The HMBC correlations of compound (**20**)

NMR data of compound **20**

Thunbergioside (**20**) yellow syrup; $^1\text{H-NMR}$ (500 MHz, Methanol- d_4) δ (ppm) 5.53 (m, 1H, H-1), 6.3 (1H, d, 6.3 Hz, H-3), 5.0 (1H, d, $J=6.3$ Hz, H-4), 3.61, (1H, m, H-6), 3.78 (1H, m, H-7), 3.60 (1H, m, H-8), 2.23 (1H, m, H-9), 4.56 (1H, d, $J= 8.0$ Hz, H-1'), 3.19 (1H, m, H-2'), 3.36 (1H, m, H-3'), 3.28 (1H, m, H-4'), 3.27 (1H, m, H-5'), 3.84 (1H, d, $J= 12.0$ Hz, H-6'a), 3.64 (1H, dd, $J= 12.0, 3.3$ Hz, H-6'b); $^{13}\text{C-NMR}$ (125 MHz, Methanol- d_4) 93.6 (C-1), 141.9 (C-3), 109.7 (C-4), 67.8 (C-5), 83.1 (C-6), 69.3 (C-7), 75.3(C-8), 54.7 (C-9), 99.7 (C-1'), 74.4 (C-2'), 77.5 (C-3'), 71.5 (C-4'), 78.2 (C-5'), 62.6 (C-6').

3.3. Rat intestine α -glucosidase inhibition of isolated compounds

All isolated compounds were evaluated for the inhibition against rat intestinal glucosidase. The active components belong to phenolic class including lignan, phenyl propanoid, and xanthone. Syringaresinol (**6**), caffeic acid (**8**), ferulic acid (**9**), rosmarinic acid (**11**), 1,2,8-trihydroxyxanthone (**17**), and isojacareubin (**18**) showed most potent inhibition among isolated compounds; while furano naphthoquinones (**1-5**), some methoxyxanthenes (**12, 14-16**), cytidine (nucleoside) (**19**), and iridoid glucosides (**20**) illustrated no-inhibition. Although iridoid glucosides are representative metabolites of genus *Thunbergia*, their antidiabetic activity has never been reported. To our knowledge, a variety of iridoids and their glycosides isolated from *Scrophularia ningpoensis* were evaluated for α -glucosidase inhibition. However, they showed weak to no inhibition against yeast α -glucosidase [41]. This result indicated that phenolic moiety played an important role in inhibiting enzyme function. The α -glucosidase inhibitory potency was likely to increase according to the number of free phenolic on the aromatic ring. Nevertheless, the above assumption could be adopted for compounds possessing the same core structure. For instance, in phenyl propanoid group, rosmarinic acid (**11**), whose structure contained four phenolic groups, showed higher inhibition against sucrase than caffeic acid (**8**) and ferulic acid (**9**); both of which contained two phenolic moieties. However, rosmarinic acid (**11**) demonstrated slightly weaker inhibition than xanthenes **17** and **18**, whose structures contain less number phenolic moiety. These observations also suggested that the

inhibition trend depended at least on the number of phenolic groups and the core structure of the compound. The α -glucosidase inhibition of isolated compounds was summarized in Figure 3.9 and Table 3.1.



Table 3.1 α -Glucosidase inhibitory effect of isolated compounds

Compound	IC ₅₀	
	Maltase (μ M)	Sucrase (μ M)
1	^a NI	NI
2	NI	NI
3	NI	NI
4	NI	NI
5	NI	NI
6	61.58	60.53
7	1165.21	1084.15
8	119.44	125.69
9	202.07	103.41
10	303.12	312.50
11	78.28	72.21
12	NI	NI
13	1024.05	1080.01
14	NI	NI
15	NI	NI
16	NI	NI
17	162.19	59.4
18	153.51	45.22

19	NI	NI
20	NI	NI
Acarbose	2.76	5.13

^aNI: no-inhibition

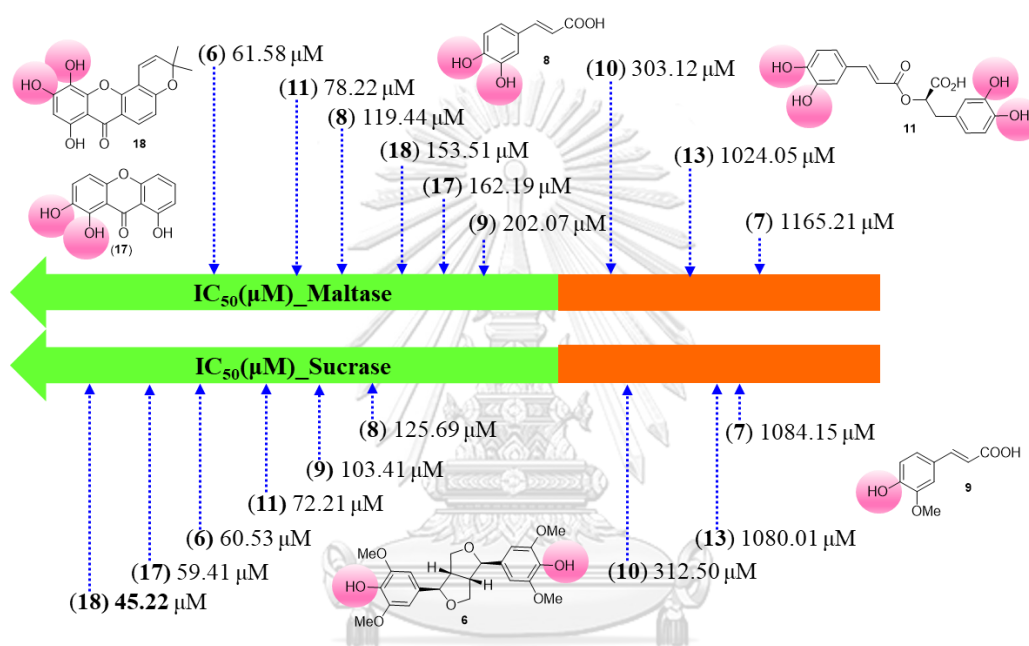


Figure 3.12 Schematic diagram presenting inhibition trend of isolated compounds.

Noted that compounds with definite IC₅₀ values are shown

3.4. Kinetic study of syringaresinol (6) and rosmarinic acid (11), 1,2,8-trihydroxyxanthone (17), and isoquercetin (18)

To gain the inhibition mechanism for rat intestinal α -glucosidase, kinetic study of syringaresinol (6), rosmarinic acid (11), 1,2,8-trihydroxyxanthone (17), and isoquercetin (18) was conducted. The kinetic parameters were identified by varying concentration of substrates (maltose and sucrose) and rat intestinal α -glucosidases

(maltase and sucrase). The Lineweaver-Burk plots of syringaresinol (**6**) (Figures 1A, 1B) showed that V_{\max} decreased with unchanged K_m in the increased concentration of this compound. The result indicated that syringaresinol inhibit maltase and sucrase in the non-competitive mechanism (Figure 3.19) with K_i value of 37.01 and 57.05 μM respectively.

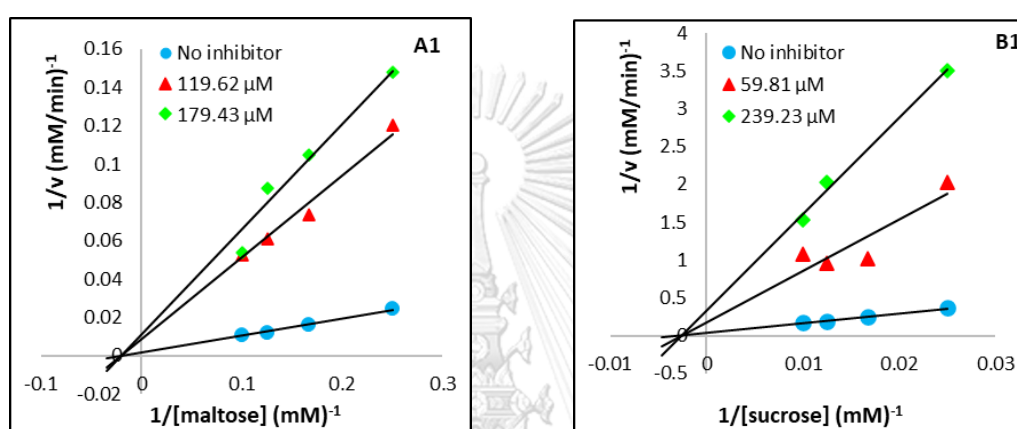


Figure 3.13 Lineweaver-Burk plots for inhibitory activity of syringaresinol (**6**)

against **A1** (maltase) and **B1** (sucrase)

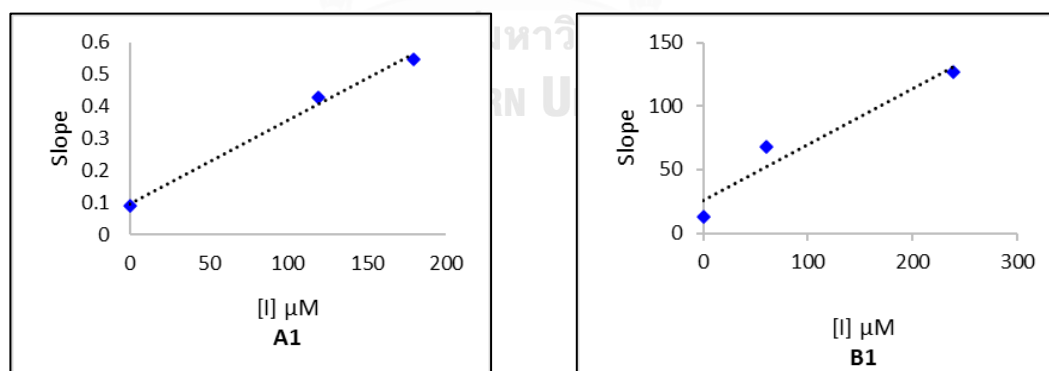


Figure 3.14 Secondary replot of slope vs. $[I]$ from a primary Lineweaver-Burk plot for the determination of K_i of (**6**)

In addition, kinetic study of rosmarinic acid (**11**) was observed allowing a non-competitive mechanism (Figure 3.20-A2) against maltase with K_i value of 53.71 μM

(Figure 2A). On the other hand, the Lineweaver-Burk plot of rosmarinic acid (Figure 2B) with sucrose substrate described that V_{\max} decreased with increased K_m in the increasing of concentration of rosmarinic acid. The result indicated that rosmarinic acid retarded sucrase by mixed manner (Figure 3.20-B2) with K_i and K_i' values of 137.22 and 129.51 μM , respectively.

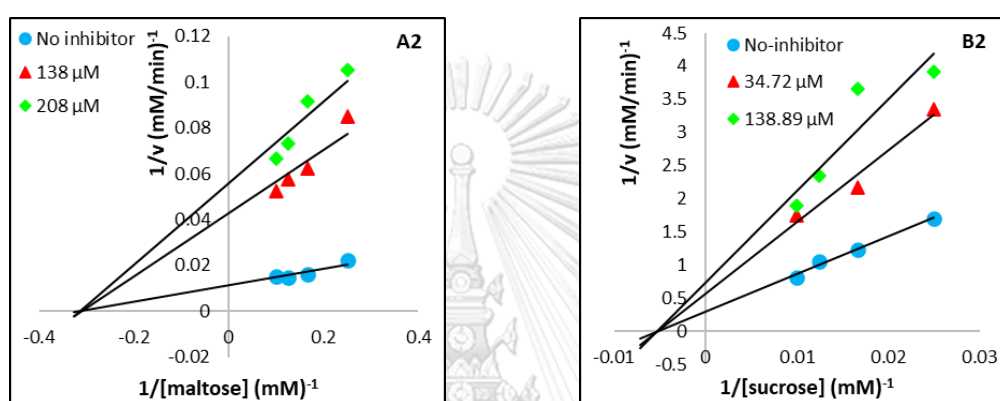


Figure 3.15 Lineweaver-Burk plots for inhibitory activity of rosmarinic acid (11) against A2 (maltase) and B2 (sucrase)

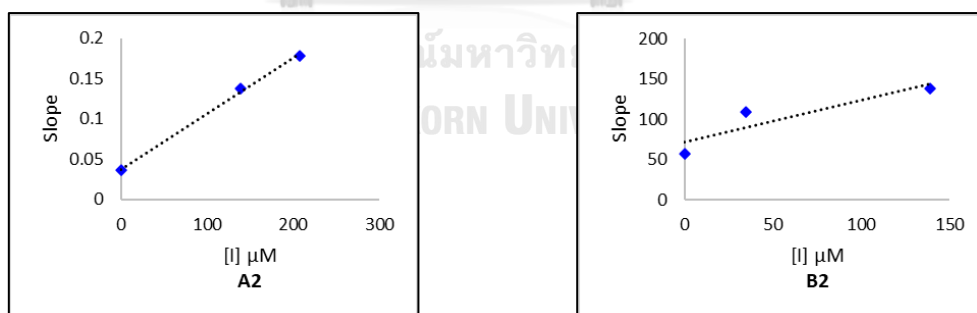


Figure 3.16 Secondary replot of slope vs. [I] from a primary Lineweaver-Burk plot for the determination of K_i of (11)

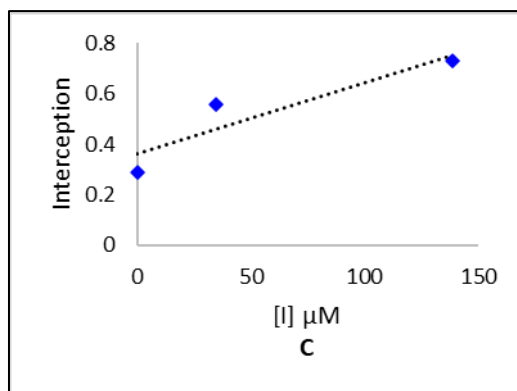


Figure 3.17 Secondary replot of intercept vs. $[I]$ from a primary Lineweaver-Burk plot for the determination of K_i' of **(11)**

In Figures 3.15 and 3.17, the intersection on the X-axis was observed allowing the identification of a non-competitive mechanism (Figure 3.21 and Figure 3.22) against maltase and sucrase. The Lineweaver-Burk Plots of 1,2,8-trihydroxyxanthone (**17**) and isojacareubin (**18**) (Figure 3.15, 3.17) showed that V_{max} decreased with unchanged K_m in the increased concentration of these compounds. The K_i values of **17** and **18** were calculated as 118.86 and 103.79 against maltase, and 72.6 and 74.36 against sucrase respectively (Table 3.2).

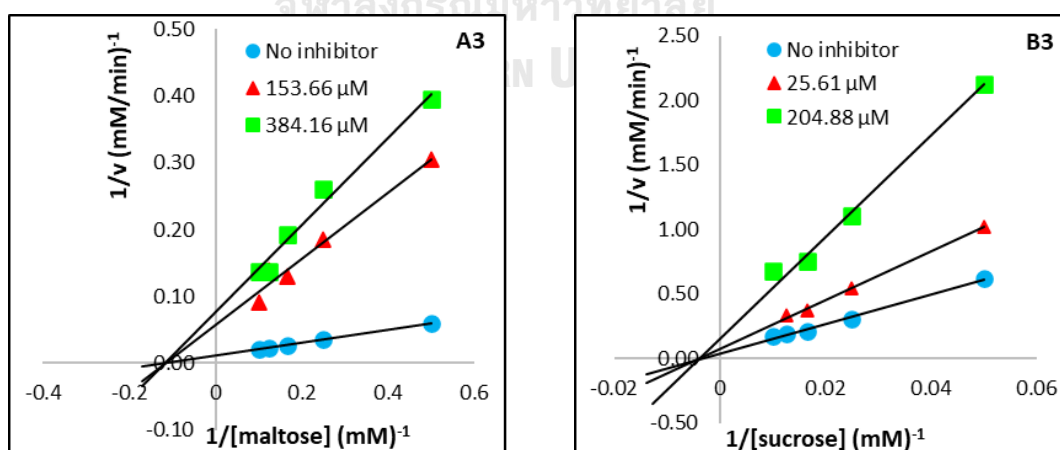


Figure 3.18 Lineweaver-Burk plots for inhibitory activity of 1,2,8-trihydroxyxanthone (**17**) against **A3** (maltase) and **B3** (sucrase)

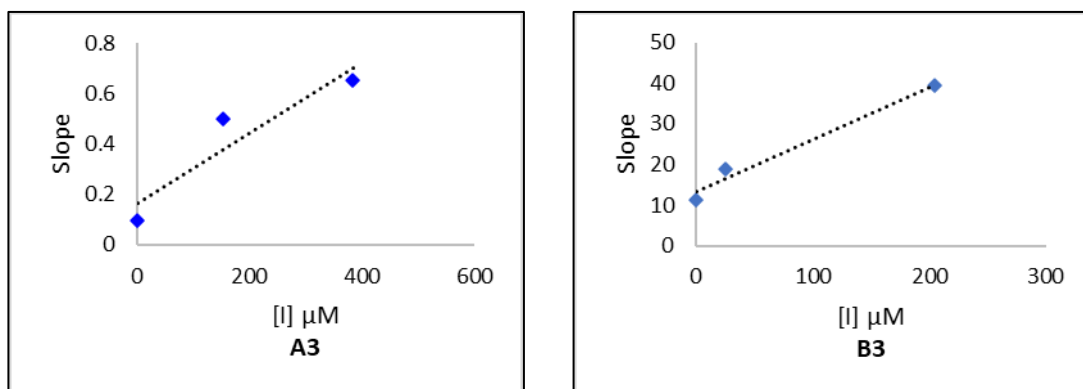


Figure 3.19 Secondary replot of slope vs. $[I]$ from a primary Lineweaver-Burk plot for the determination of K_i of (17)

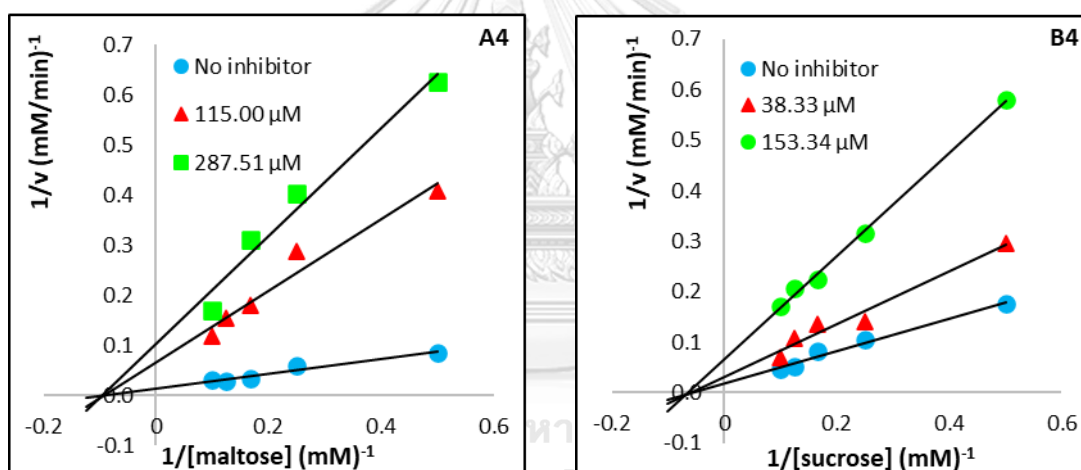


Figure 3.20 Lineweaver-Burk plots for inhibitory activity of isojacareubin (18)

against **A4** (maltase) and **B4** (sucrase)

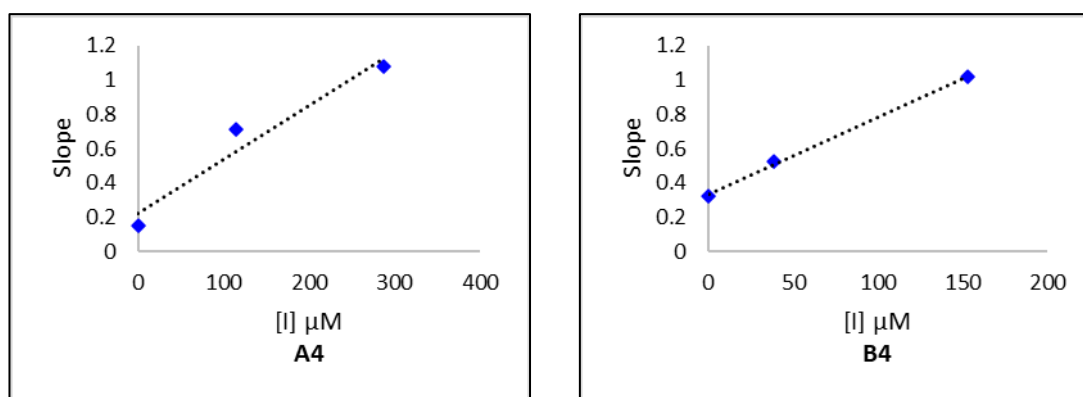


Figure 3.21 Secondary replot of slope vs. $[I]$ from a primary Lineweaver-Burk plot for

the determination of K_i of (18)

Table 3.2 Inhibition types and kinetic parameters of syringaresinol (6), rosmarinic acid (11), 1,2,8-trihydroxyxanthone (17), and isojacareubin (18) on α -glucosidase

		Maltase	Sucrase
	Inhibition type	Non-competitive	Non-competitive
Syringaresinol (6)	K_i (μM)	37.00	57.05
	K_i' (μM)	-	-
	Inhibition type	Non-competitive	Mixed
Rosmarinic acid (11)	K_i (μM)	53.71	137.22
	K_i' (μM)	-	129.51
1,2,8-trihydroxyxanthone (17)	Inhibition type	Non-competitive	Non-competitive
	K_i (μM)	118.86	103.79
	K_i' (μM)	-	-

Isojacareubin	Inhibition type	Non-competitive	Non-competitive
(18)	K_i (μM)	72.6	74.36
	K_i' (μM)	-	-

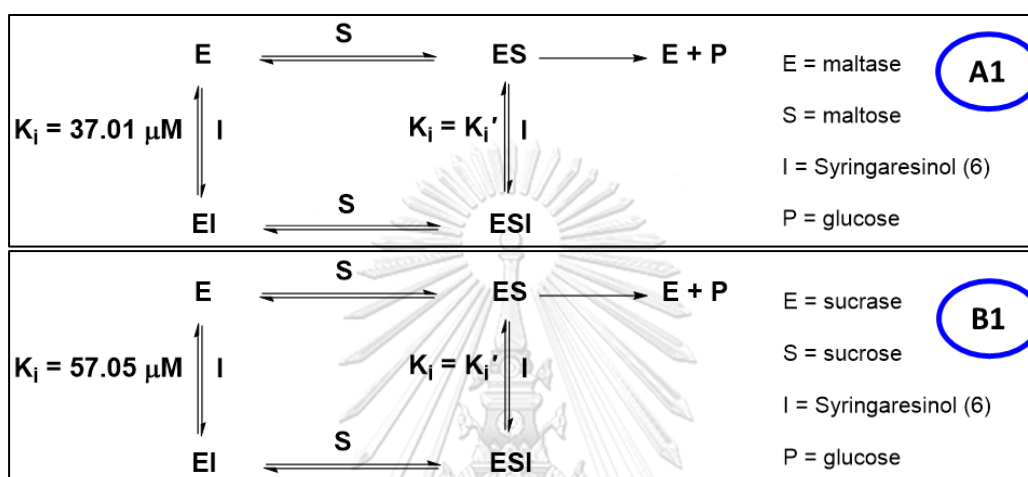


Figure 3.22 Putative mechanism pathway of syringaresinol (6) for non-competitive inhibition (A1, B1) against maltase and sucrase

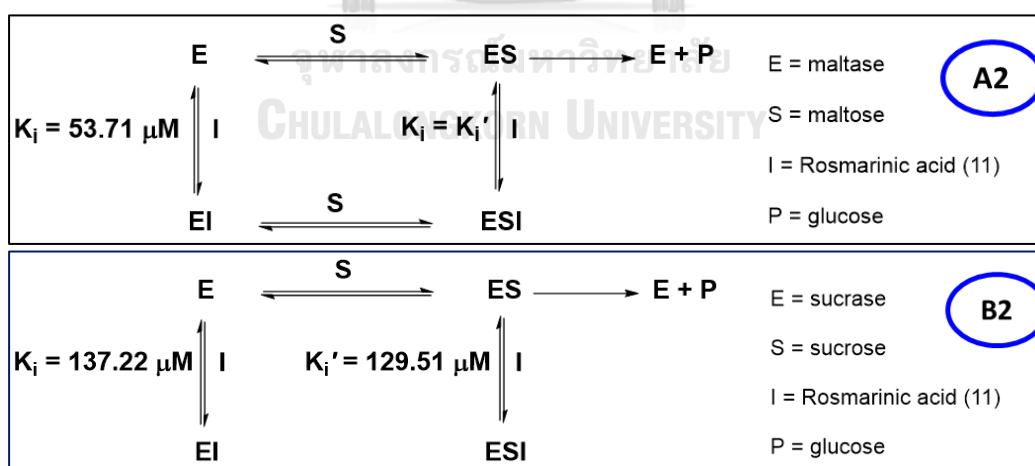


Figure 3.23 Putative mechanism pathway of rosmarinic acid (11) for non-competitive

(A2) and mixed (B2) inhibition against maltase and sucrase

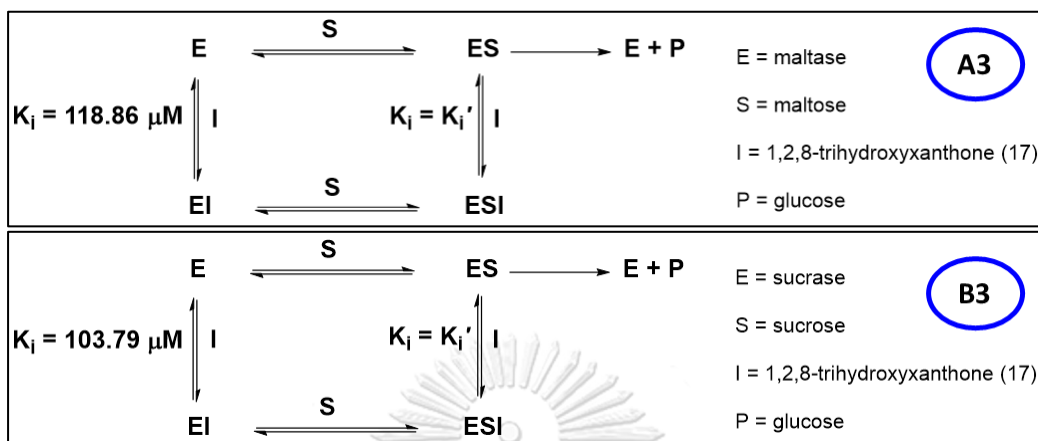


Figure 3.24 Putative mechanism pathway of 1,2,8-trihydroxyxanthone (17) for non-competitive inhibition (A3, B3) against maltase and sucrase

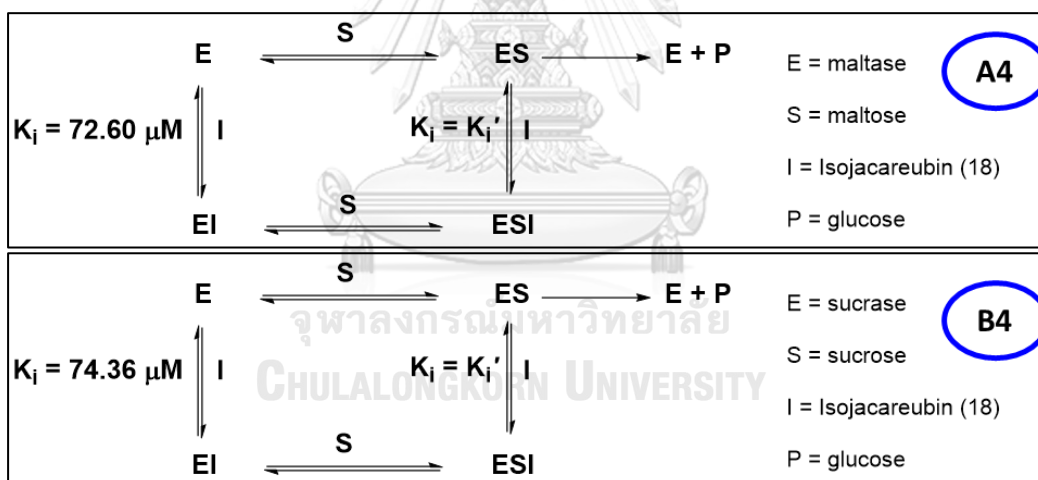


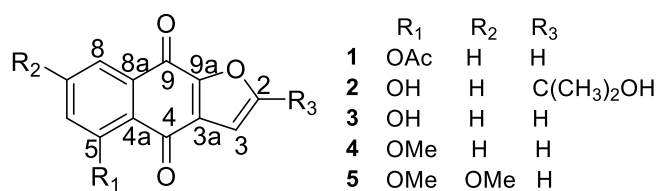
Figure 3.25 Putative mechanism pathway of isojacareubin (18) for non-competitive inhibition (A4, B4) against maltase and sucrase

Chapter 4

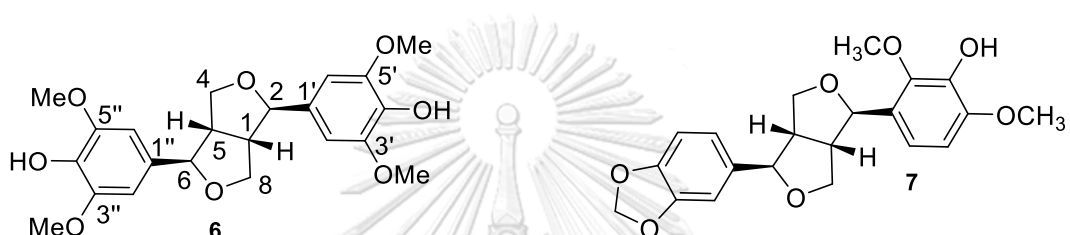
Conclusions

This research is the first identification of α -glucosidase inhibitors from the stem of *Thunbergia laurifolia*. Based on α -glucosidase inhibition guided, one new compound named 5-acetoxynaphthoquinone (1) was isolated, together nineteen known compounds including, 5-hydroxyisopropynaphtho[2,3-b]furan-4,9quinone (2), 5-hydroxynaphtho[2,3-b]furan-4,9quinone (3), 5-methoxynaphtho[2,3-b]furan-4,9quinone (4), 5,7-dimethoxynaphtho[2,3-b]furan-4,9quinone (5), syringaresinol (6), lignan α -7a (7), caffeic acid (8), ferulic acid (9), 3',4'-methylenedioxybenzoic acid (10), rosmarinic acid (11), 1-hydroxy-7-methoxyxanthone (12), euxanthone (13), 1,7-dimethoxyxanthone (14), 1,2-dimethoxy-8-hydroxyxanthone (15), 2,8-dihydroxy-1-methoxyxanthone (16), 1,2,8-trihydroxyxanthone (17), cytidine (19), isojacareubin (18), thunbergioside (20). In addition, this is a comprehensive work on phytochemical study of *T. laurifolia*. Five different classes of natural products, namely furanonaphthoquinone, furofuran lignan, phenyl propanoid, xanthone and iridoid were isolated. Furthermore, furanonaphthoquinone, furofuran lignan, and xanthone were isolated for the first time in this genus. This information would fulfil phytochemical study of this plant, in which iridoid has been recognized as a representative metabolite. In addition to rosmarinic acid (11) that has been reported as a sole bioactive inhibitor, compounds 6, 17, and 18 were also discovered as equivalent inhibitors in this work.

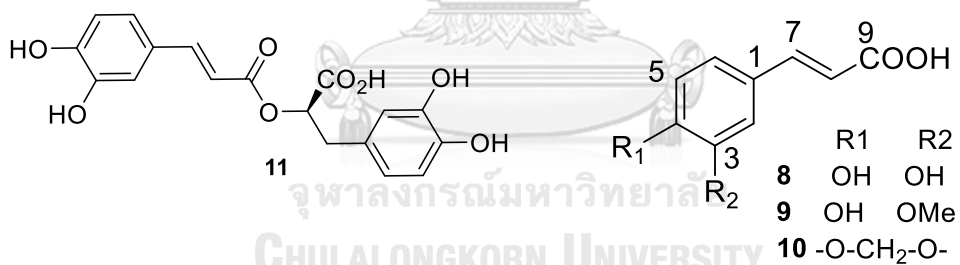
● Furanonaphthoquinone



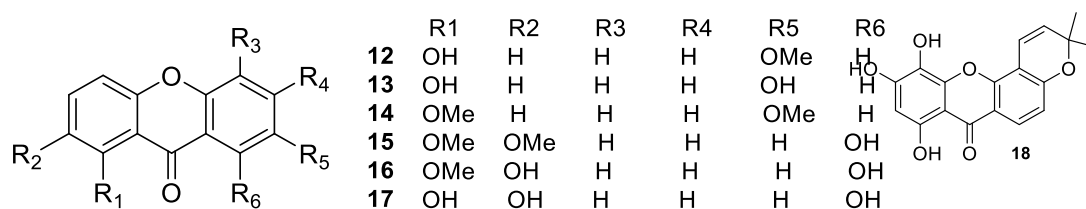
● Furofuran lignan



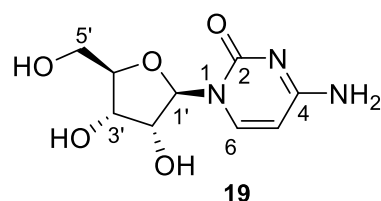
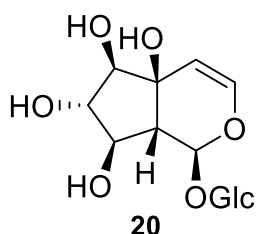
● Phenyl propanoid



● Xanthone



- Iridoid and another skeleton



All isolated compounds were evaluated for the α -glucosidase inhibition. syringaresinol (**6**), rosmarinic acid (**11**), 1,2,8-trihydroxyxanthone (**17**), and isojacareubin (**18**) showed highest activity among isolated compounds. Although they were catabolised into different classes, they were similar to each other in the presence of phenolic moiety. It is likely that α -glucosidase inhibitory potency increases according to the number of free phenolic group on the aromatic ring. The kinetic study of the most active compounds indicated that syringaresinol (**6**), 1,2,8-trihydroxyxanthone (**17**), and isojacareubin (**18**) showed the non-competitive mechanism against maltase and sucrase whereas rosmarinic acid (**11**) showed the non-competitive mechanism against maltase and mixed mechanism against sucrase.

This investigation has disclosed that *Thunbergia laurifolia* had the potential to provide medicinal compounds. Therefore, it is necessary to continue to isolate more compounds and evaluate their biological activities for applying on medicinal fields. Notably, syringaresinol (**6**), rosmarinic acid (**11**), 1,2,8-trihydroxyxanthone (**17**), and isojacareubin (**18**) revealed the potent candidates for α -glucosidase inhibitory

activity, thus the further studies such as molecular docking could be investigated. Furthermore, synthesis of their derivatives is one of the excellent directions to enhance the potential activity of natural products.



APPENDIX

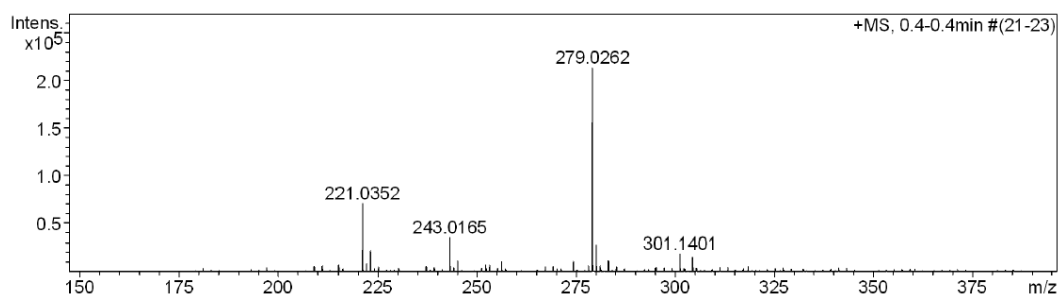
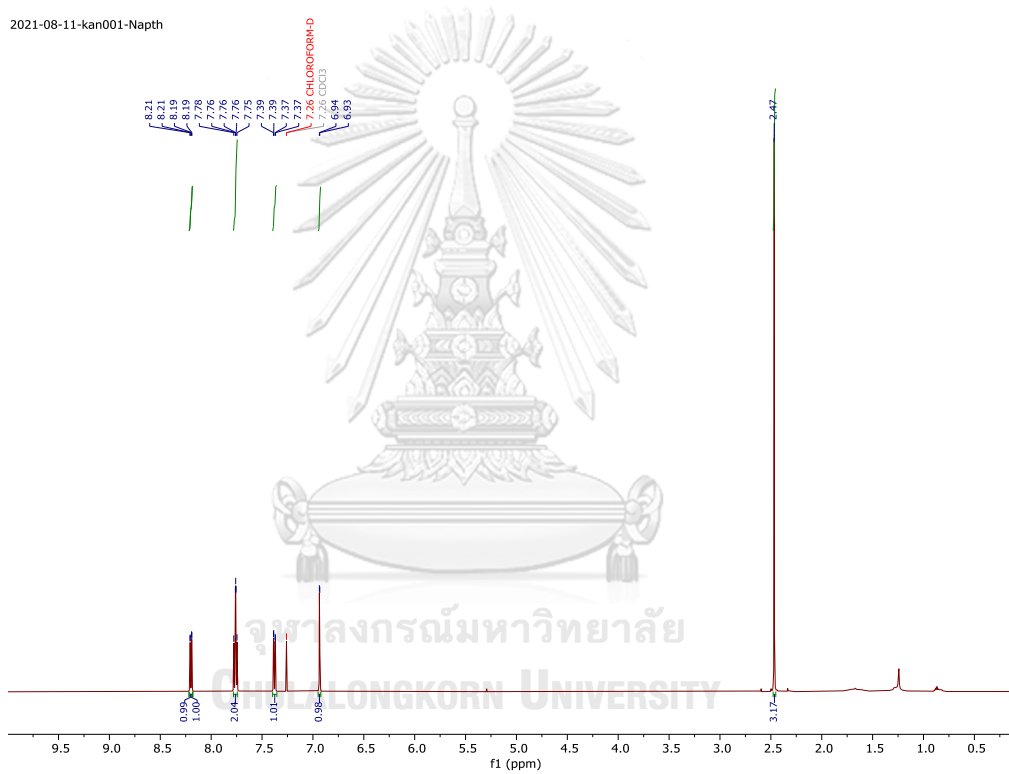


Figure S1 HR-ESI-MS spectrum of furanonaphthoquinone (1)

Figure S2 The ¹H-NMR spectrum of furanonaphthoquinone (1) in Chloroform-d

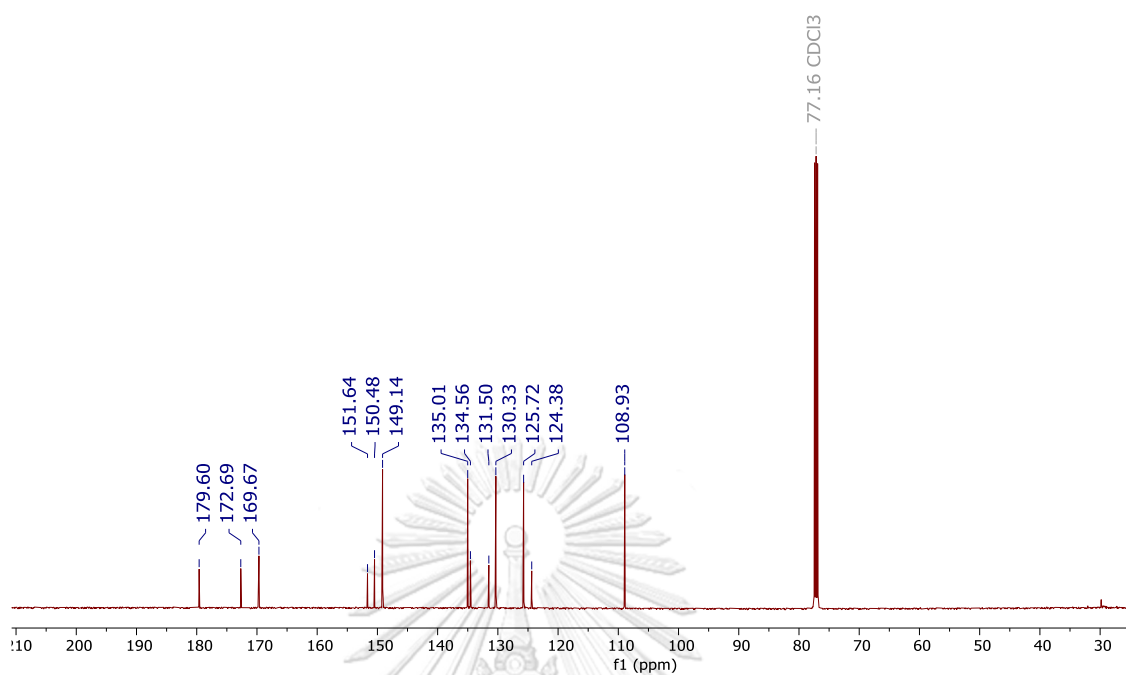


Figure S3 The ^{13}C -NMR spectrum of furanonaphthoquinone (**1**) in Chloroform-*d*

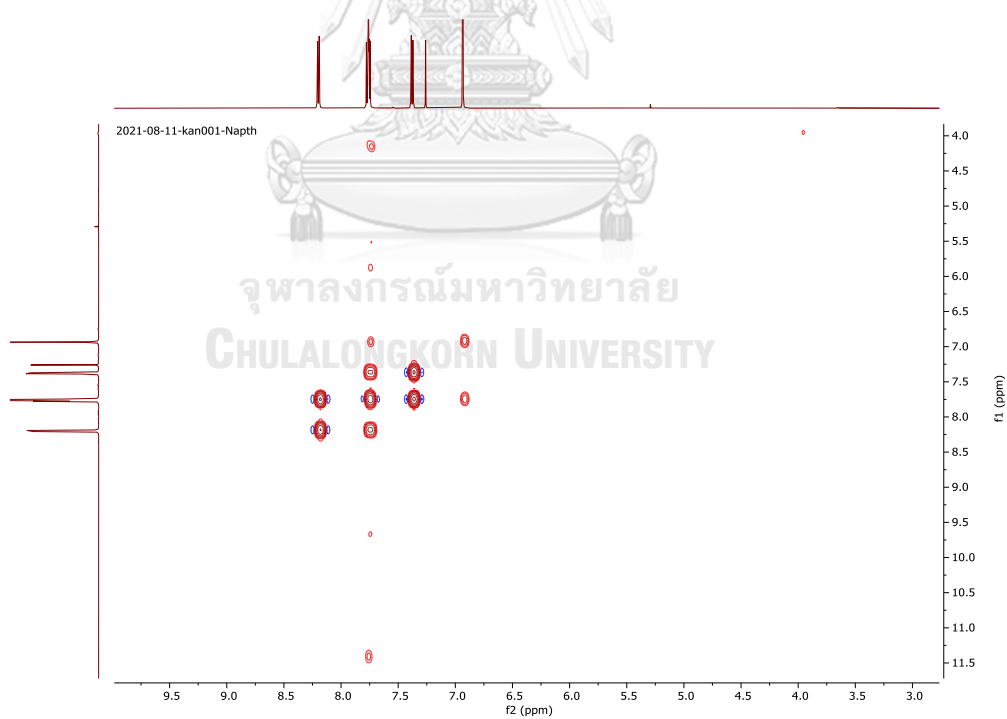


Figure S4 The COSY spectrum of furanonaphthoquinone (**1**) in Chloroform-*d*

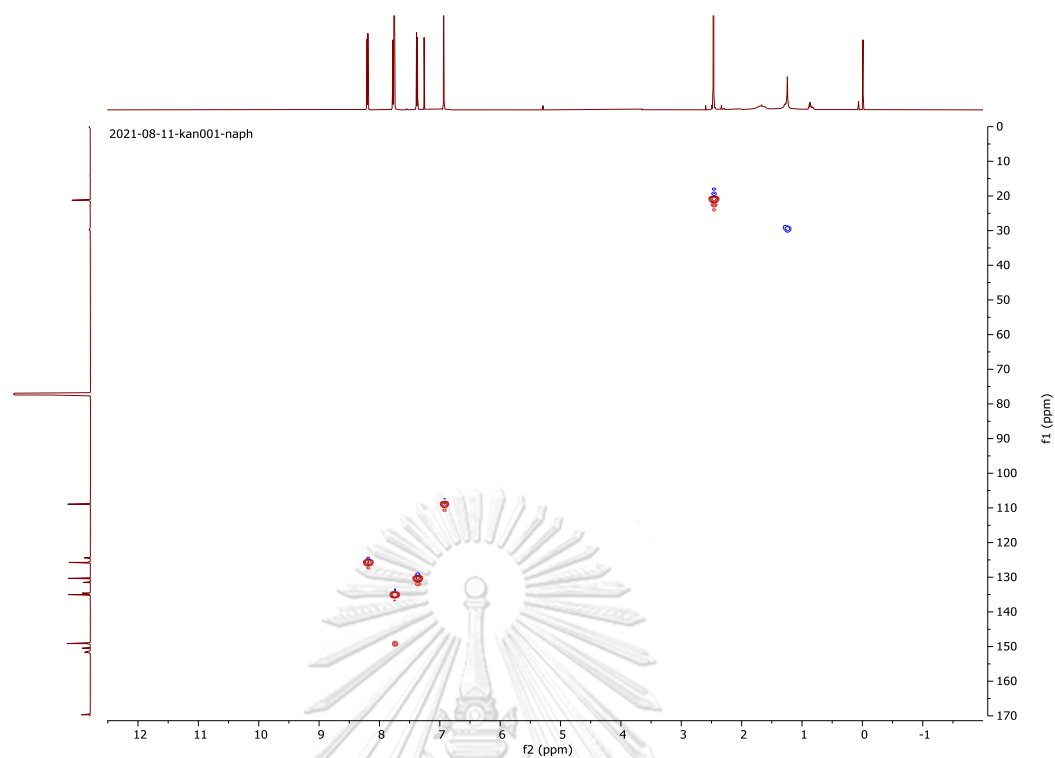


Figure S5 The HSQC spectrum of furanonaphthoquinone (**1**) in Chloroform-*d*

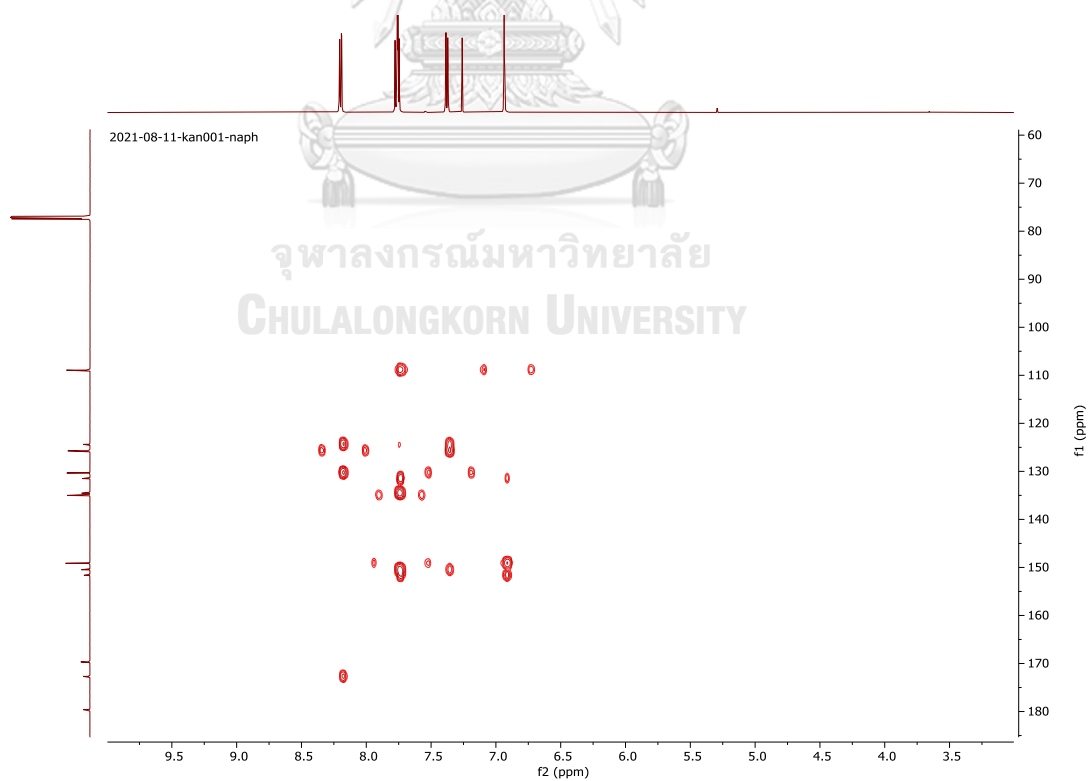


Figure S6 The HMBC spectrum of furanonaphthoquinone (**1**) in Chloroform-*d*

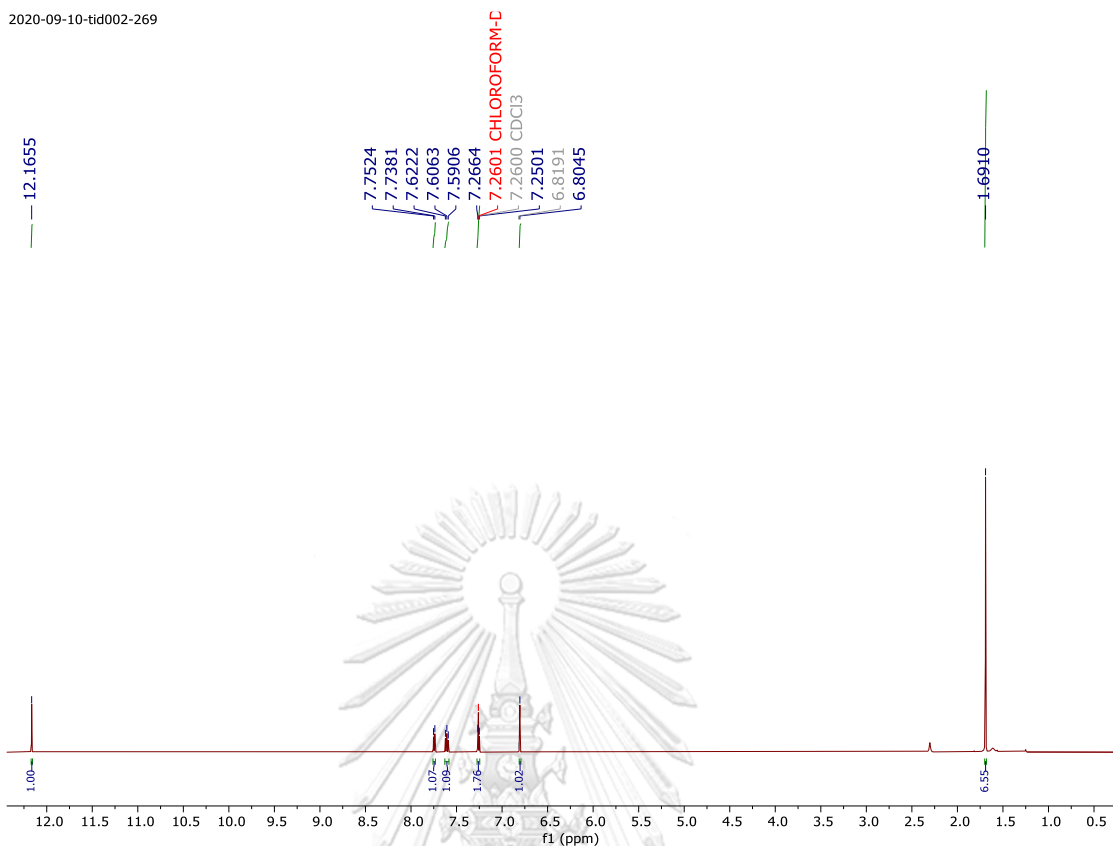


Figure S7 The ^1H -NMR spectrum of compound (2) in Chloroform-*d*

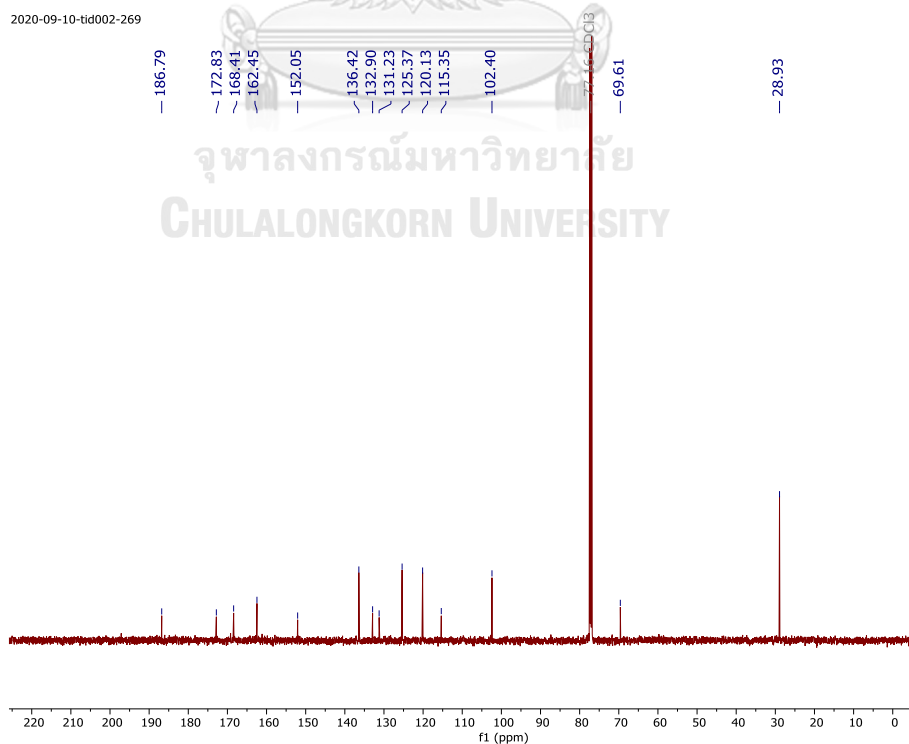


Figure S8 The ^{13}C -NMR spectrum of compound (2) in Chloroform-*d*

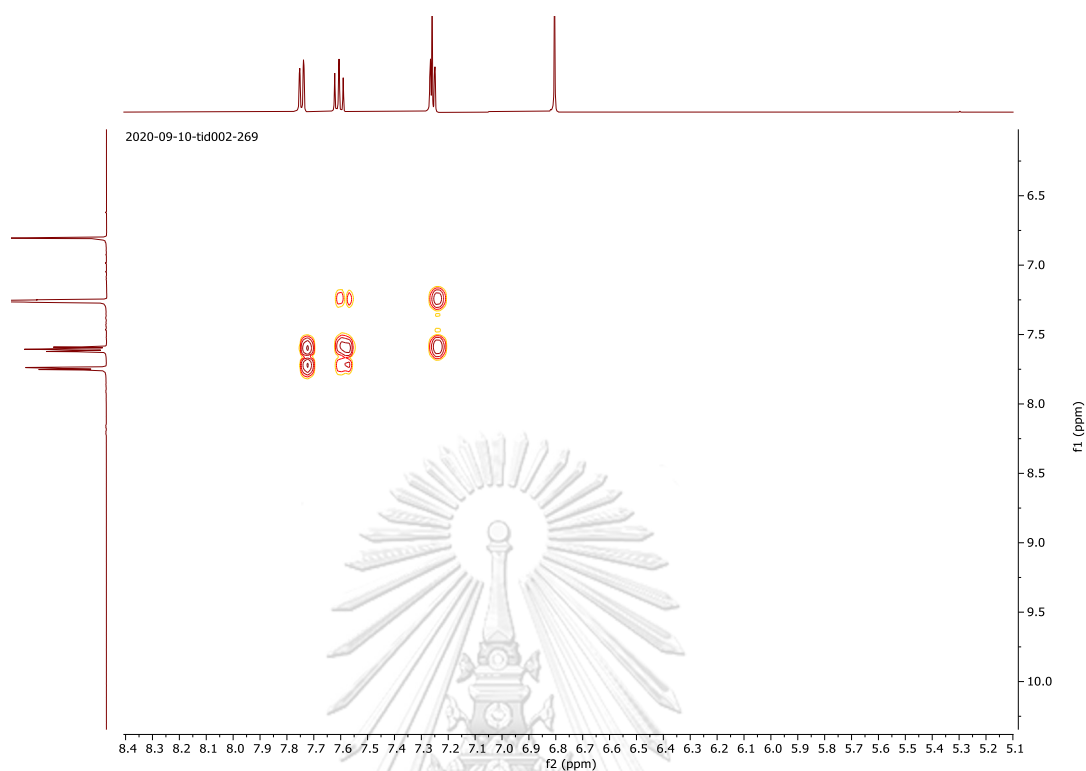


Figure S9 The COSY spectrum of compound (2) in Chloroform-*d*

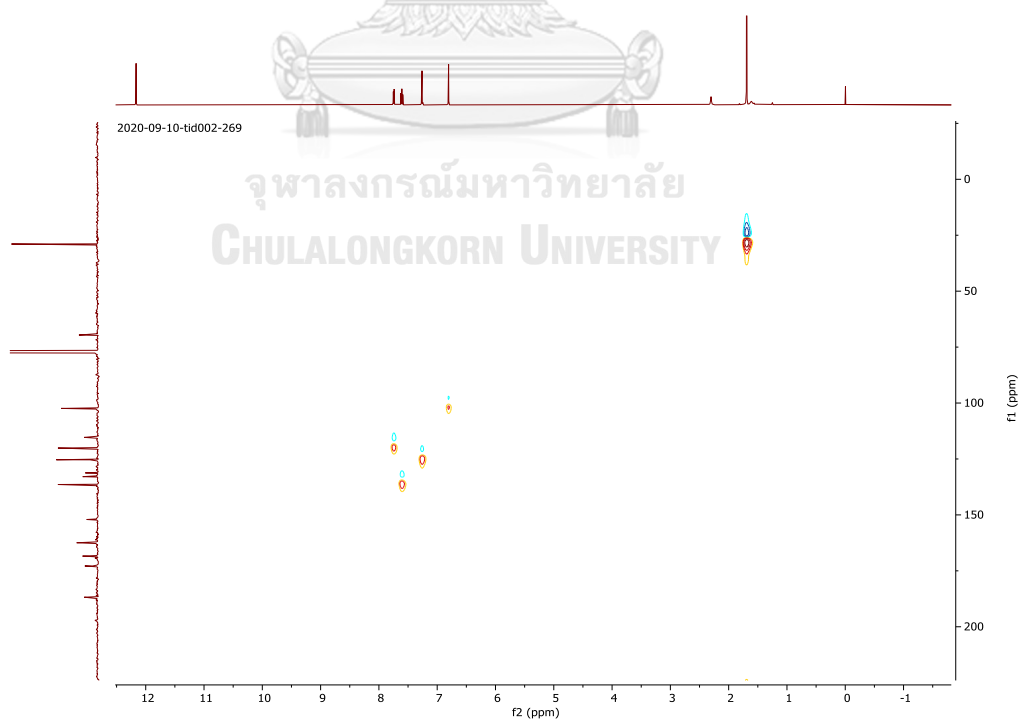


Figure S10 The HSQC spectrum of compound (2) in Chloroform-*d*

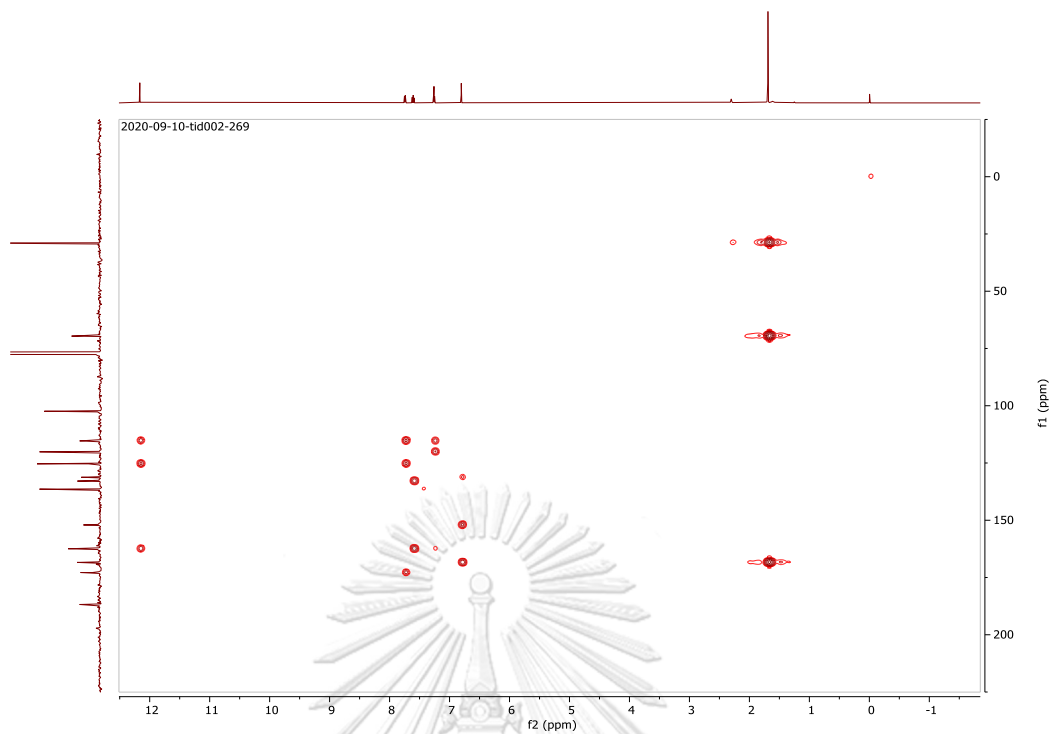


Figure S11 The HMBC spectrum of compound (2) in Chloroform-*d*

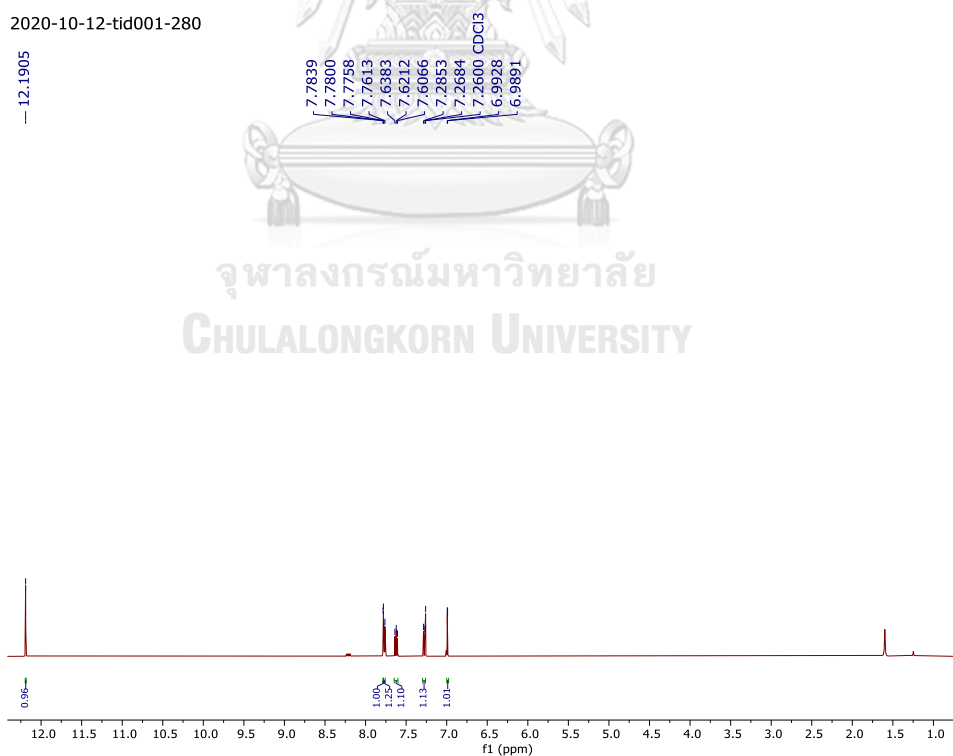


Figure S12 The ¹H-NMR spectrum of compound (3) in Chloroform-*d*

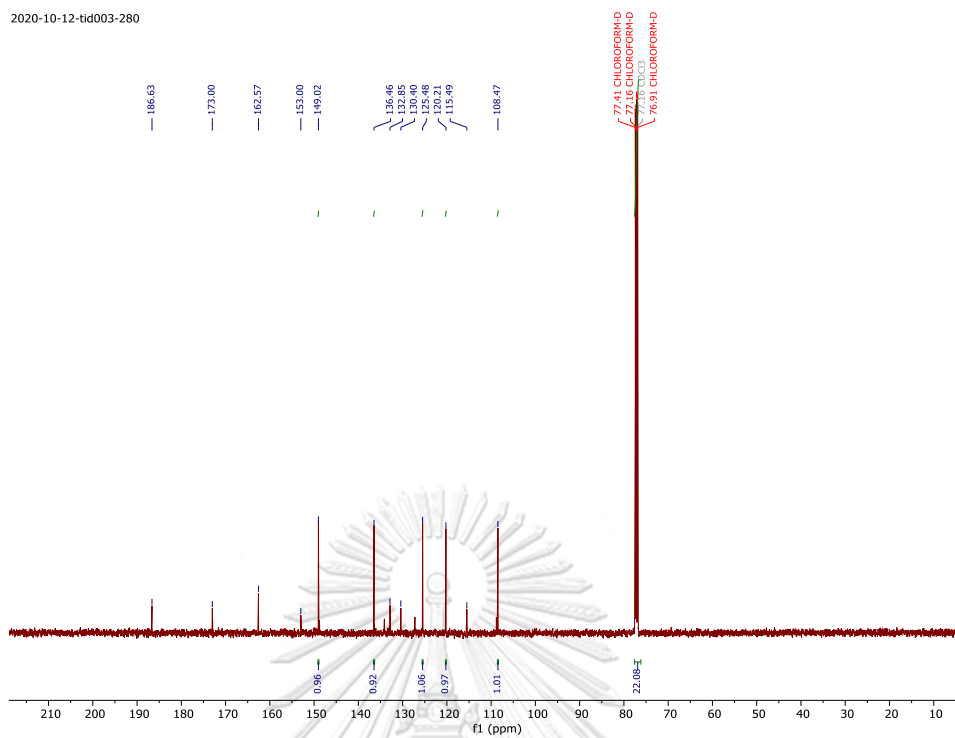


Figure S13 The ^{13}C -NMR spectrum of compound (3) in Chloroform-*d*

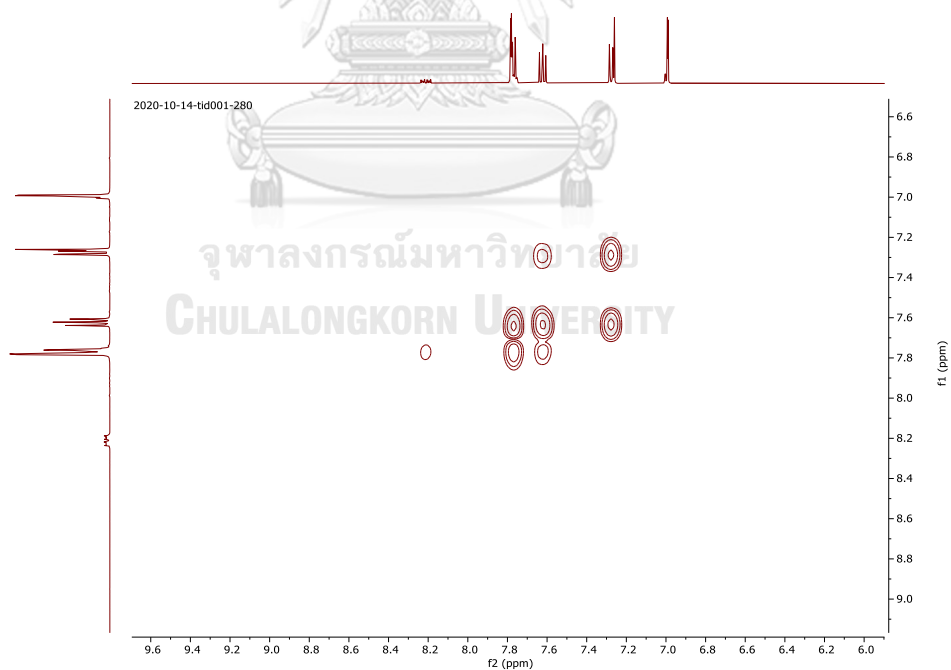


Figure S14 The COSY spectrum of compound (3) in Chloroform-*d*

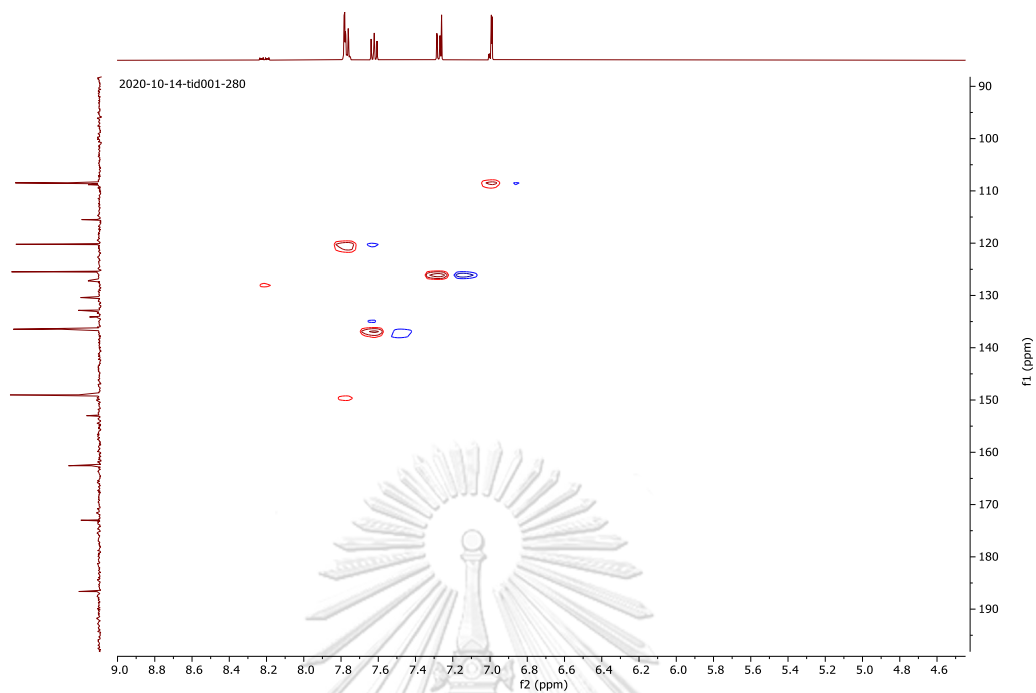


Figure S15 The HSQC spectrum of compound (3) in Chloroform-*d*

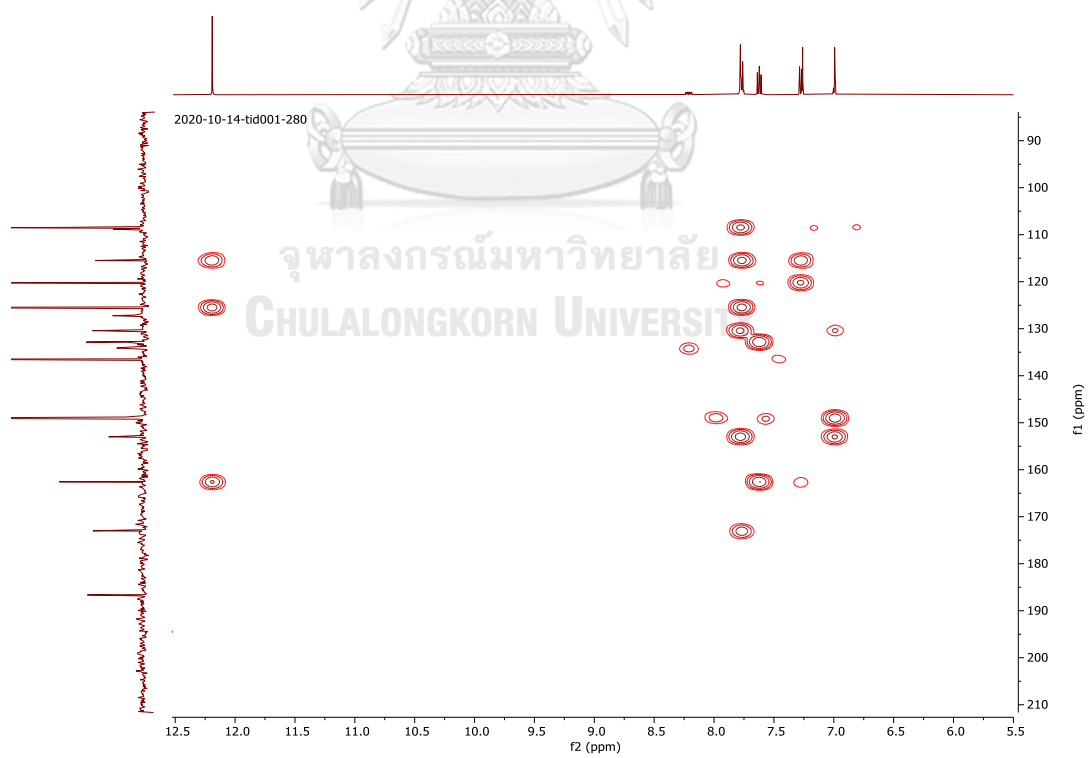
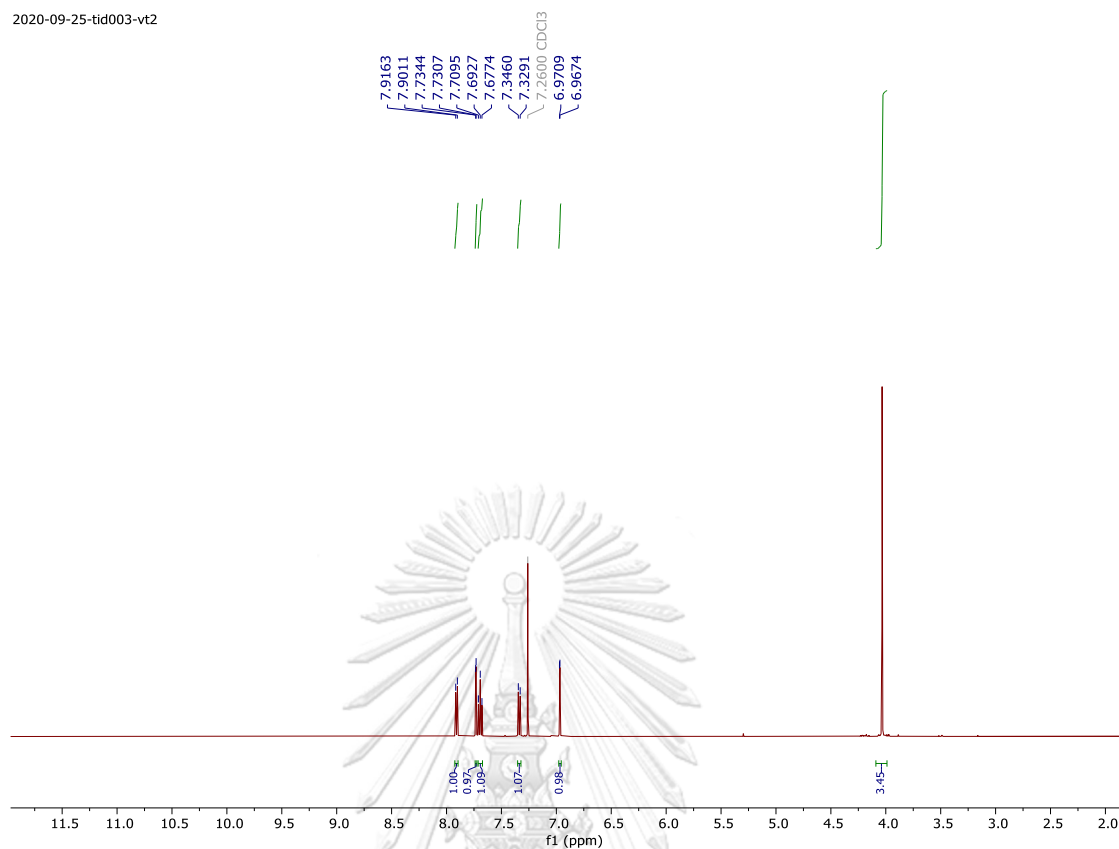
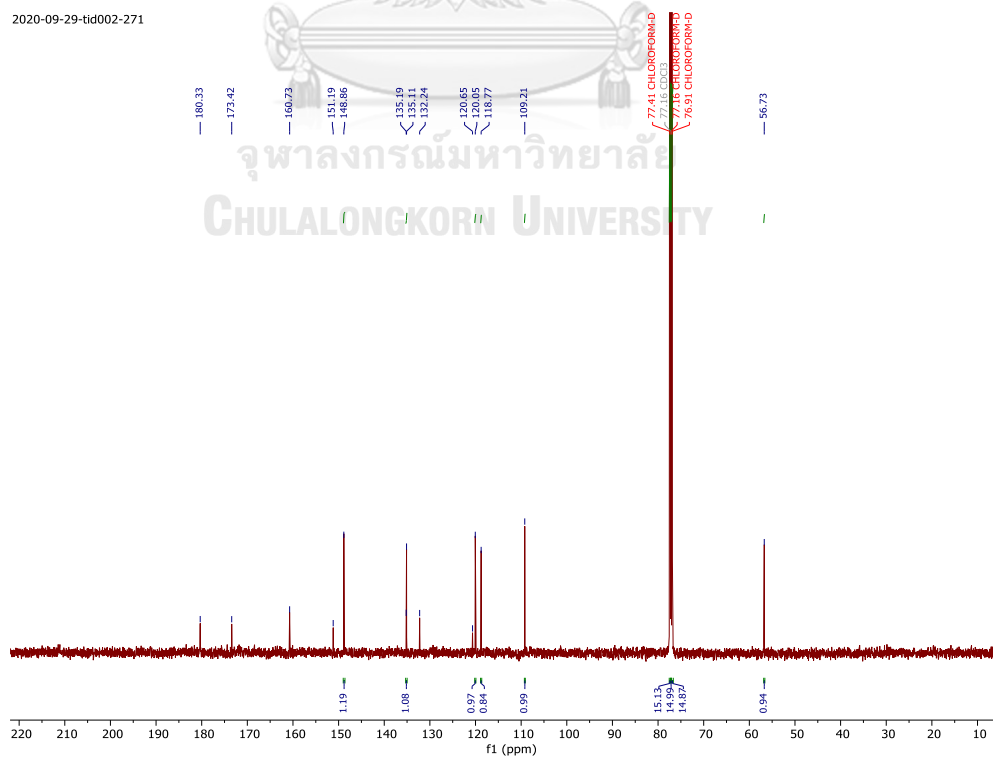


Figure S16 The HMBC spectrum of compound (3) in Chloroform-*d*

2020-09-25-tid003-vt2

Figure S17 The ^1H -NMR spectrum of compound (4) in Chloroform-*d*

2020-09-29-tid002-271

Figure S18. The ^{13}C -NMR spectrum of compound (4) in Chloroform-*d*

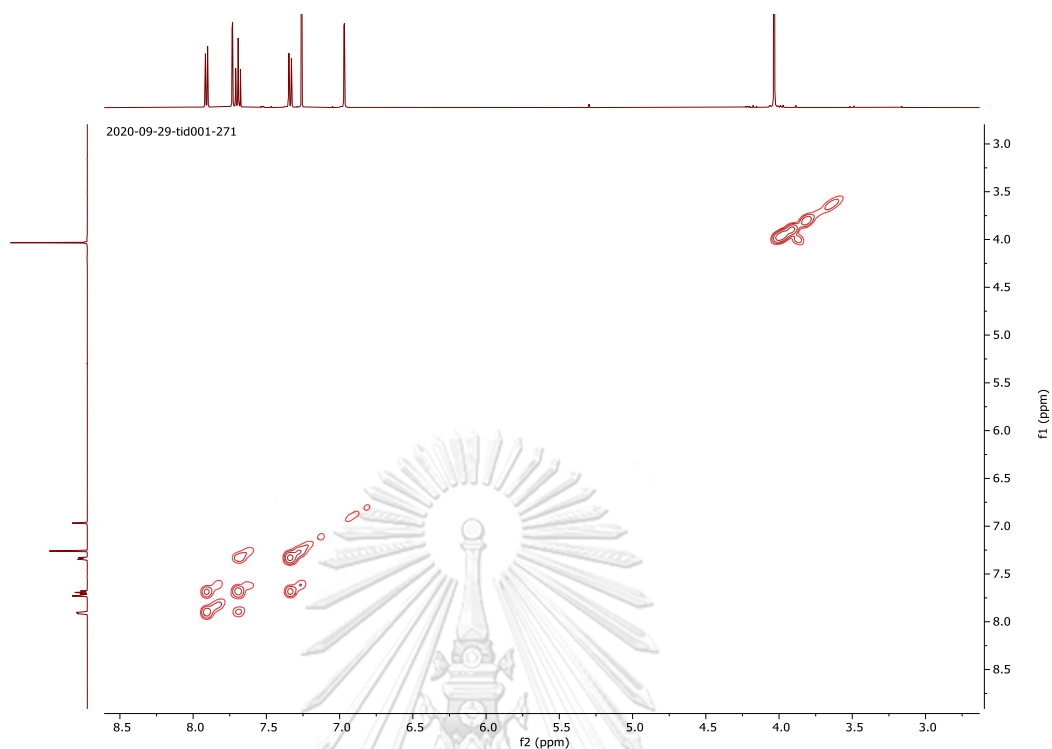


Figure S19 The COSY spectrum of compound (4) in Chloroform-*d*

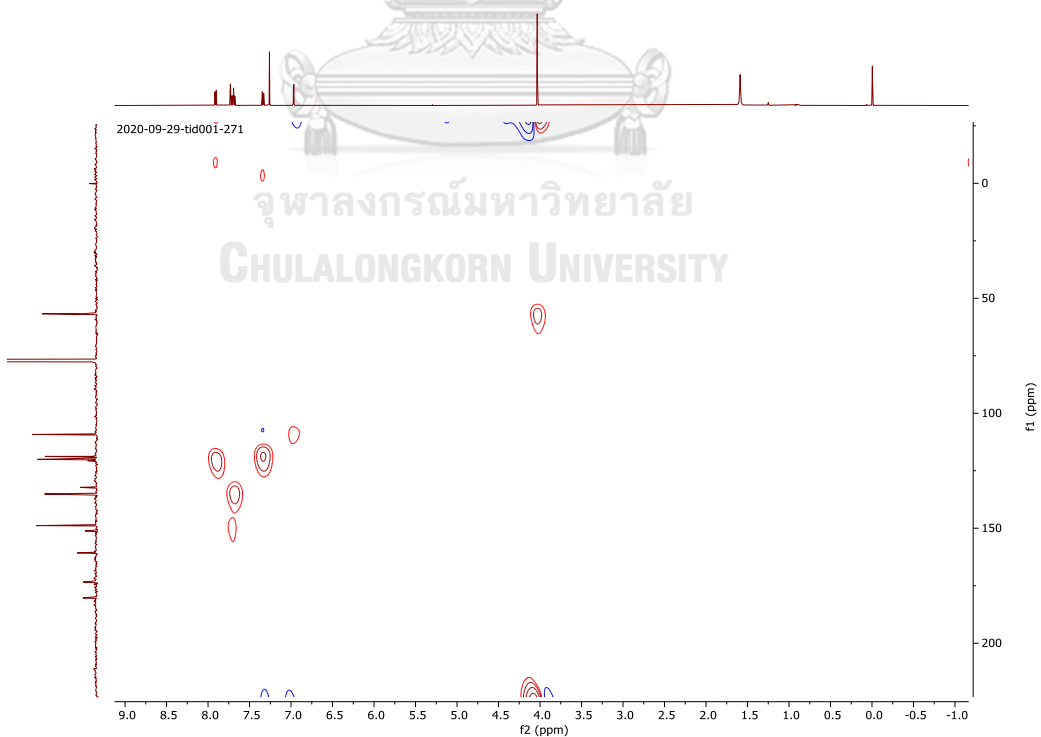


Figure S20 The HSQC spectrum of compound (4) in Chloroform-*d*

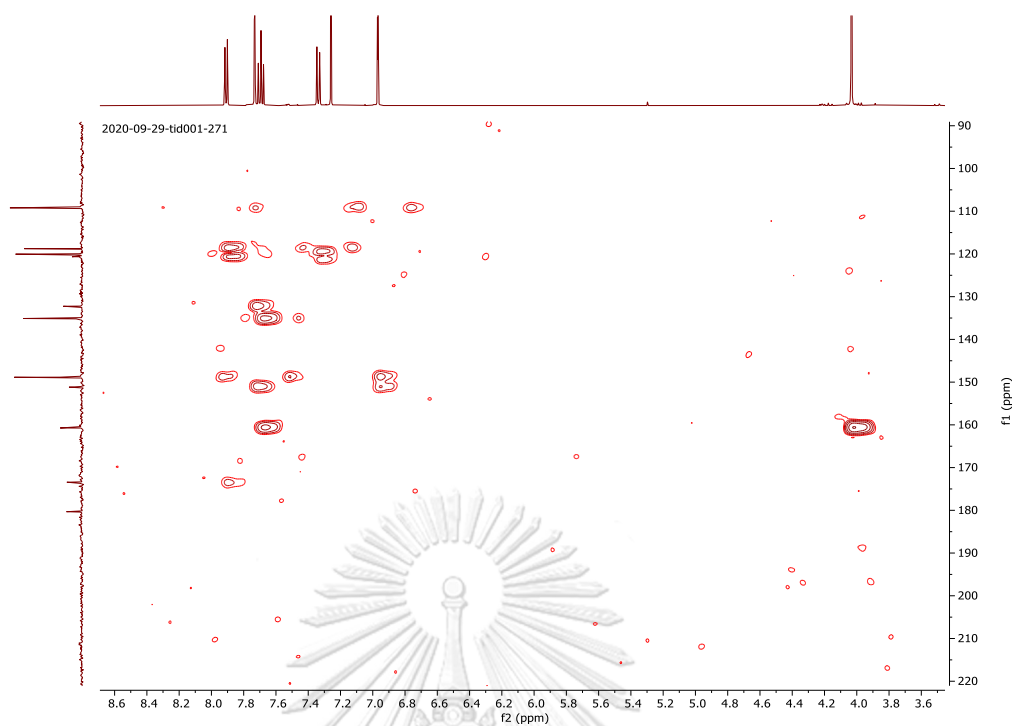


Figure S21 The HMBC spectrum of furanonaphthoquinone (**4**) in Chloroform-*d*

2020-11-16-kan004-V3T

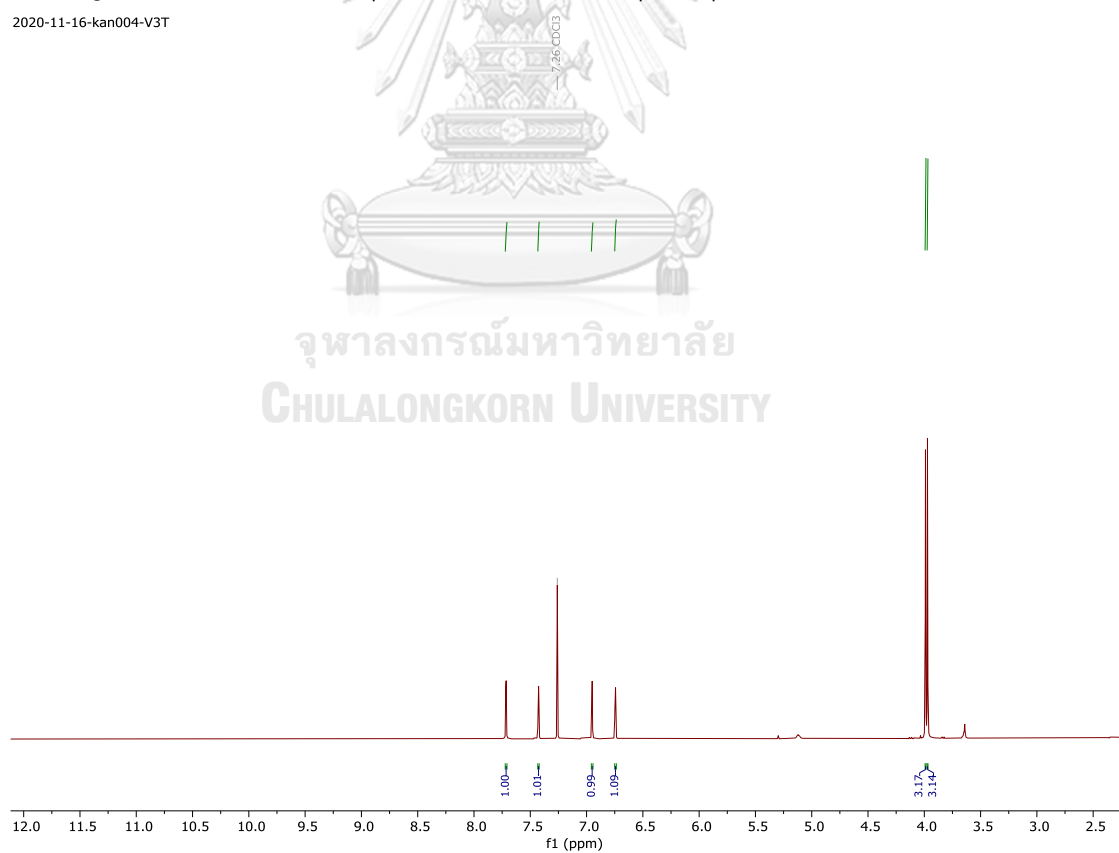


Figure S22 The ^1H -NMR spectrum of compound (**5**) in Chloroform-*d*

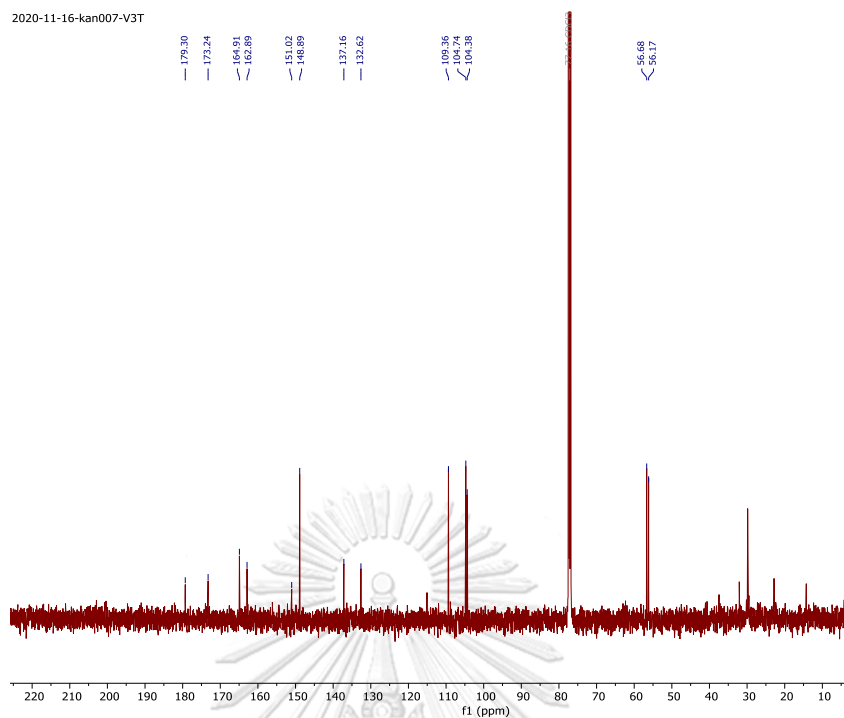


Figure S23 The ^{13}C -NMR spectrum of compound (5) in Chloroform-*d*

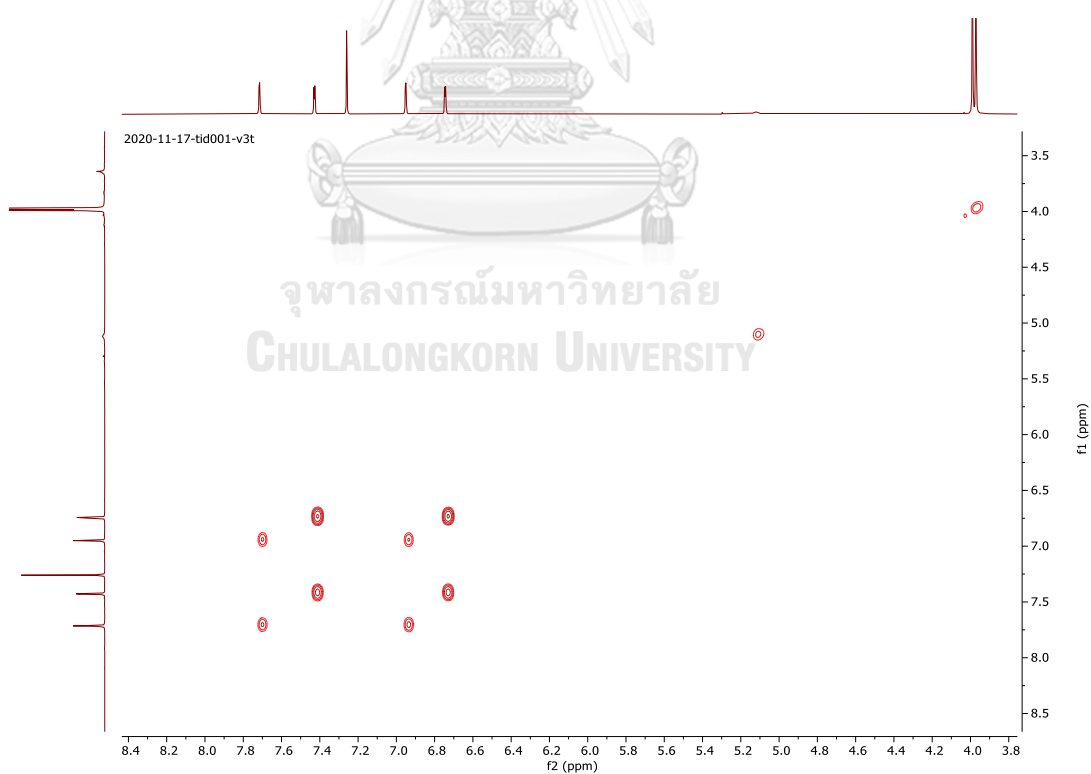


Figure S24 The COSY spectrum of compound (5) in Chloroform-*d*

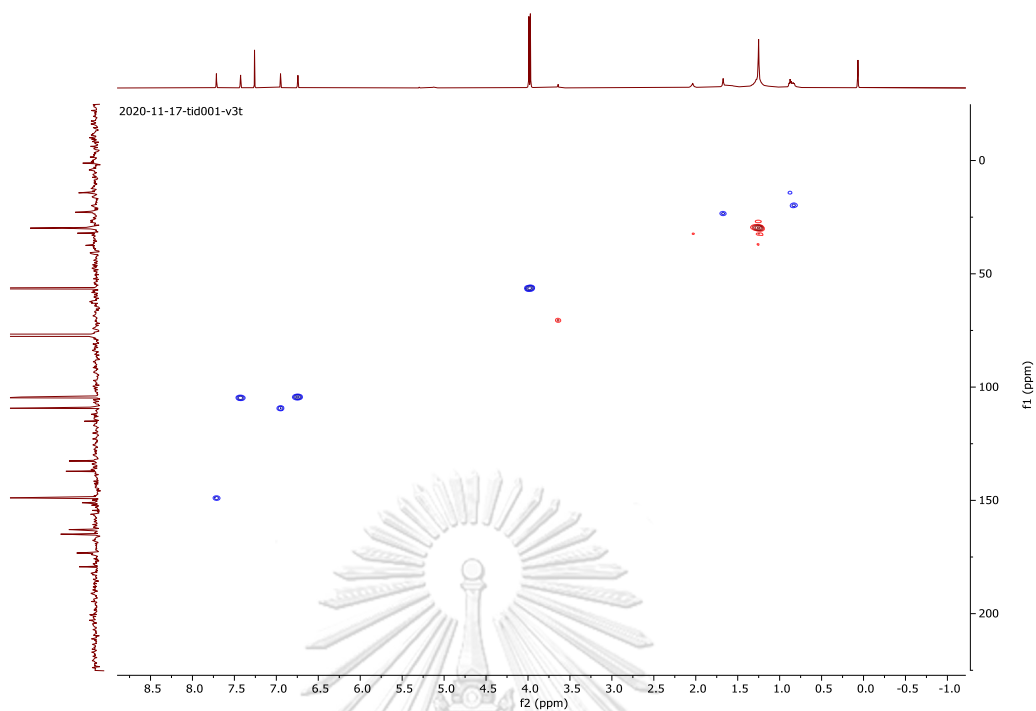


Figure S25 The HSQC spectrum of furanonaphthoquinone (5) in Chloroform-*d*

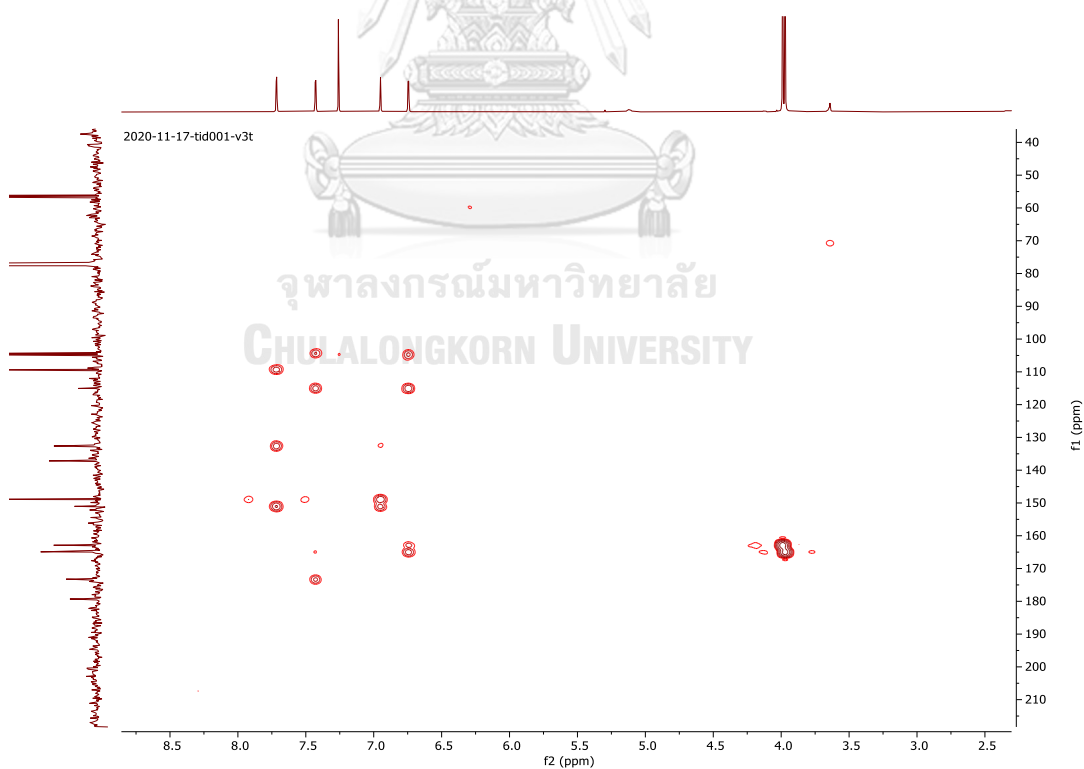


Figure S26 The HMBC spectrum of compound (5) in Chloroform-*d*

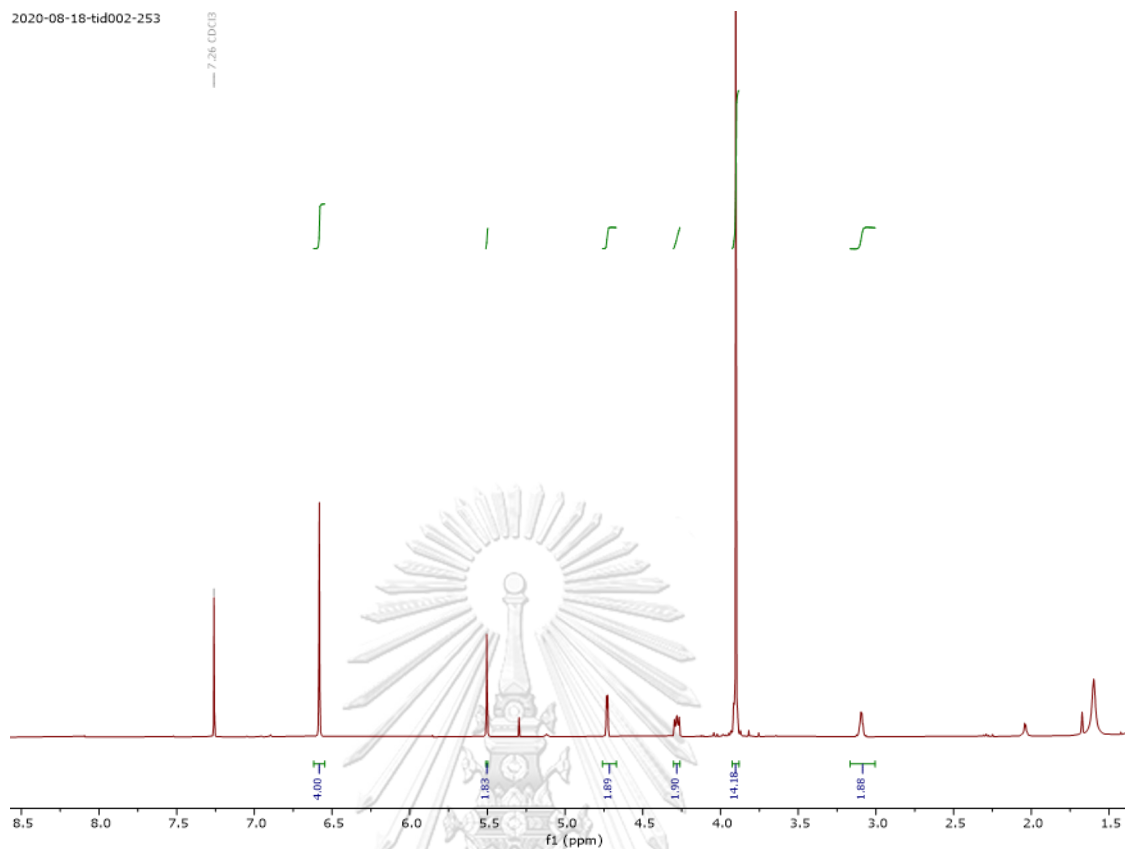


Figure S27 The ^1H -NMR spectrum of compound (6) in Chloroform-*d*

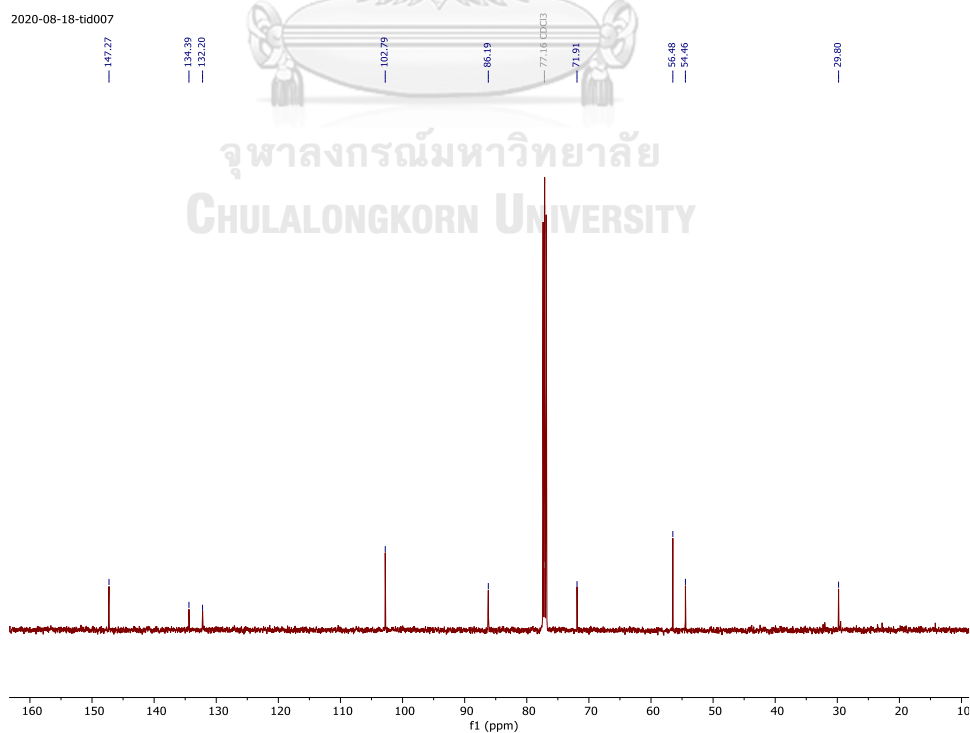


Figure S28 The ^{13}C -NMR spectrum of compound (6) in Chloroform-*d*

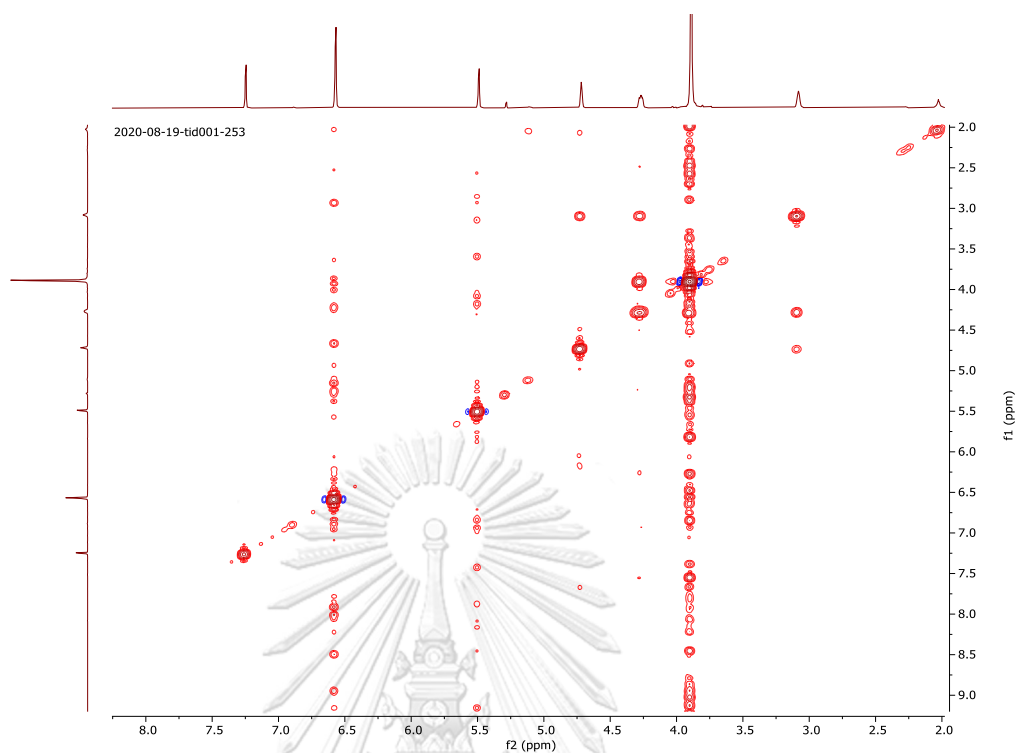


Figure S29 The COSY spectrum of compound (6) in Chloroform-*d*

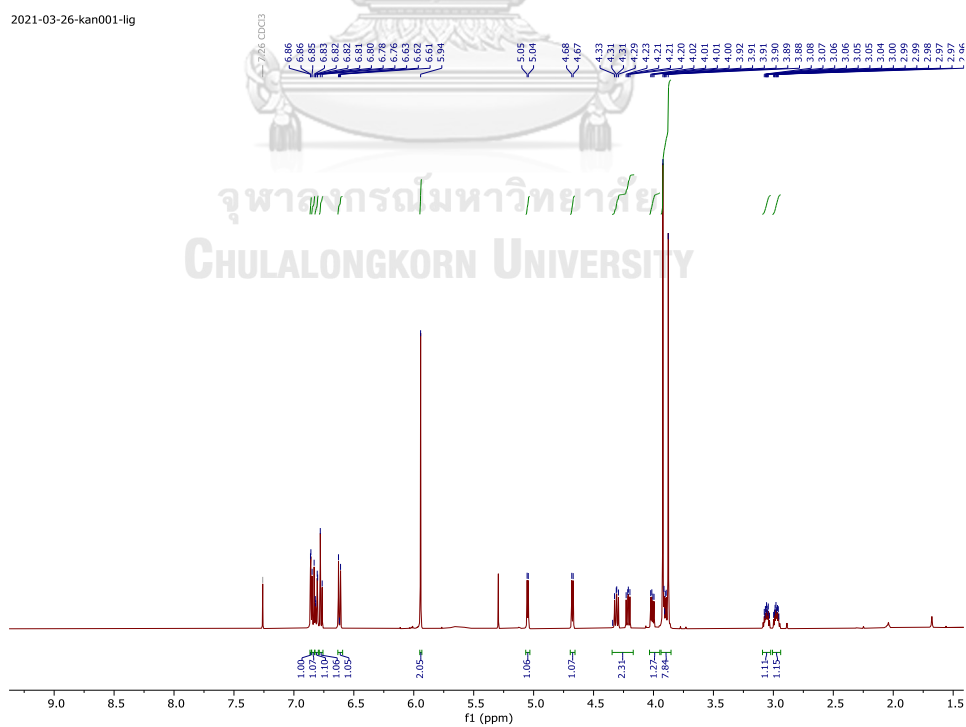


Figure S30 The ^1H -NMR spectrum of compound (7) in Chloroform-*d*

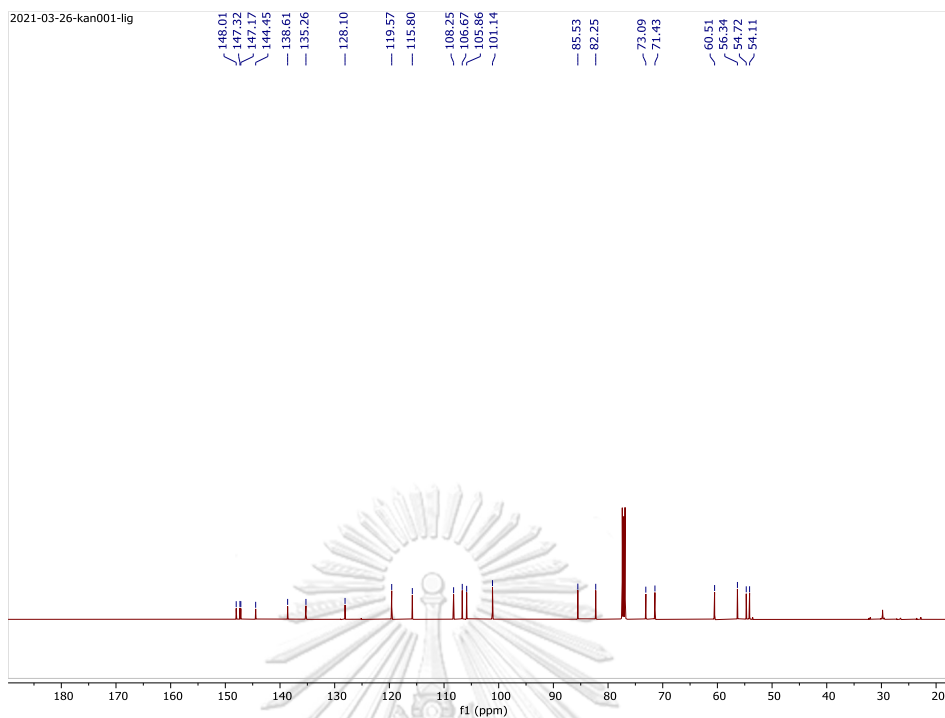


Figure S31 The ^{13}C -NMR spectrum of compound (7) in Chloroform-*d*

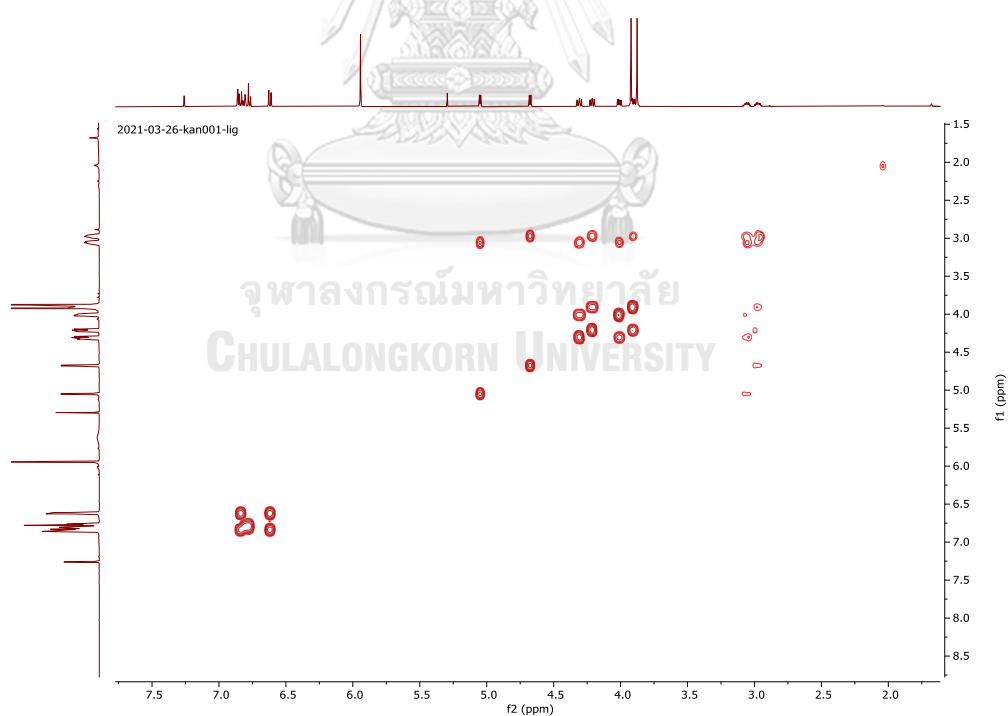


Figure S32 The COSY spectrum of compound (7) in Chloroform-*d*

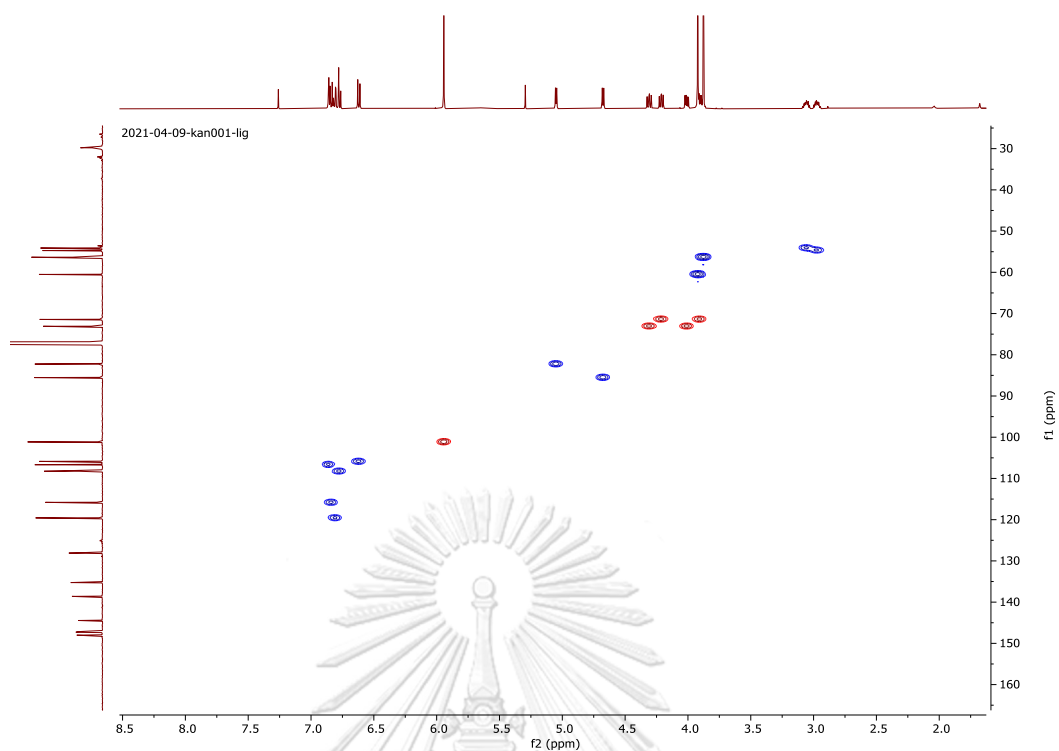


Figure S33 The HSQC spectrum of compound (7) in Chloroform-*d*

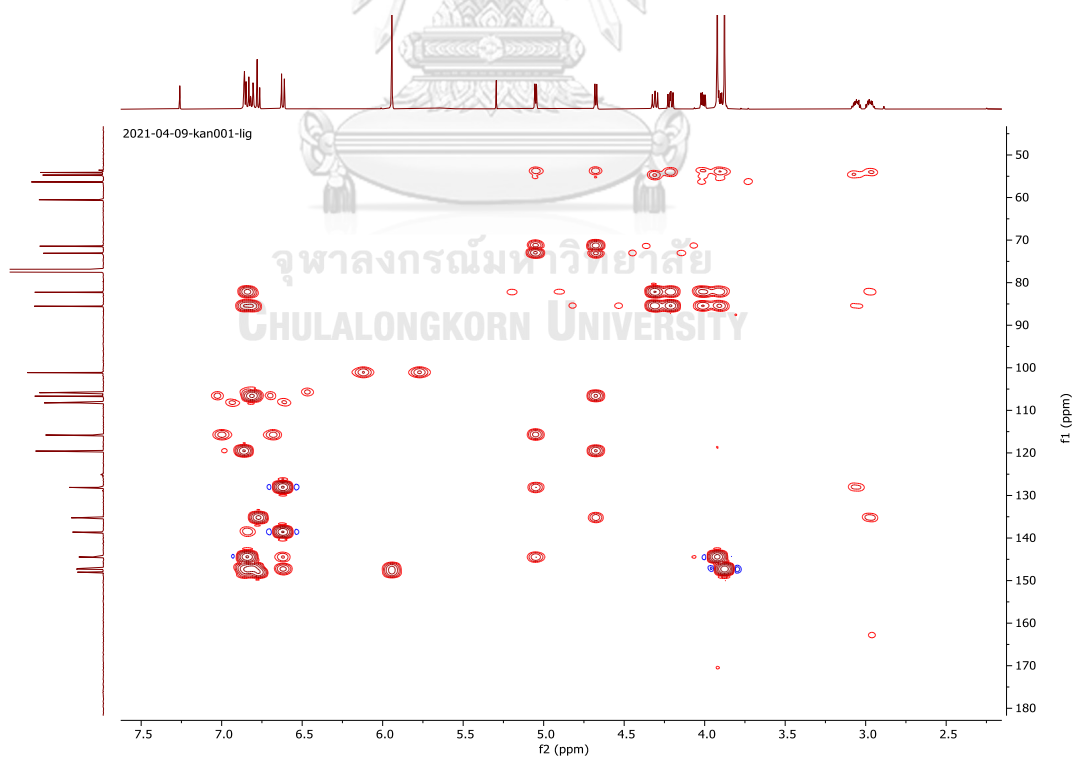


Figure S34 The HMBC spectrum of compound (7) in Chloroform-*d*

2021-02-01-kan006-Caf
single_pulse

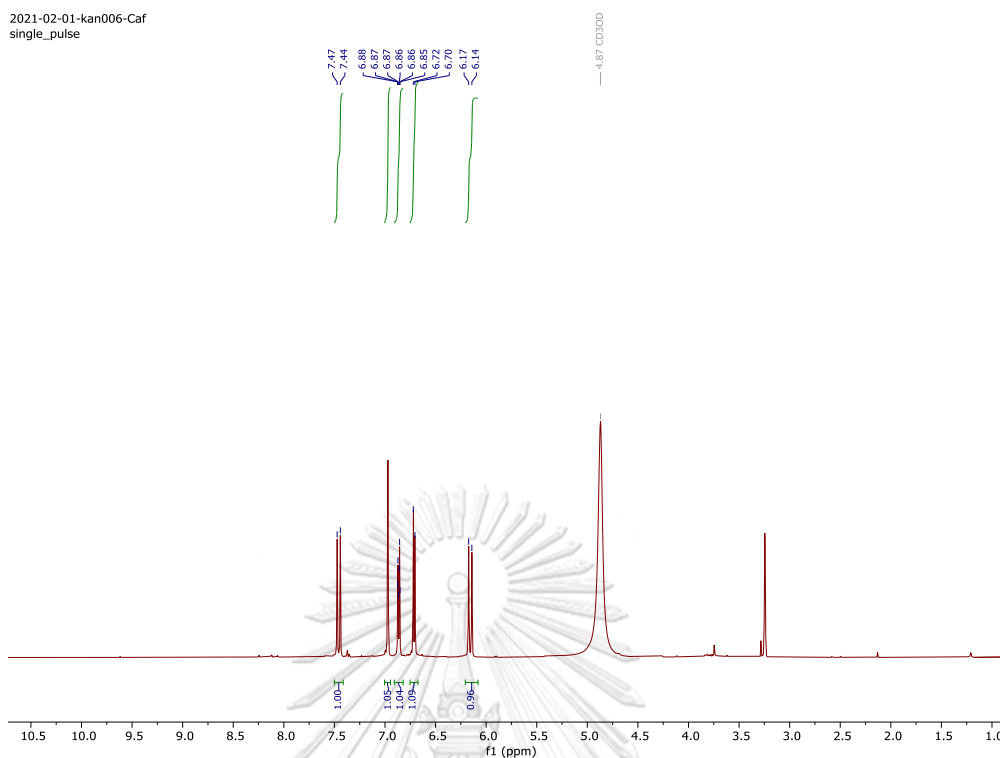


Figure S35 The ^1H -NMR spectrum of compound (8) in Methanol- d_4

2021-02-05-kan002-caf

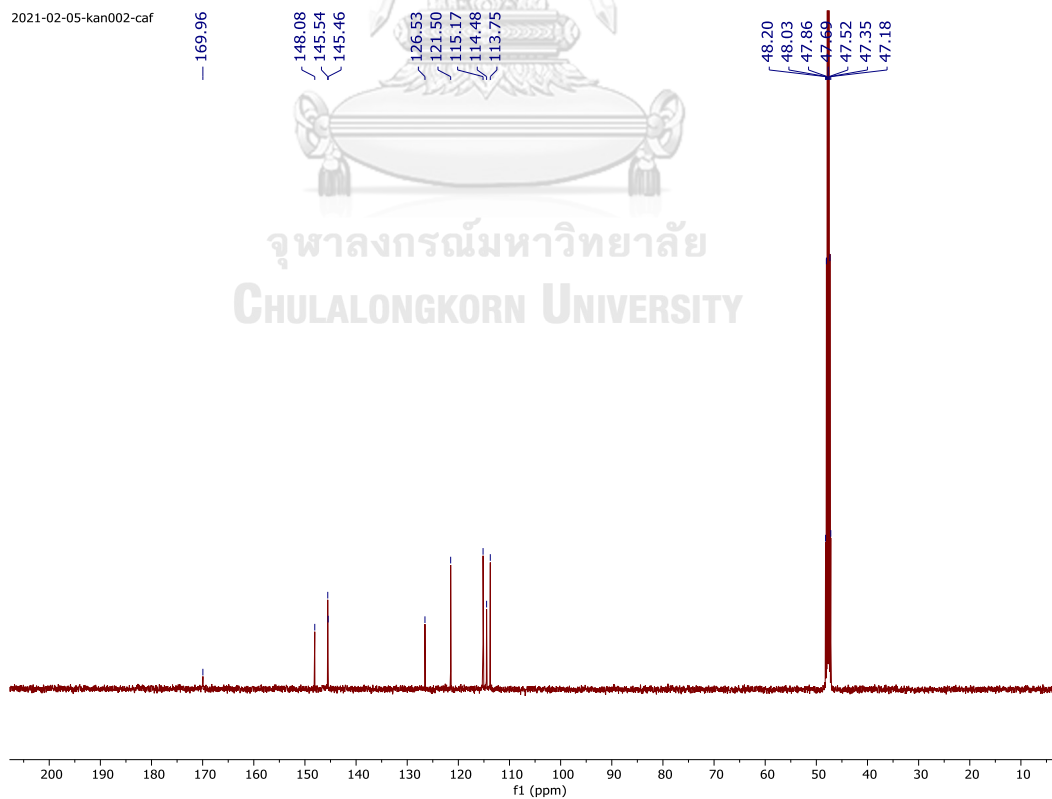


Figure S36 The ^{13}C -NMR spectrum of compound (8) in Methanol- d_4

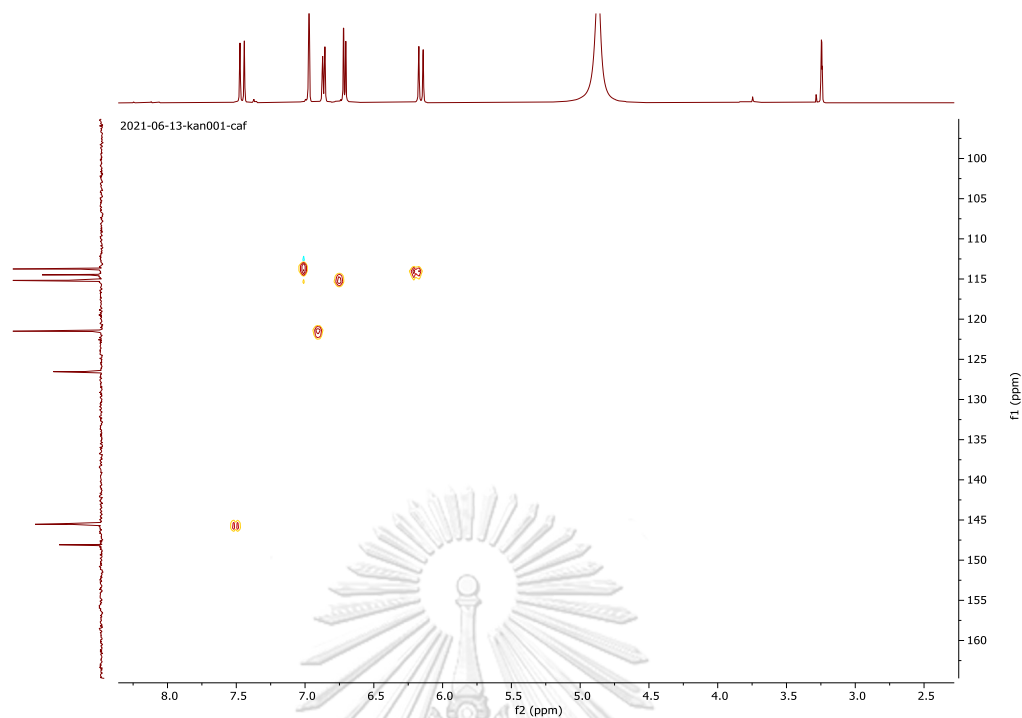


Figure S37 The HSQC spectrum of compound (8) in Methanol- d_4

2021-02-01-kan009-Fe
single_pulse

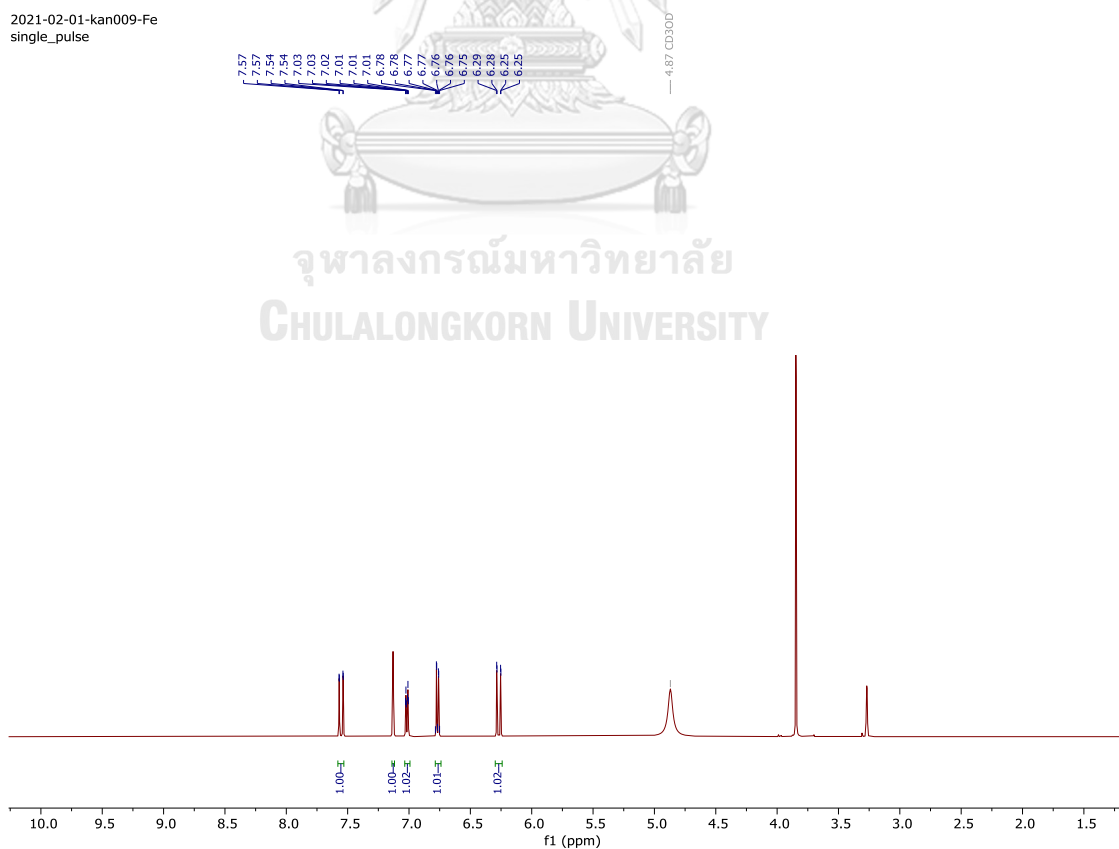


Figure S38 The ^1H -NMR spectrum of compound (9) in Methanol- d_4

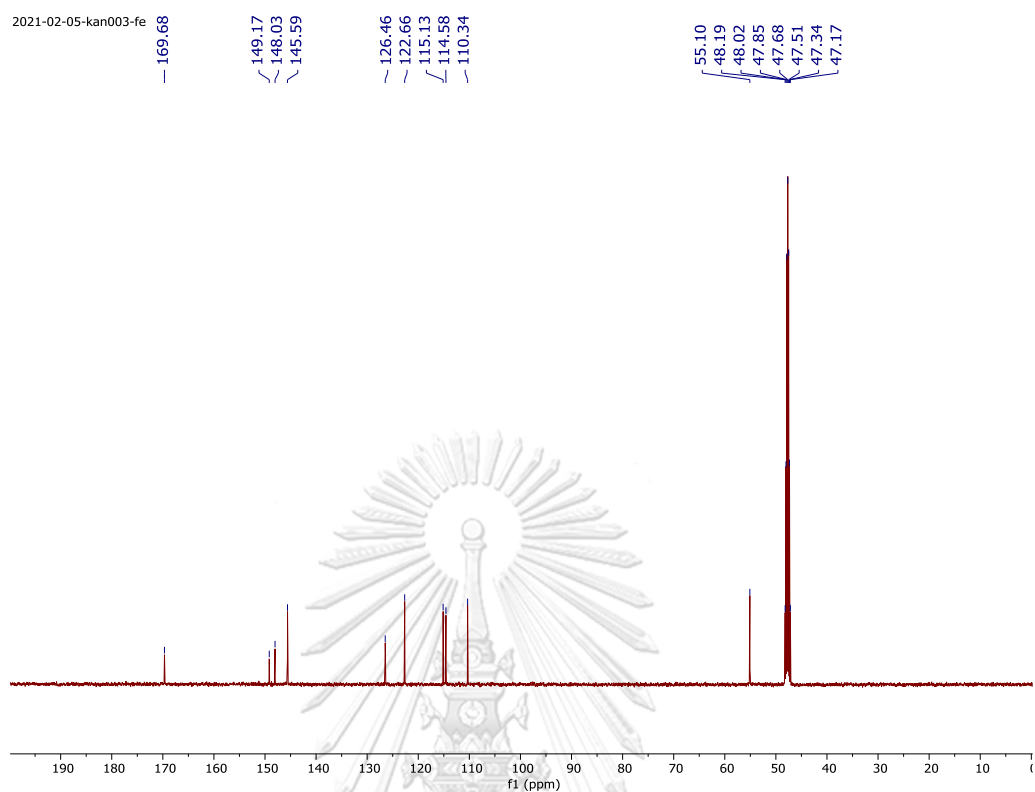


Figure S39 ^{13}C -NMR spectrum of compound (9) in Methanol- d_4

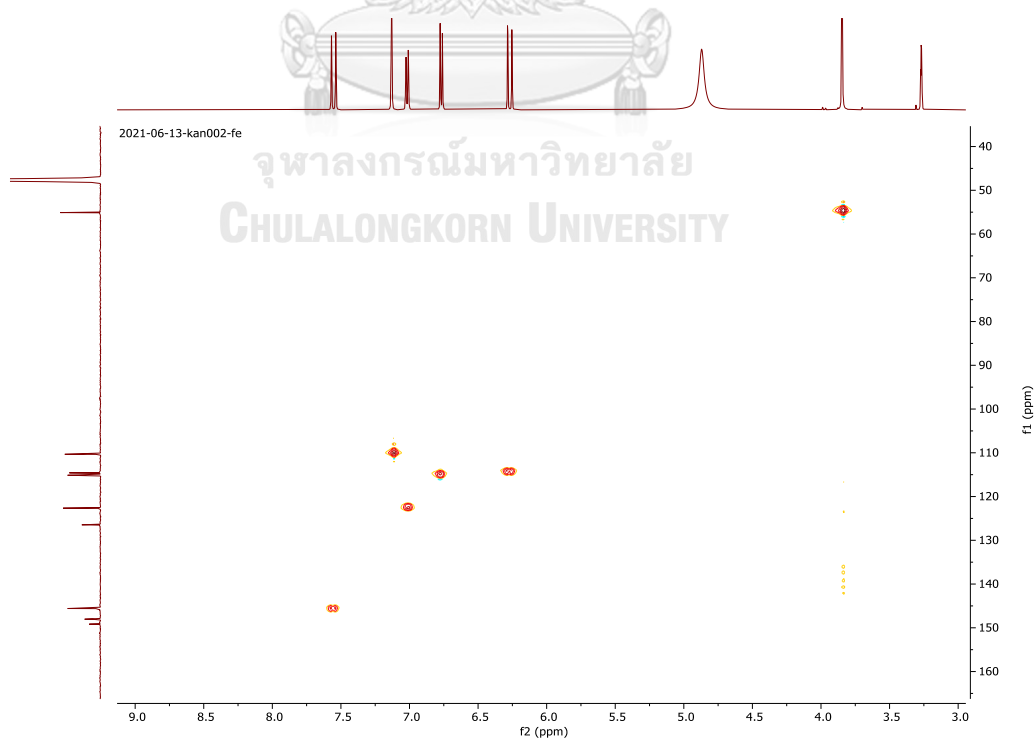


Figure S40 The HSQC spectrum of compound (9) in Methanol- d_4

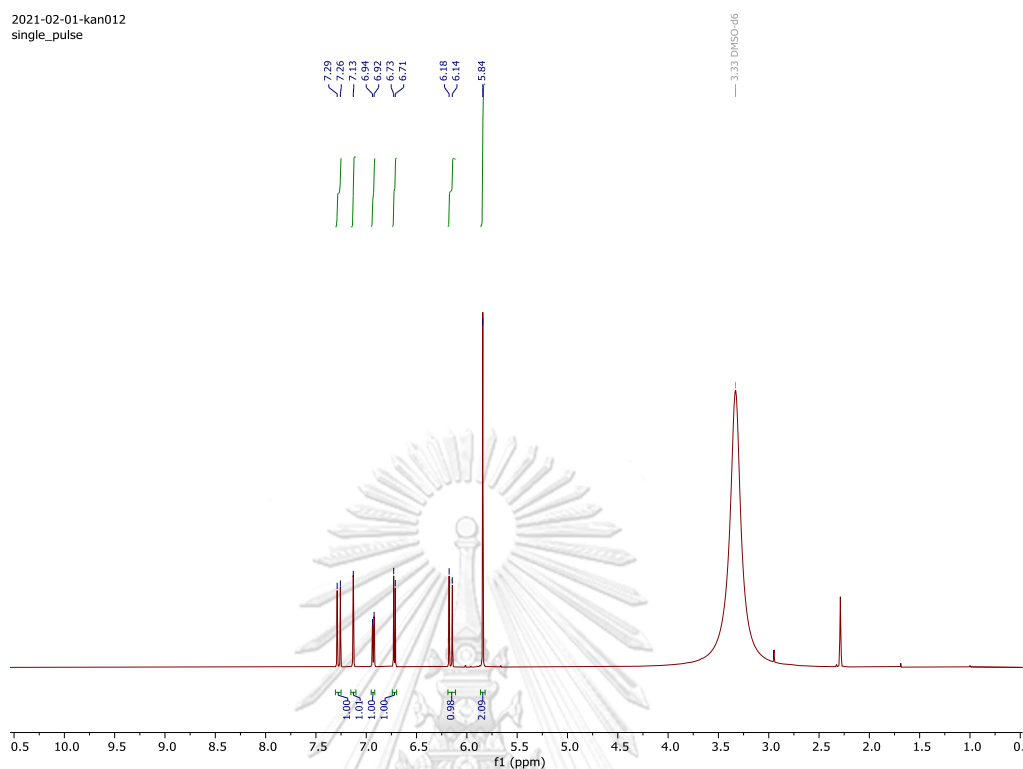


Figure S41 The ^1H -NMR spectrum of compound (10) in $\text{DMSO-}d_6$

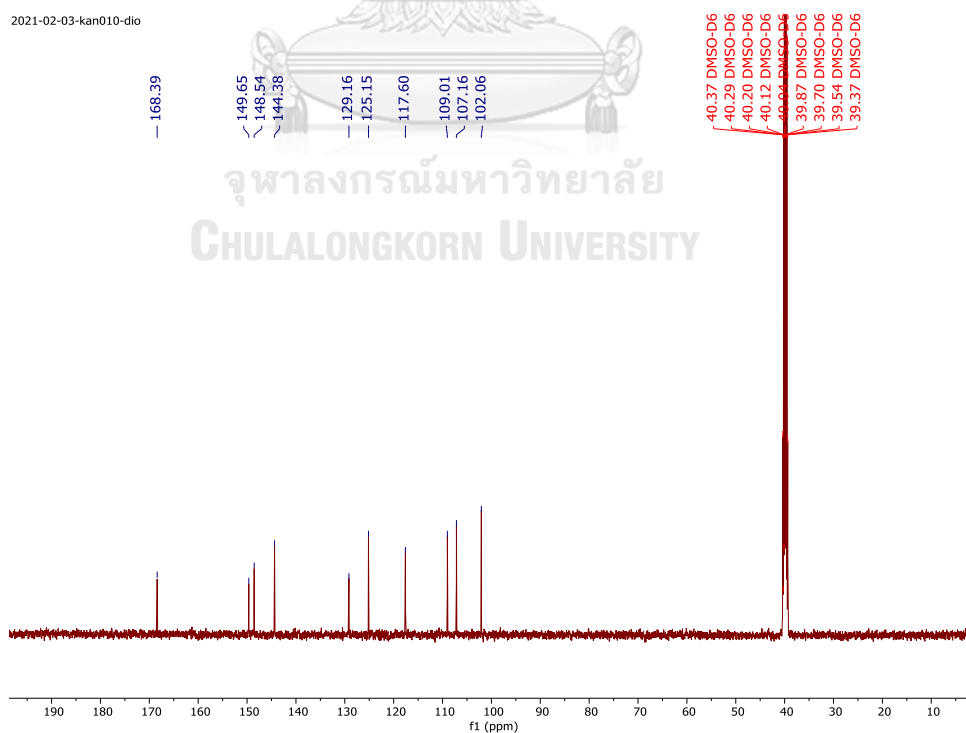


Figure S42 The ^{13}C -NMR spectrum of compound (10) in $\text{DMSO-}d_6$

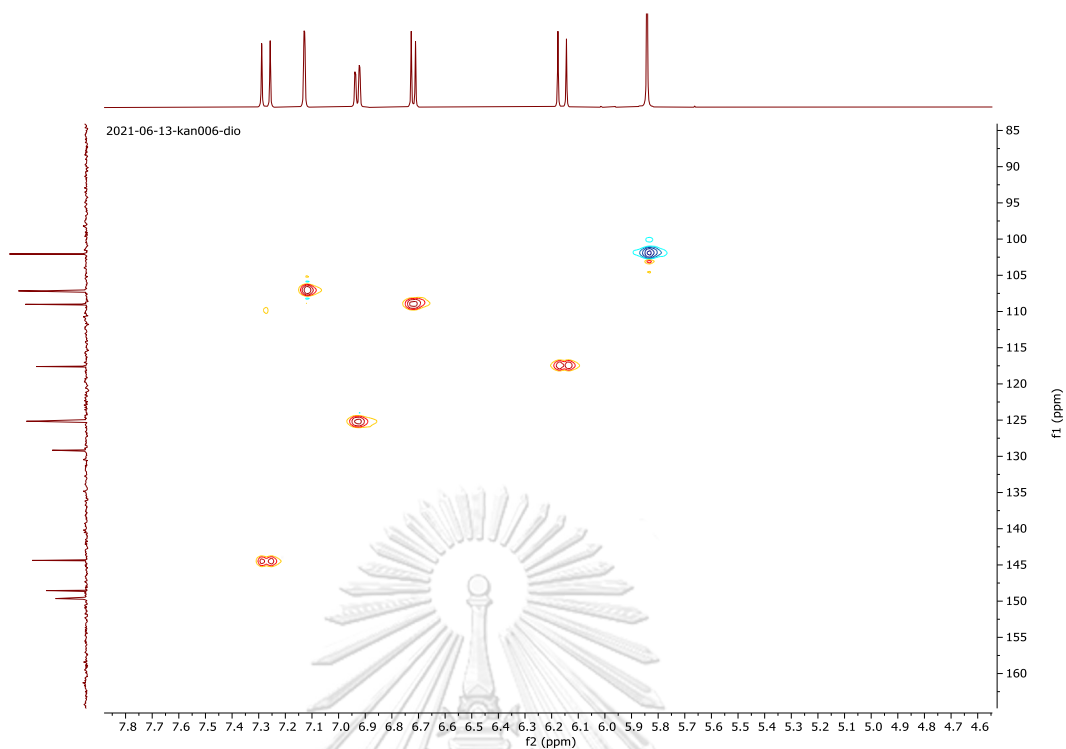


Figure S43 The HSQC spectrum of compound (10) in DMSO- d_6

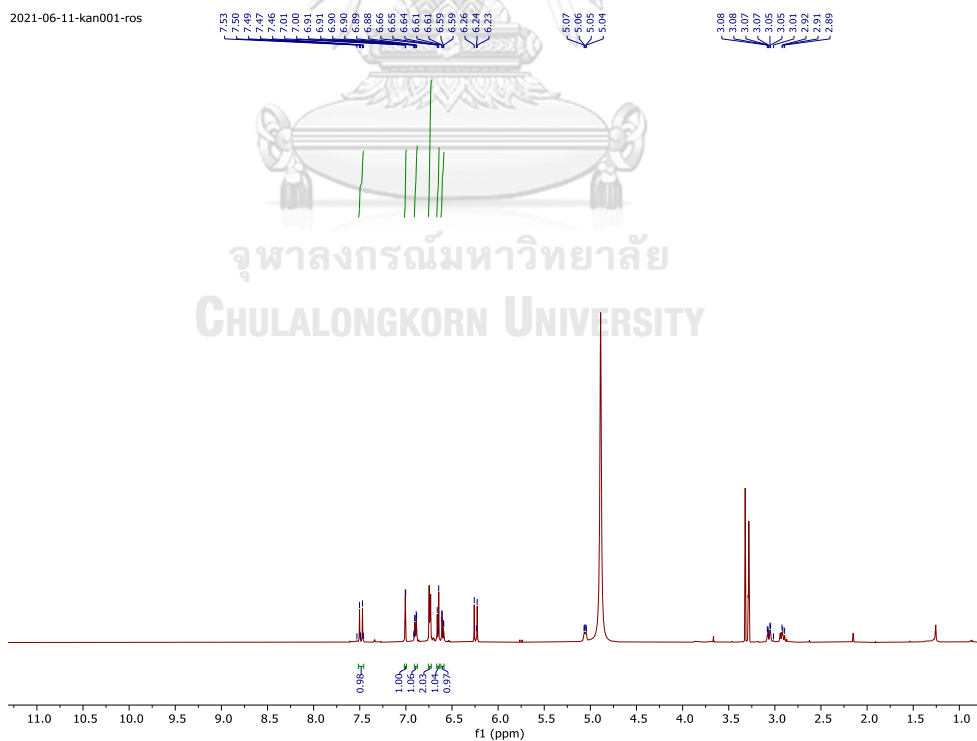


Figure S44 The ^1H -NMR spectrum of compound (11) in Methanol- d_4

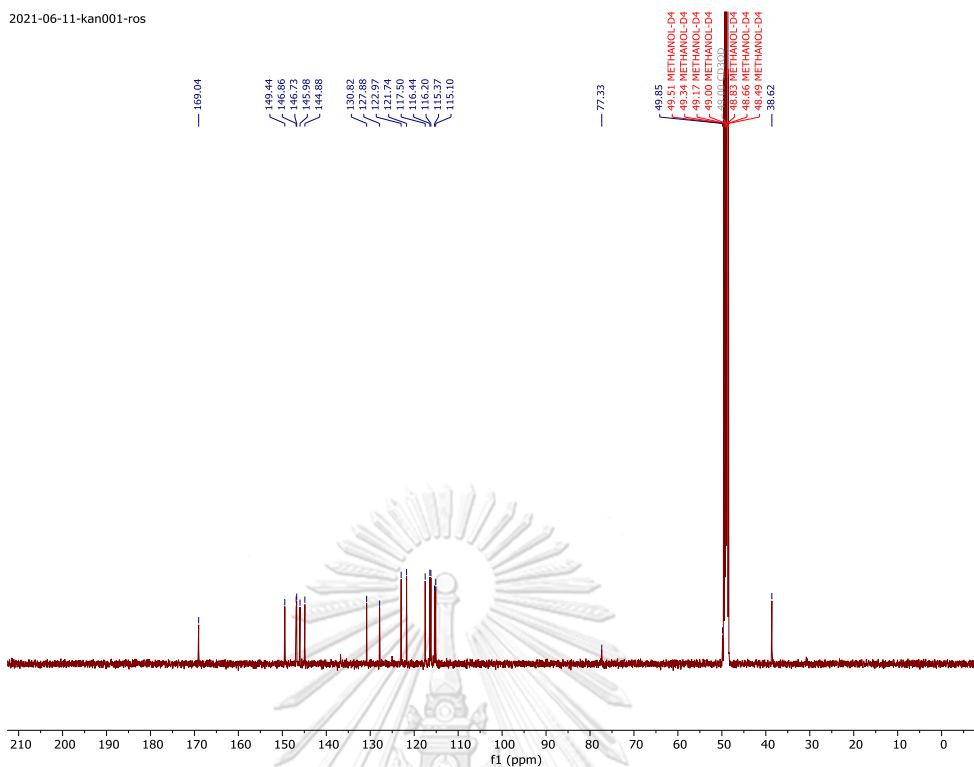


Figure S45 The ^{13}C -NMR spectrum of compound (11) in Methanol- d_4

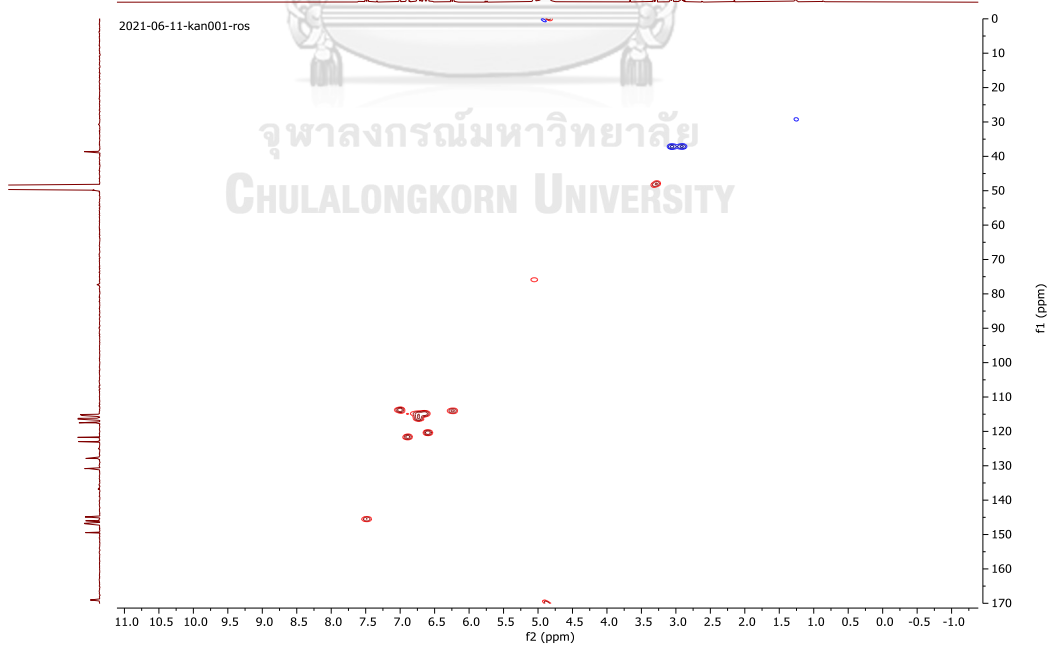


Figure S46 The HSQC spectrum of compound (11) in Methanol- d_4

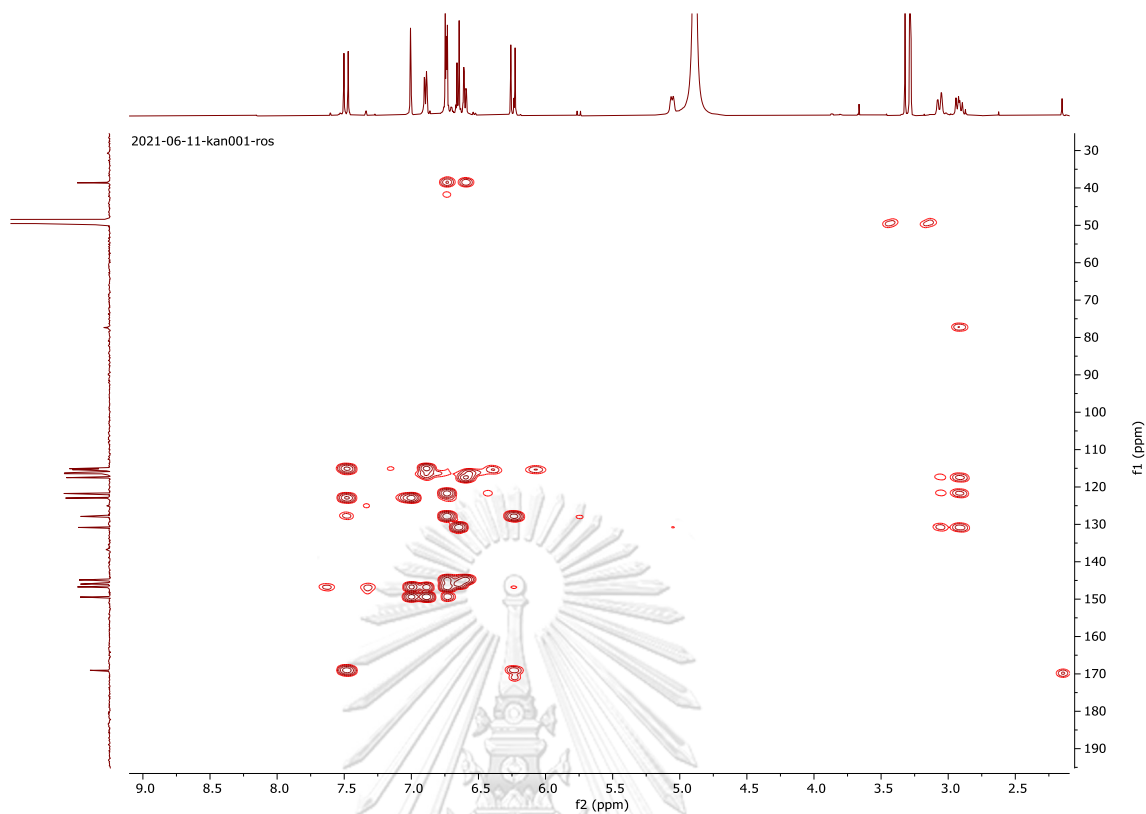


Figure S47 The HMBC spectrum of compound (11) in Methanol- d_4

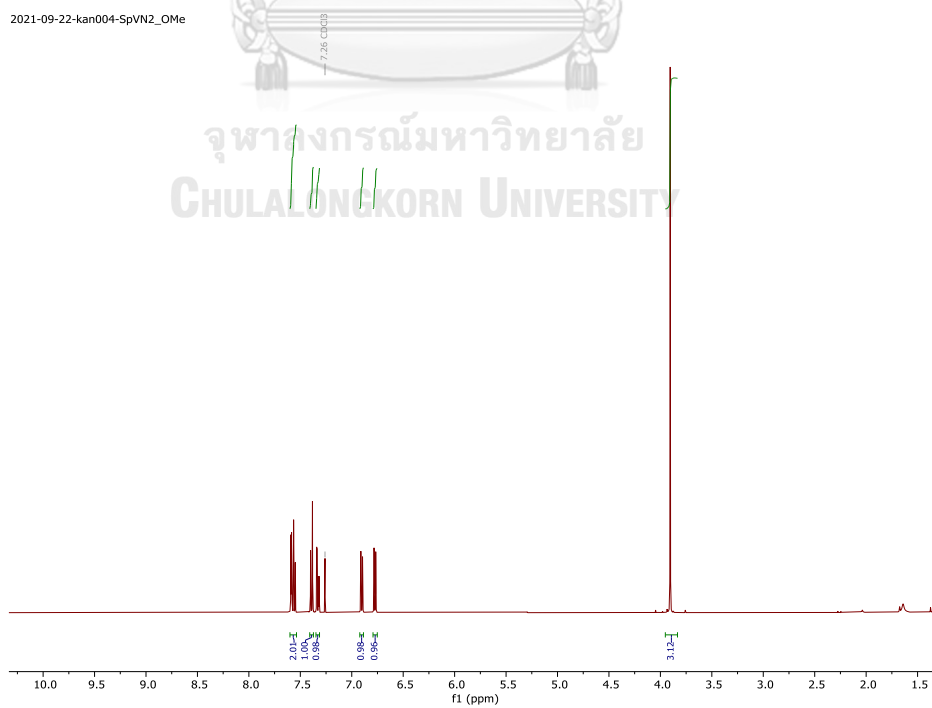


Figure S48 The ^1H -NMR spectrum of compound (12) in chloroform- d

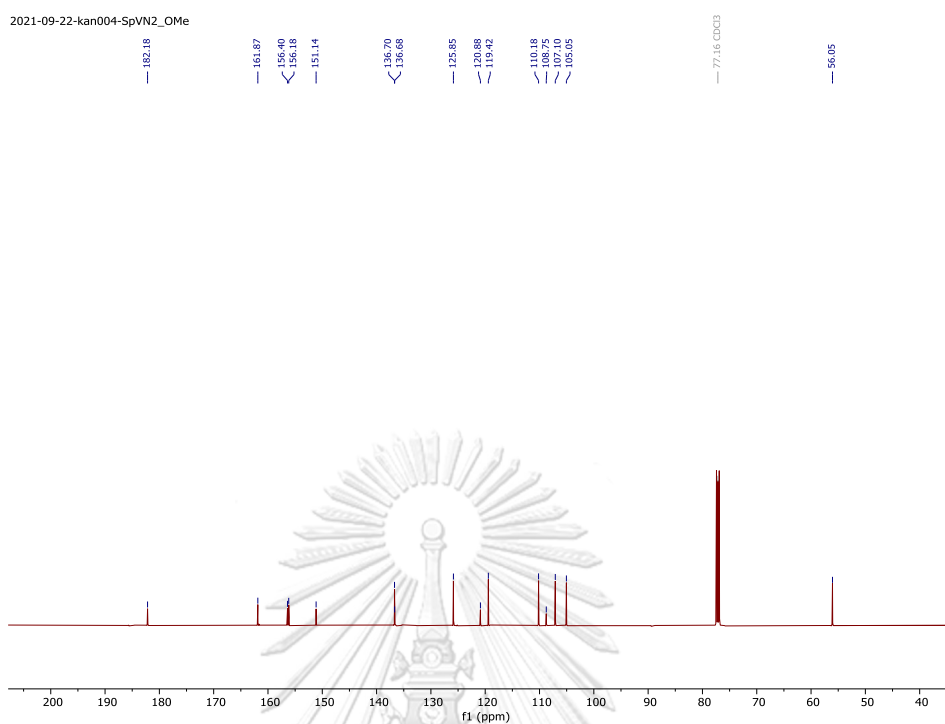


Figure S49 The ¹³C-NMR spectrum of compound (12) in chloroform-*d*

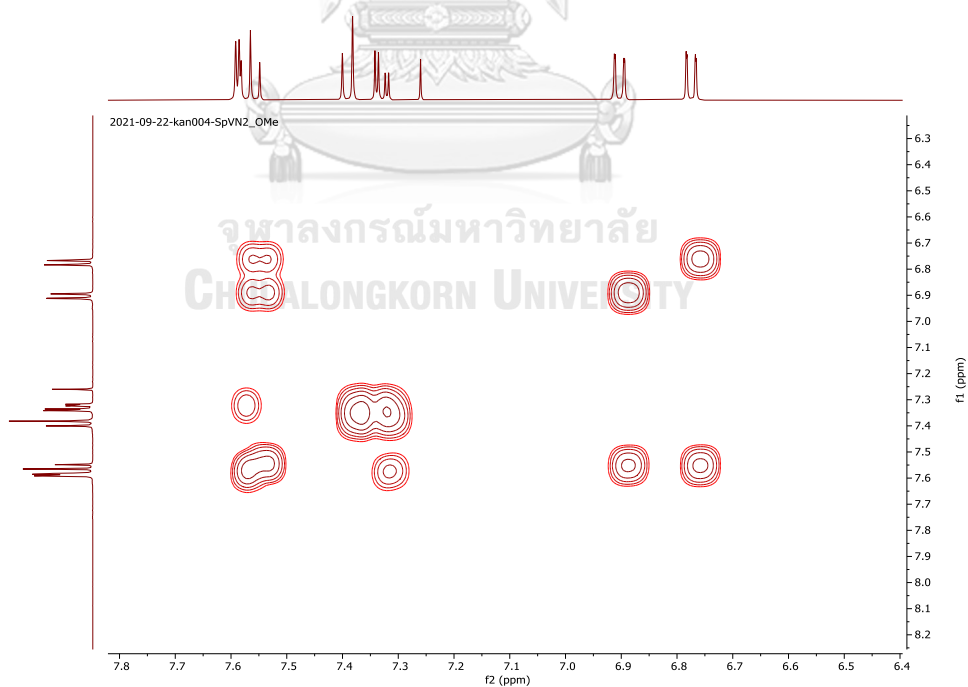


Figure S50 The COSY spectrum of compound (12) in chloroform-*d*

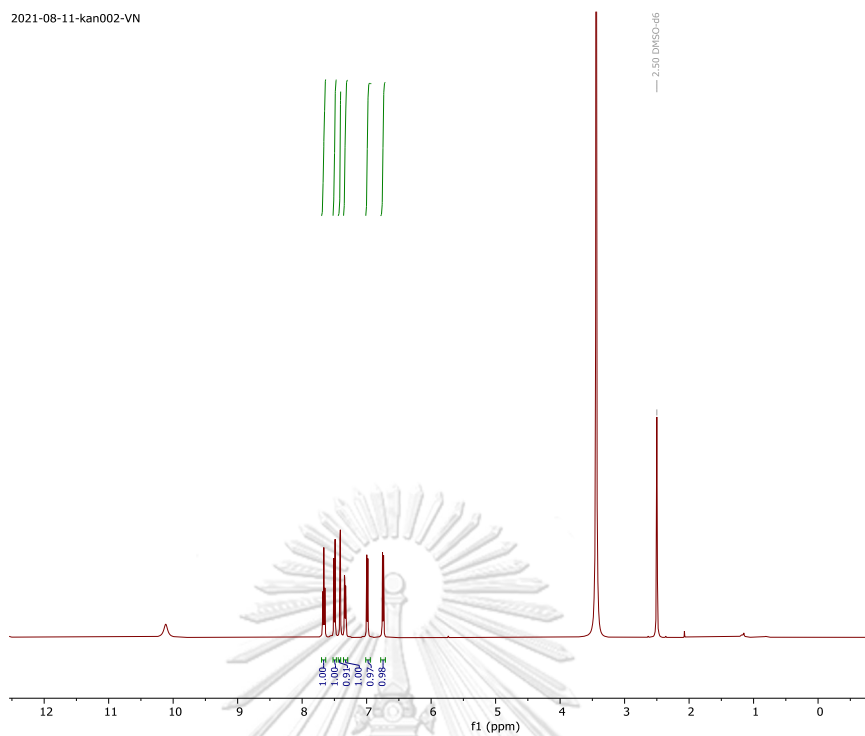


Figure S51 The ^1H -NMR spectrum of compound (13) in $\text{DMSO-}d_6$

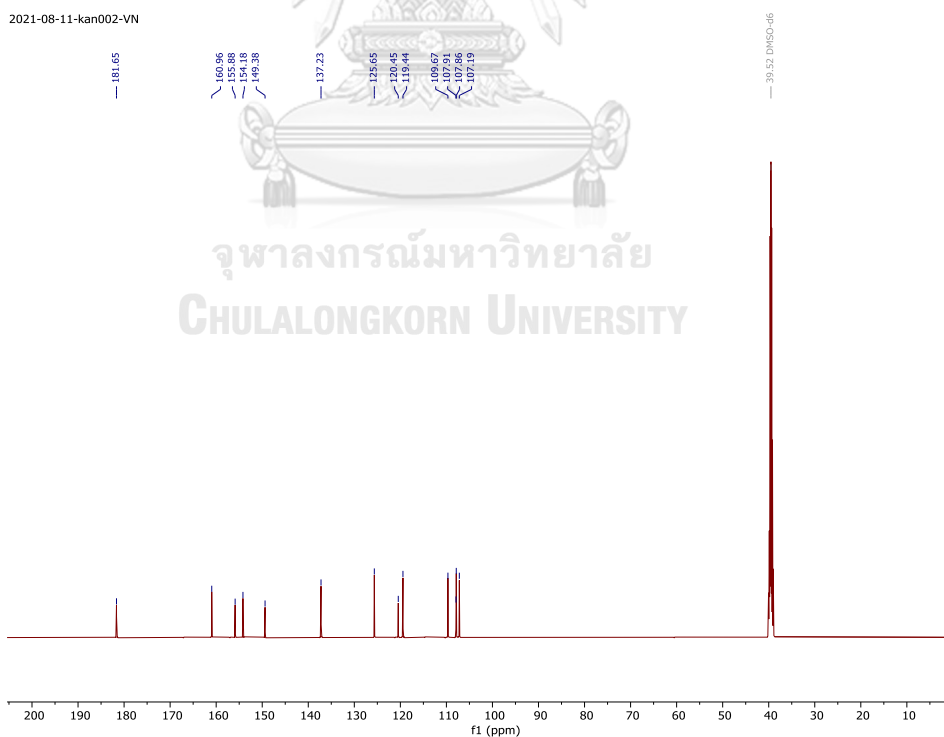


Figure S52 The ^{13}C -NMR spectrum of compound (13) in $\text{DMSO-}d_6$

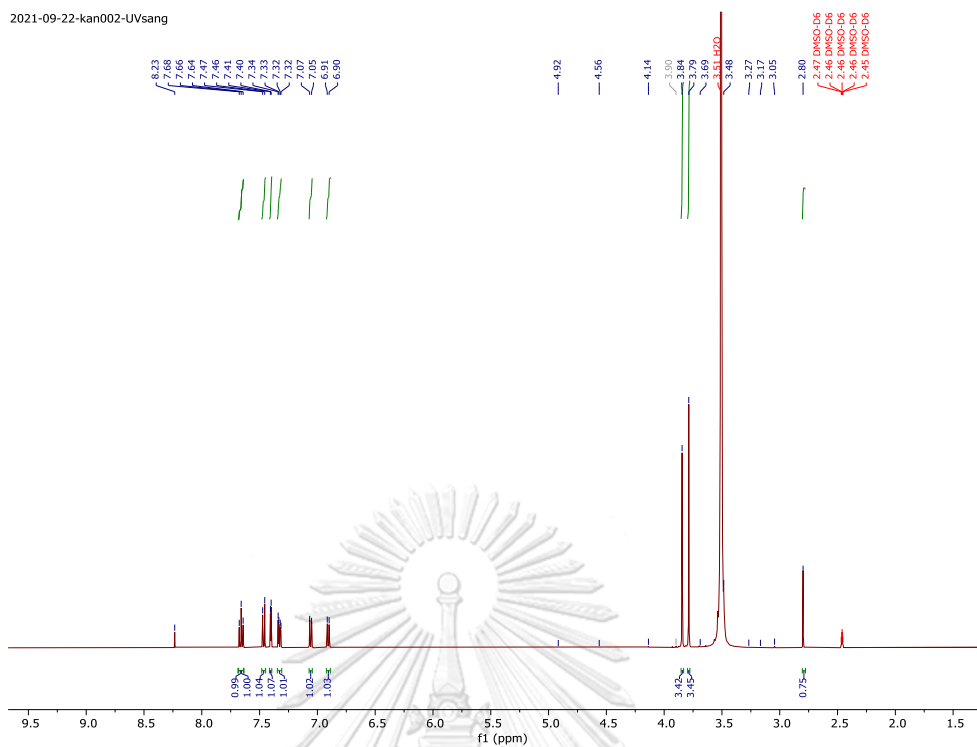


Figure S53 The ^1H -NMR spectrum of compound (14) in $\text{DMSO-}d_6$

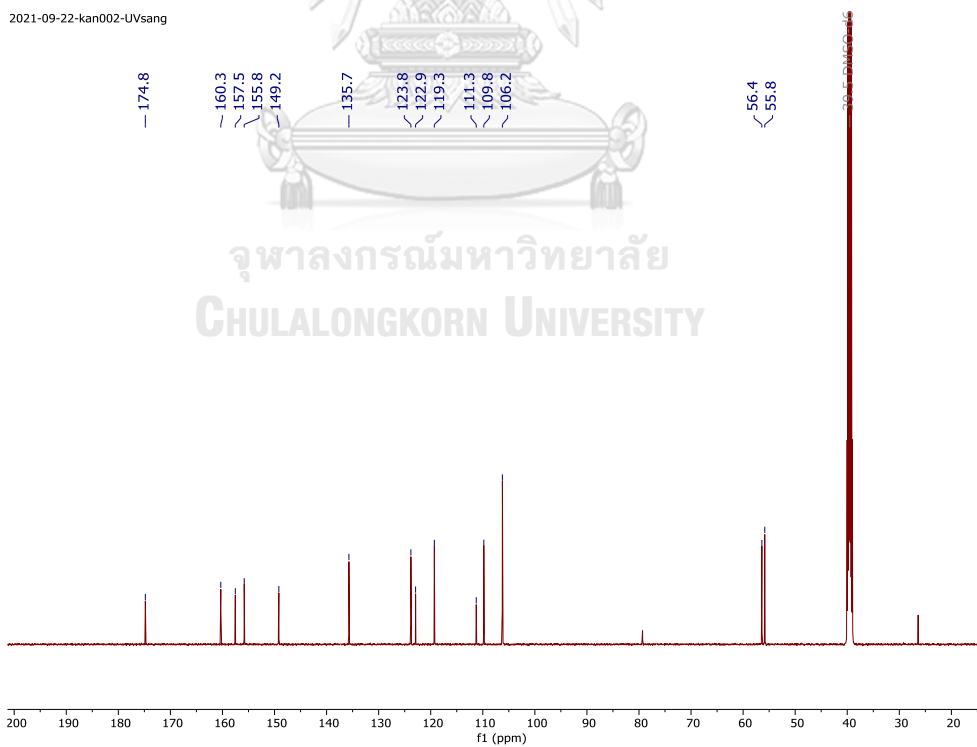


Figure S54 The ^{13}C -NMR spectrum of compound (14) in $\text{DMSO-}d_6$

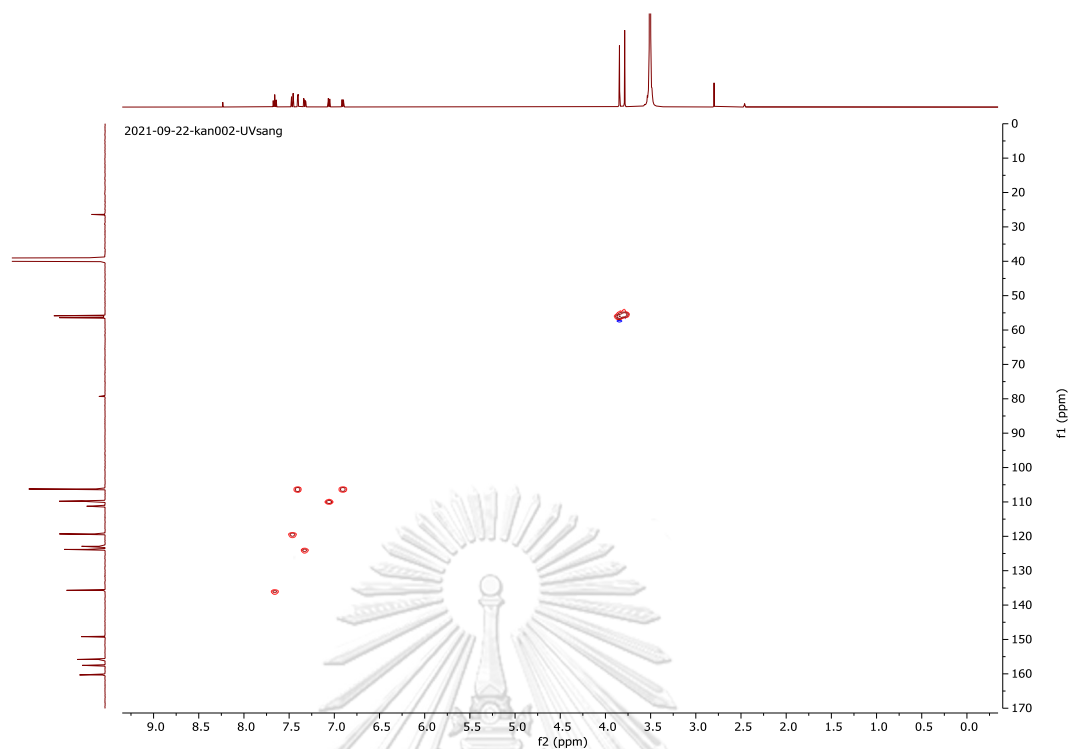


Figure S55 The HSQC spectrum of compound (14) in DMSO- d_6

2021-09-22-kan003-SpVN2

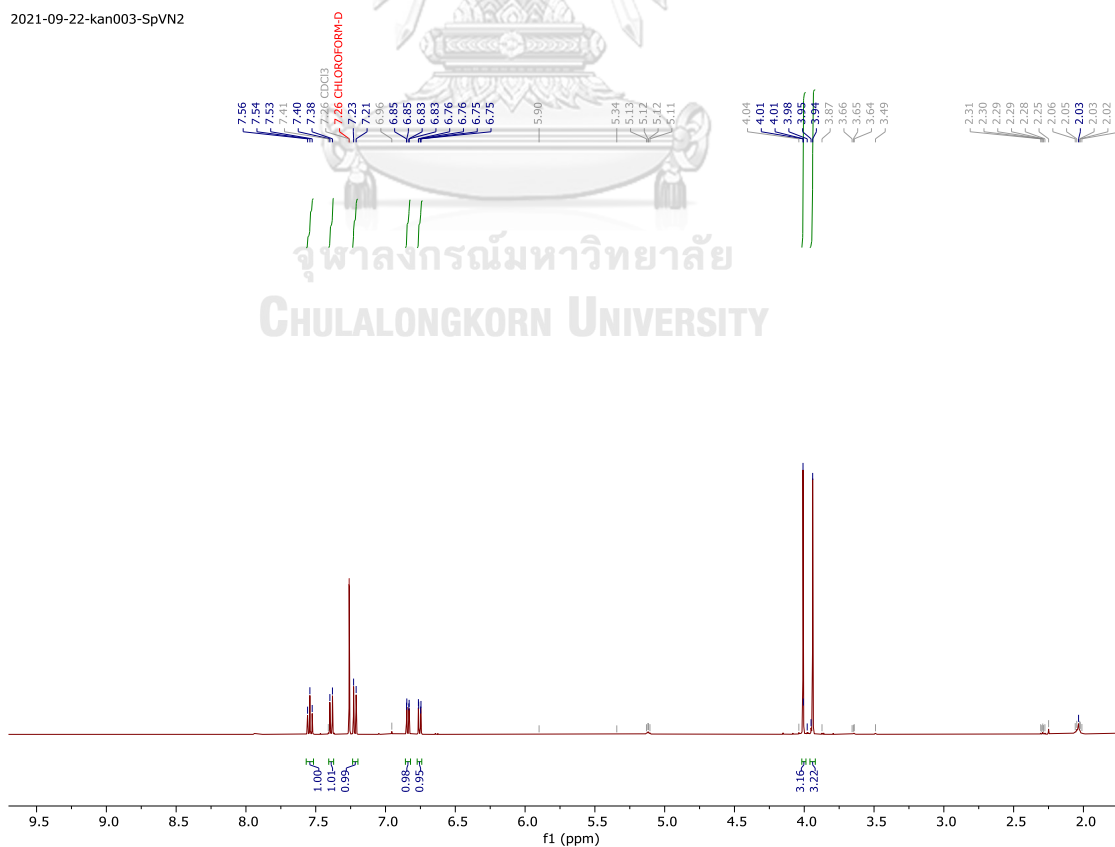


Figure S56 The ^1H -NMR spectrum of compound (15) in Chloroform- d

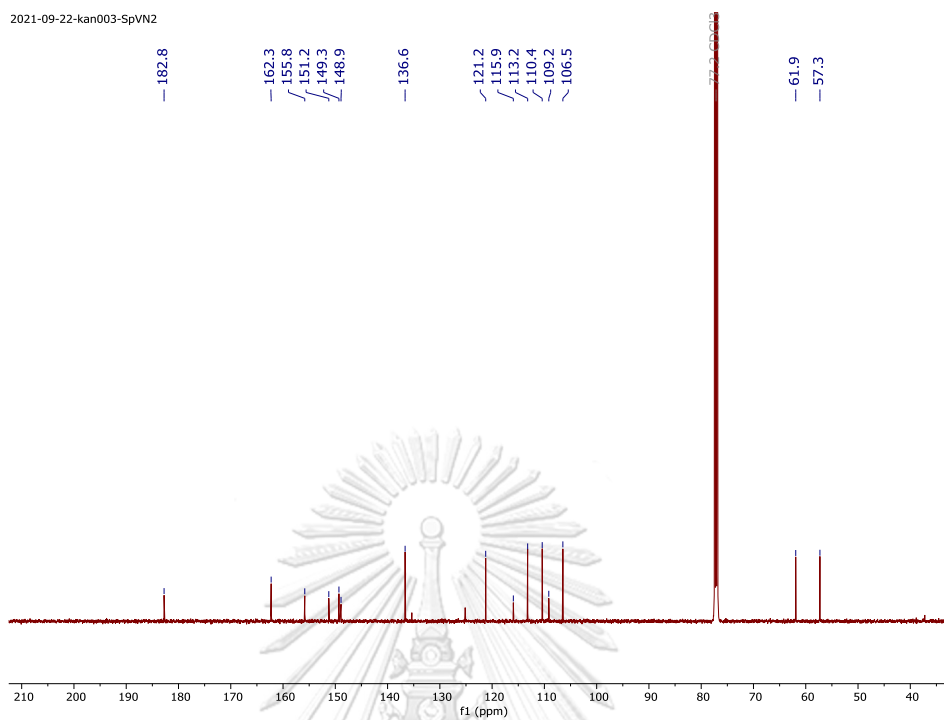


Figure S57 The ^{13}C -NMR spectrum of compound (15) in Chloroform-*d*

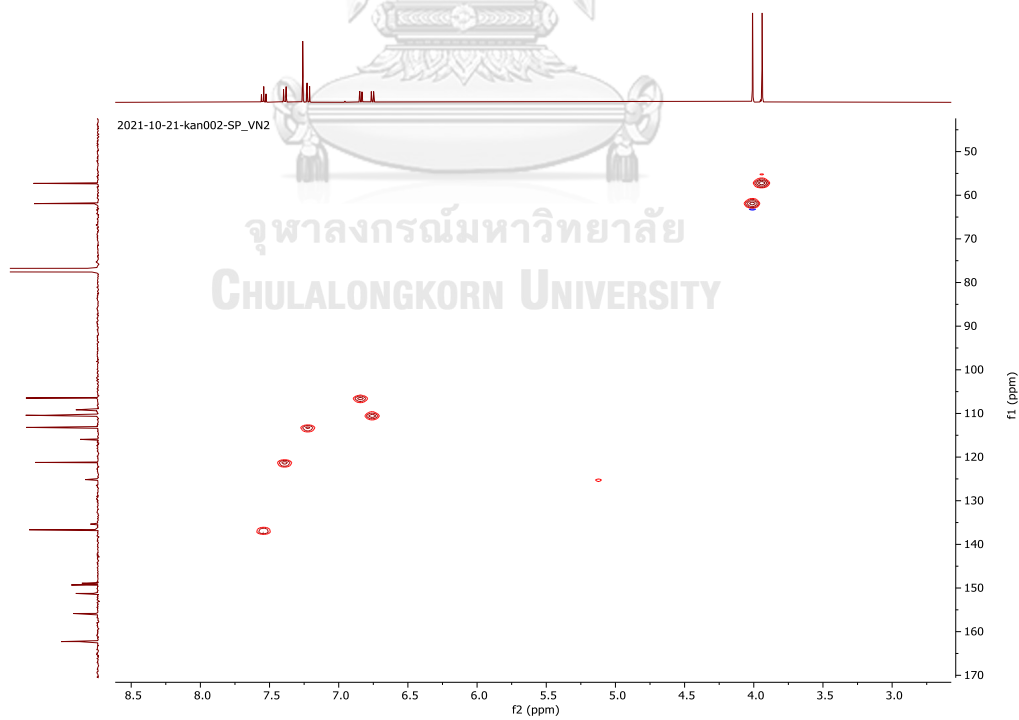


Figure S58 The HSQC spectrum of compound (15) in Chloroform-*d*

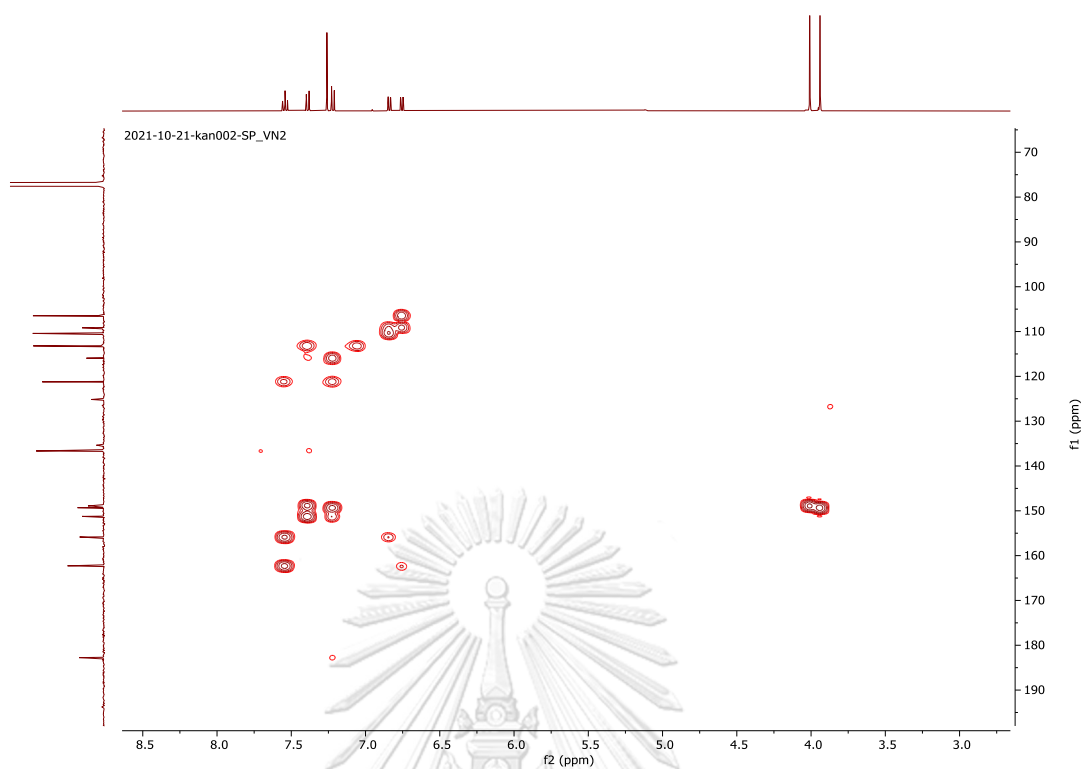


Figure S59 The HMBC spectrum of compound (15) in Chloroform-*d*

2021-08-20-kan001-VN1

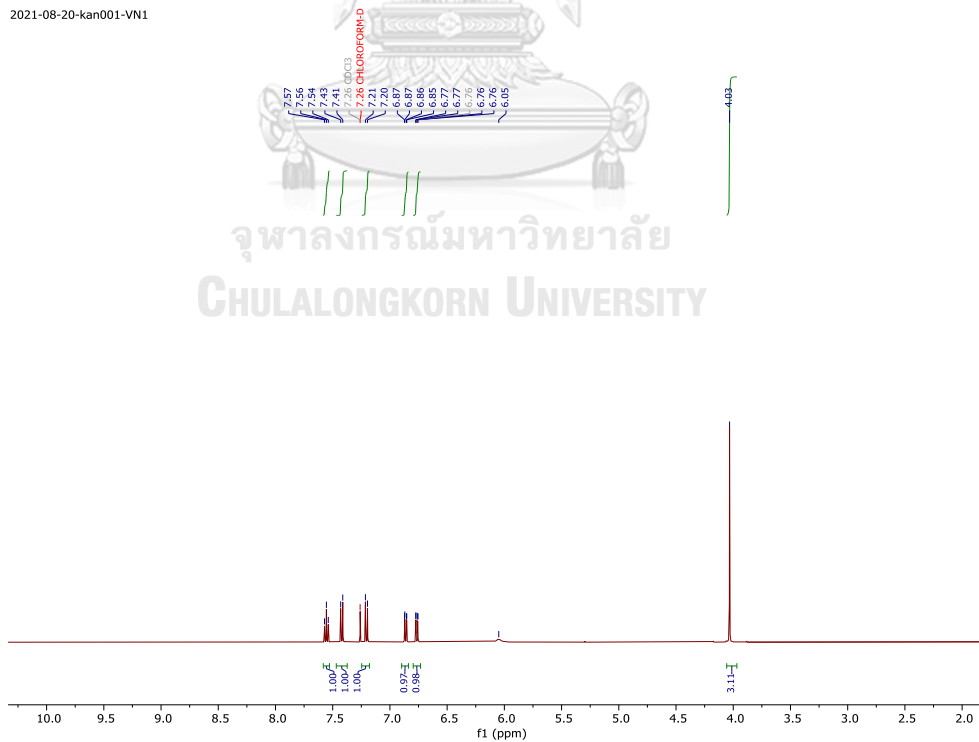


Figure S60 The ^1H -NMR spectrum of compound (16) in Chloroform-*d*

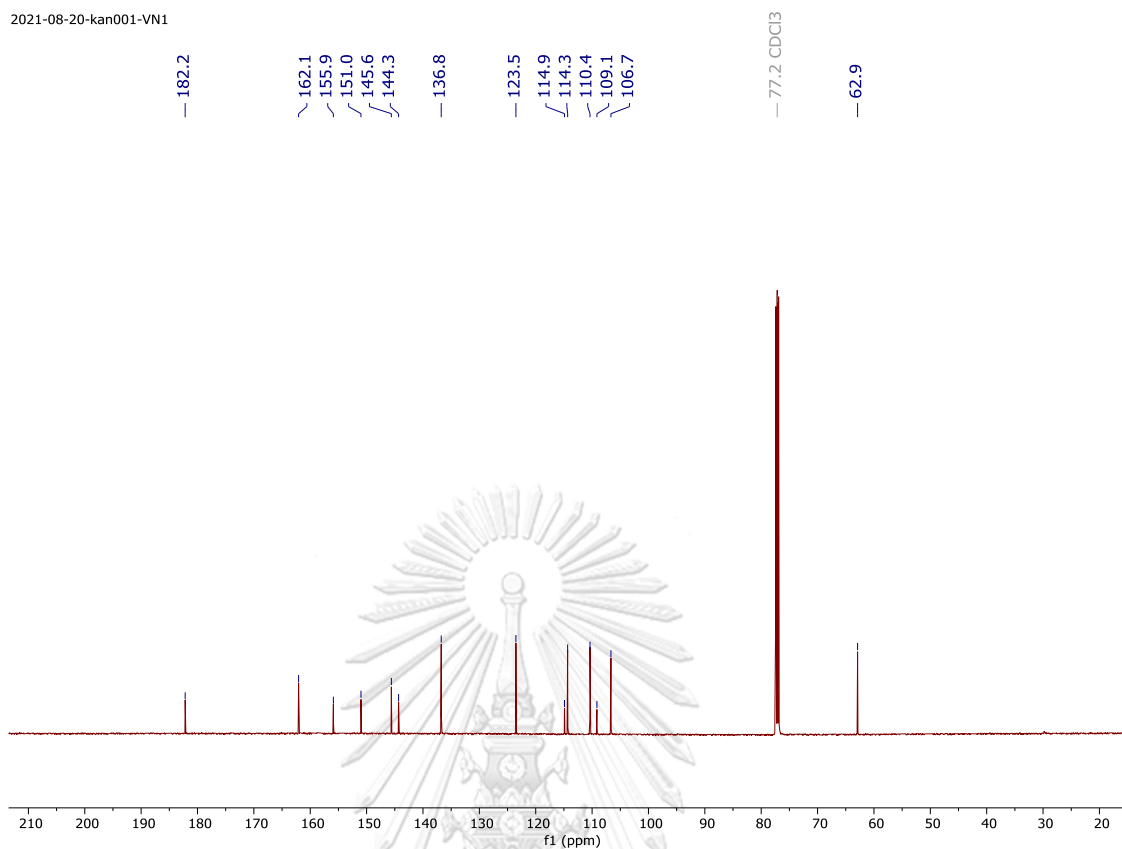


Figure S61 The ¹³C-NMR spectrum of compound (16) in Chloroform-*d*

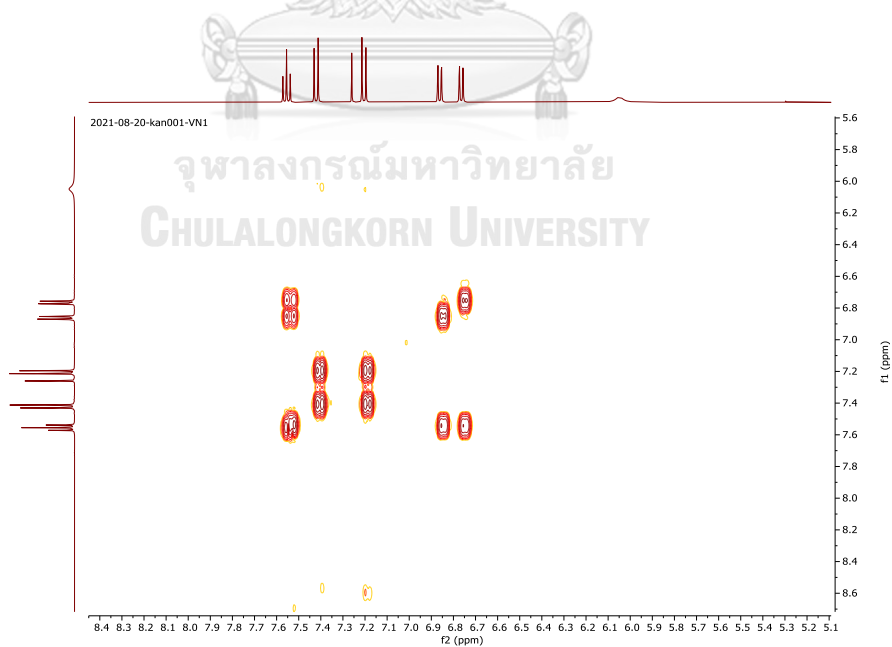


Figure S62 The COSY spectrum of compound (16) in Chloroform-*d*

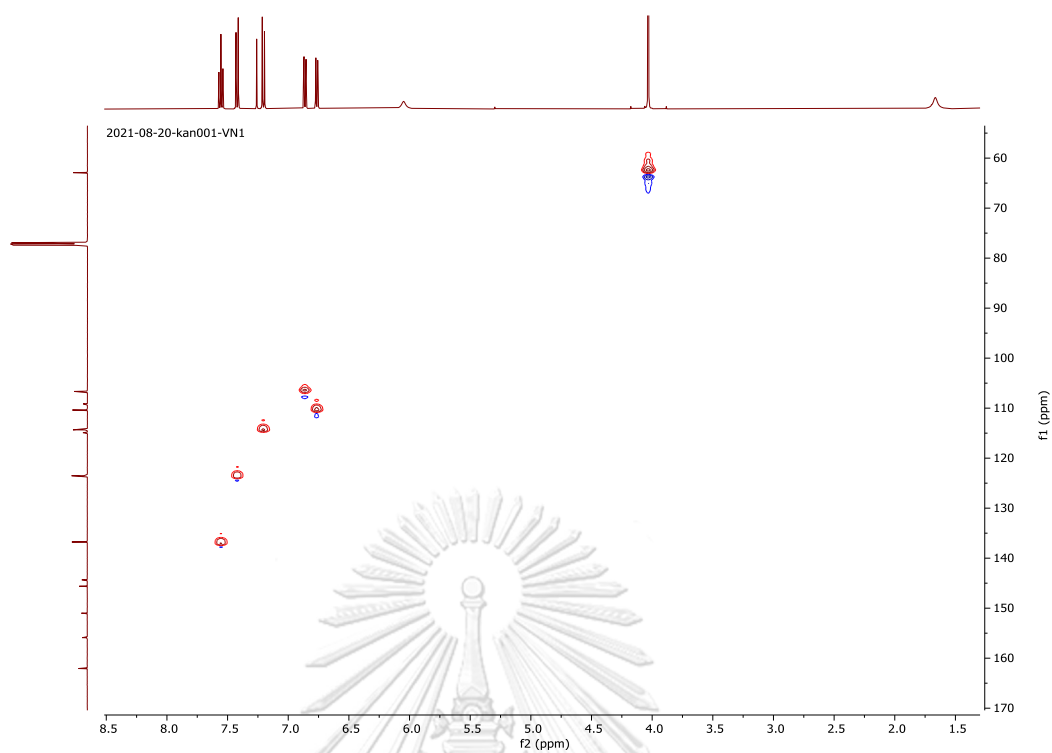


Figure S63 The HSQC spectrum of compound (16) in Chloroform-*d*

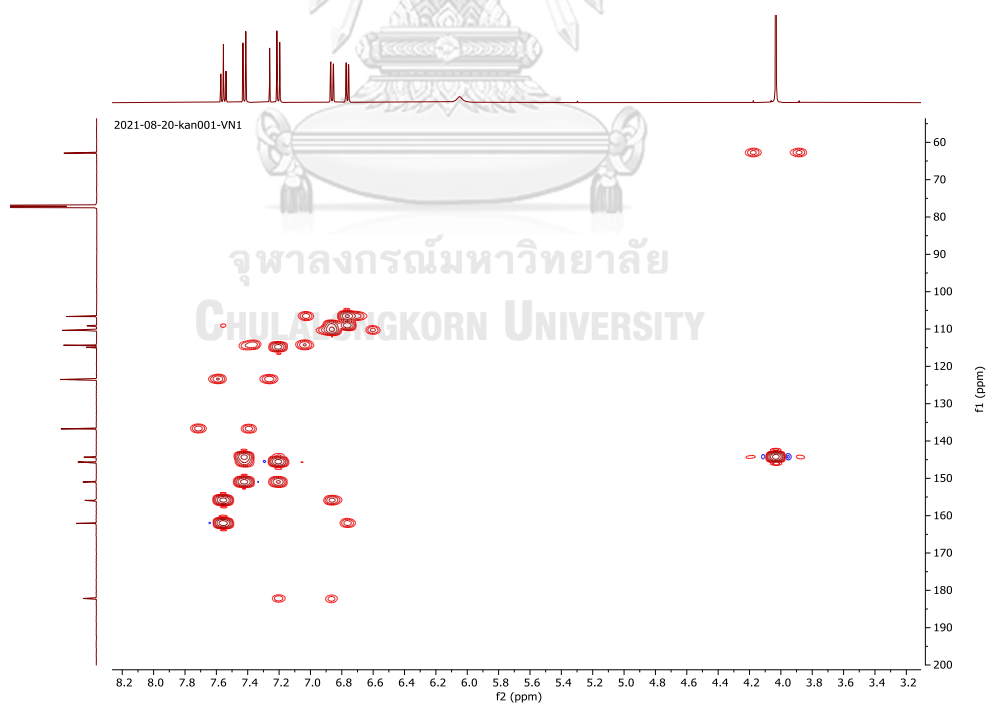


Figure S64 The HMBC spectrum of compound (16) in Chloroform-*d*

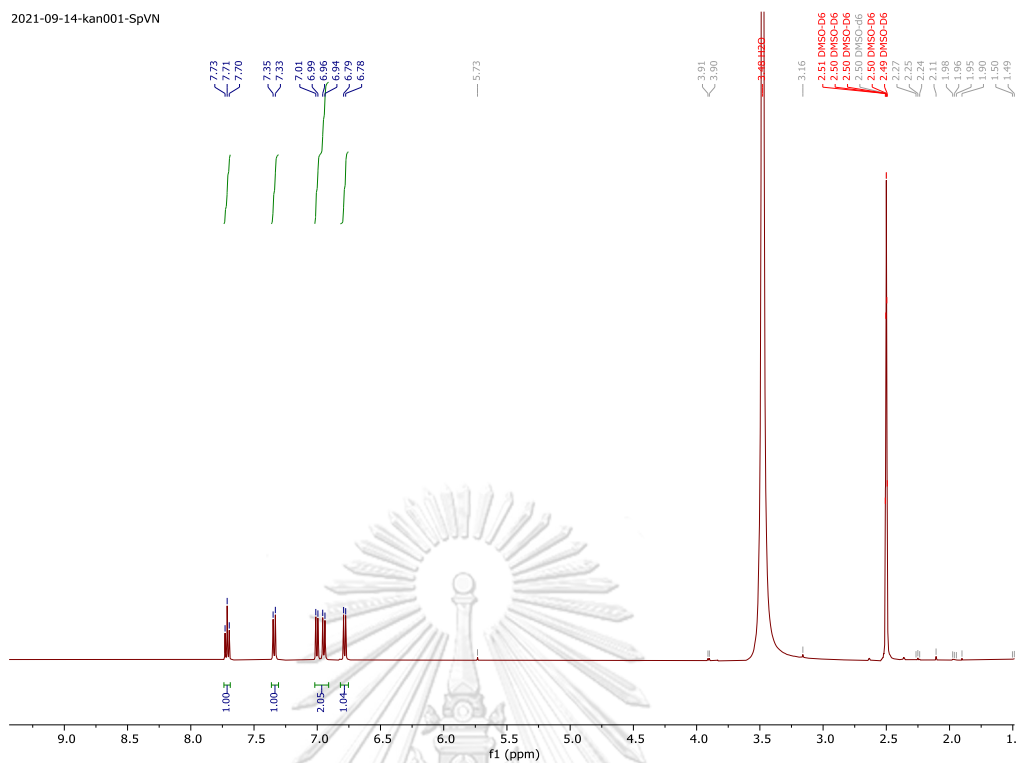


Figure S65 The $^1\text{H-NMR}$ spectrum of compound (17) in $\text{DMSO-}d_6$

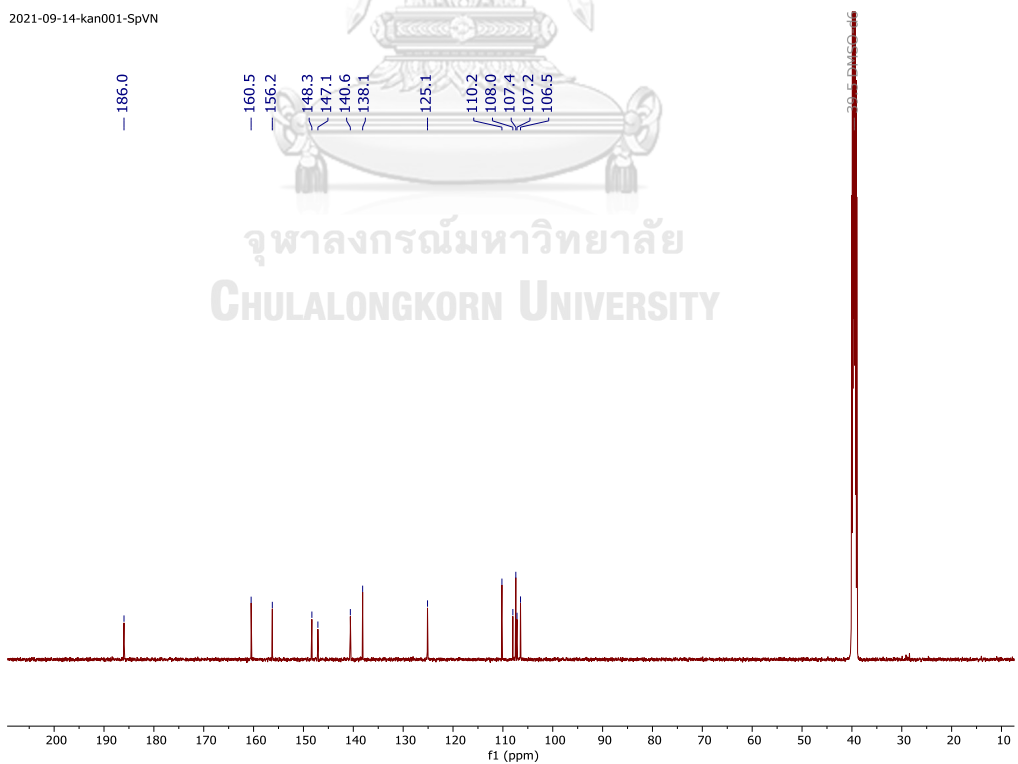


Figure S66 The $^{13}\text{C-NMR}$ spectrum of compound (17) in $\text{DMSO-}d_6$

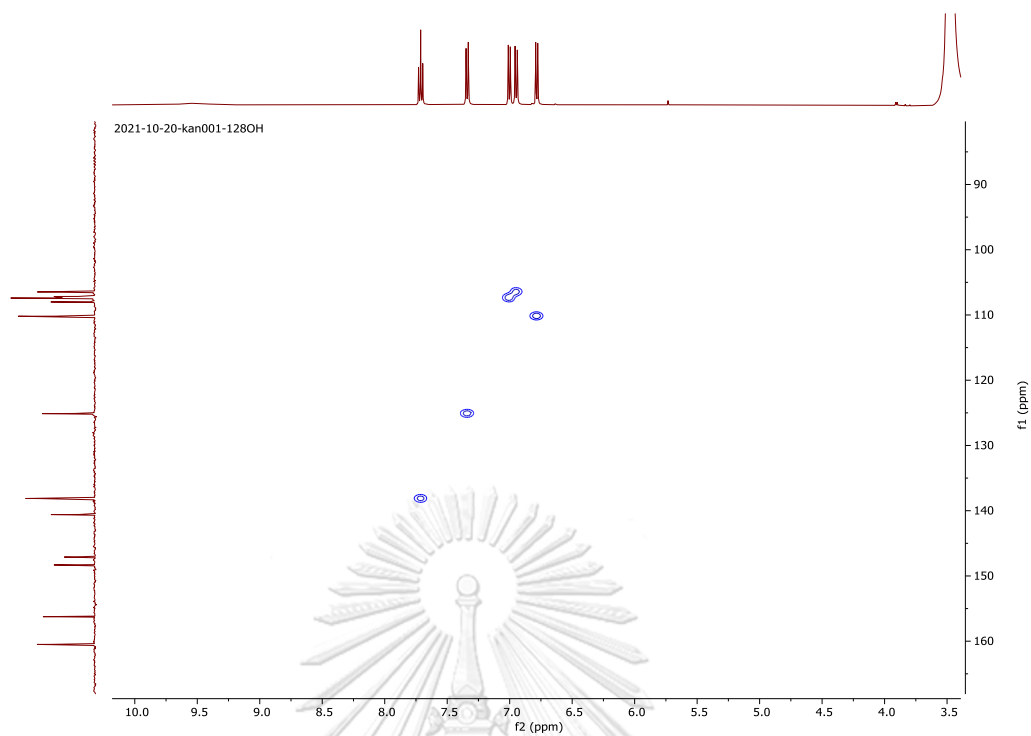


Figure S67 The HSQC spectrum of compound (17) in DMSO- d_6

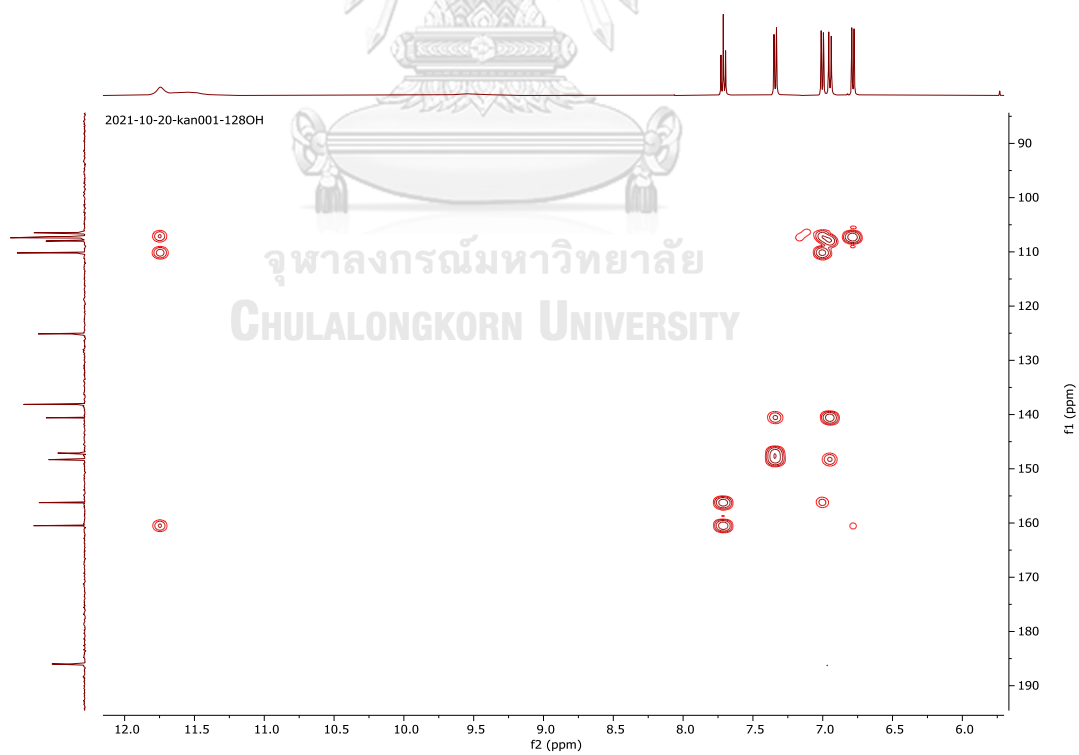
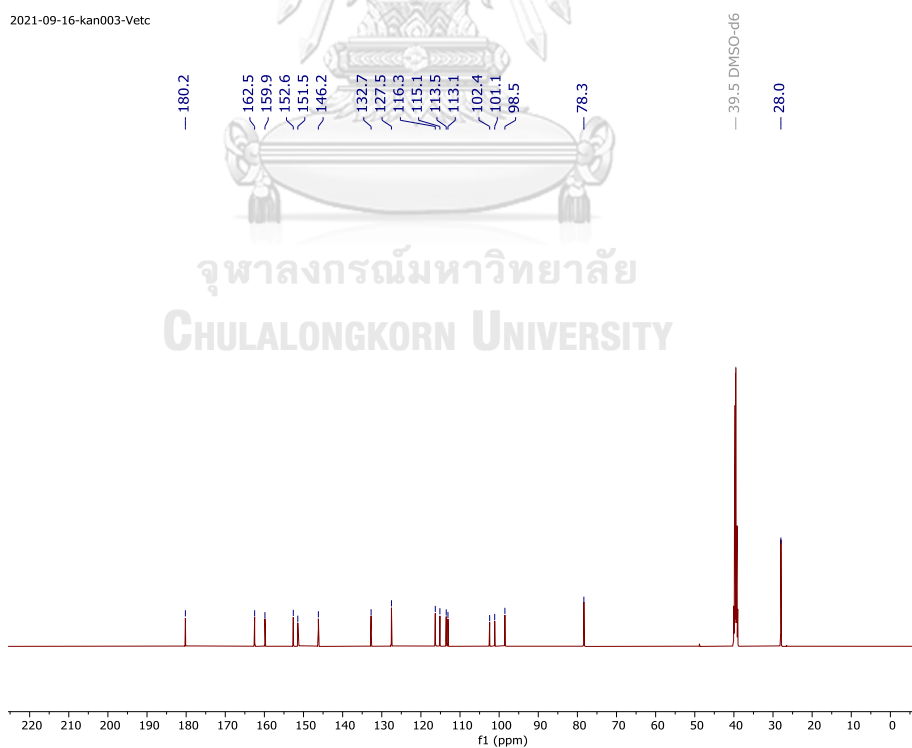
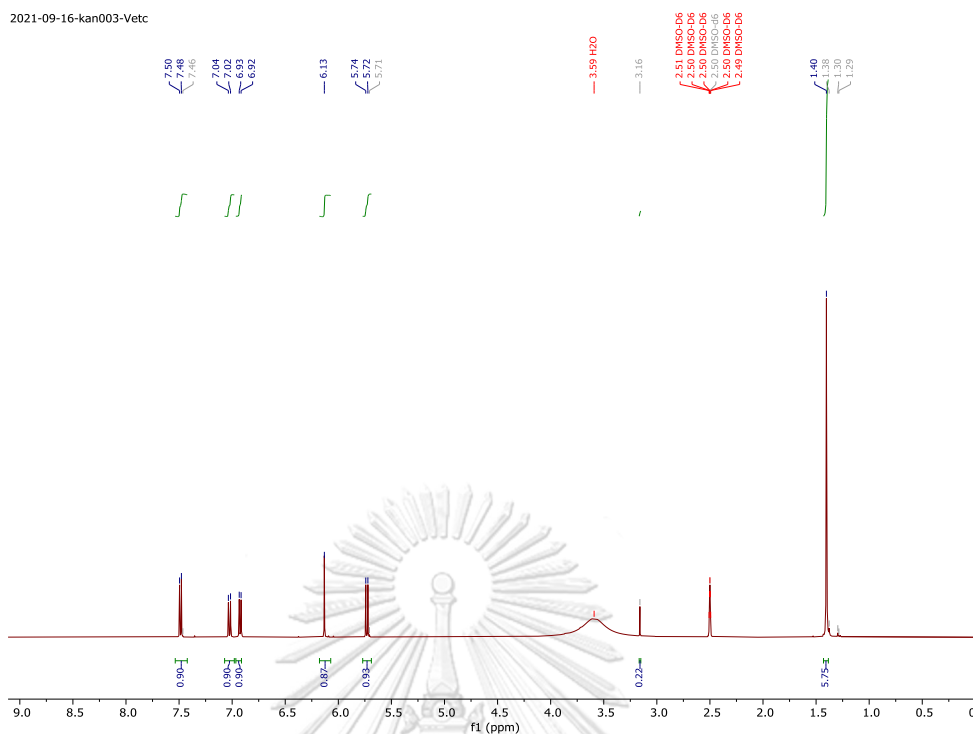


Figure S68 The HMBC spectrum of compound (17) in DMSO- d_6



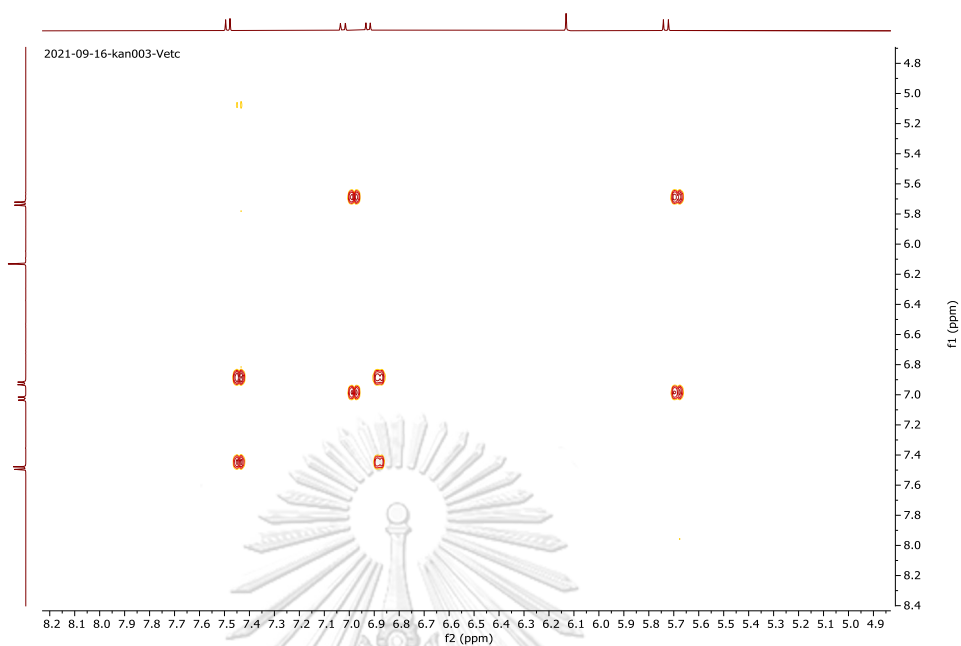


Figure S71 The COSY spectrum of compound (18) in DMSO- d_6

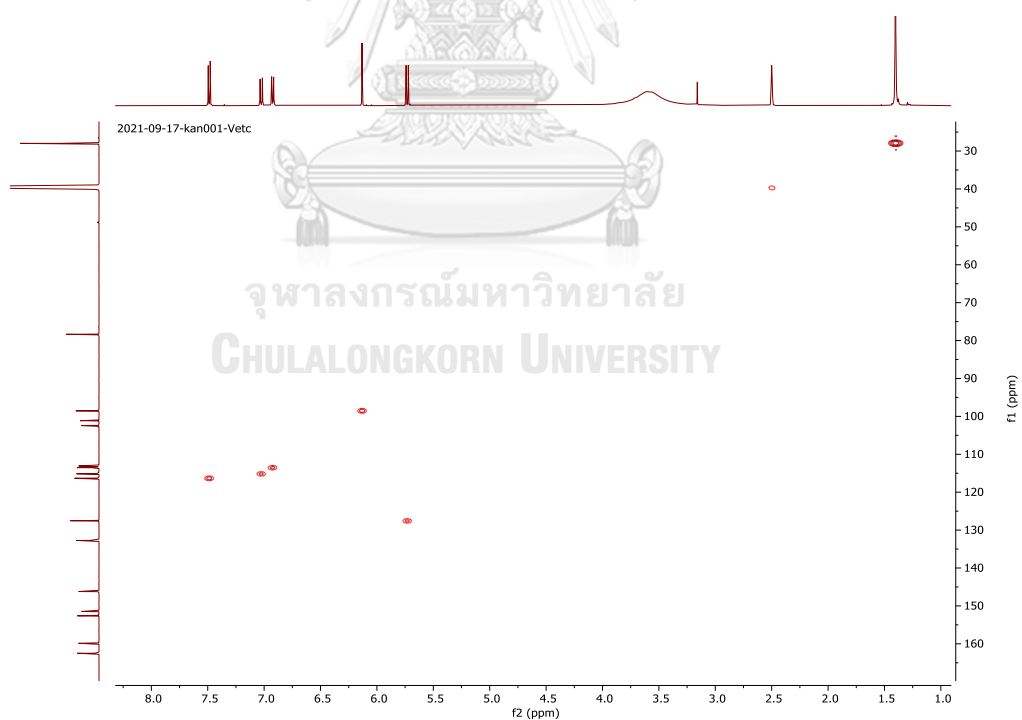


Figure S72 The HSQC spectrum of compound (18) in DMSO- d_6

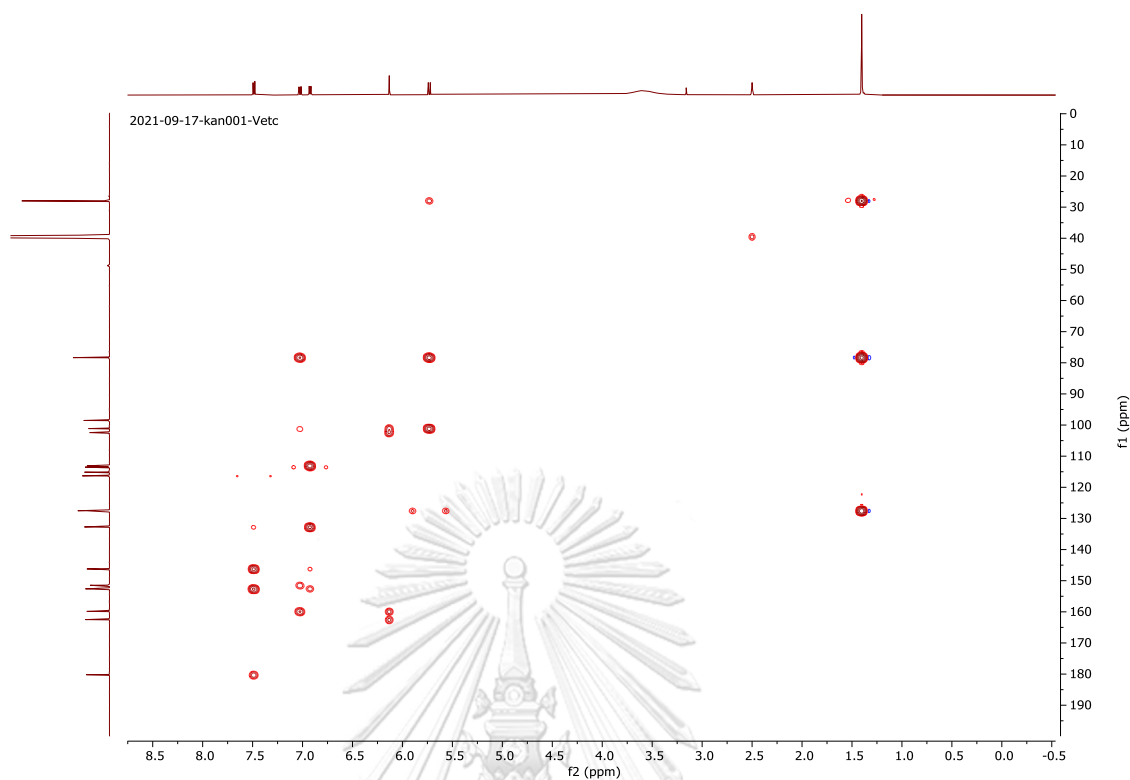


Figure S73 The HMBC spectrum of compound (18) in DMSO

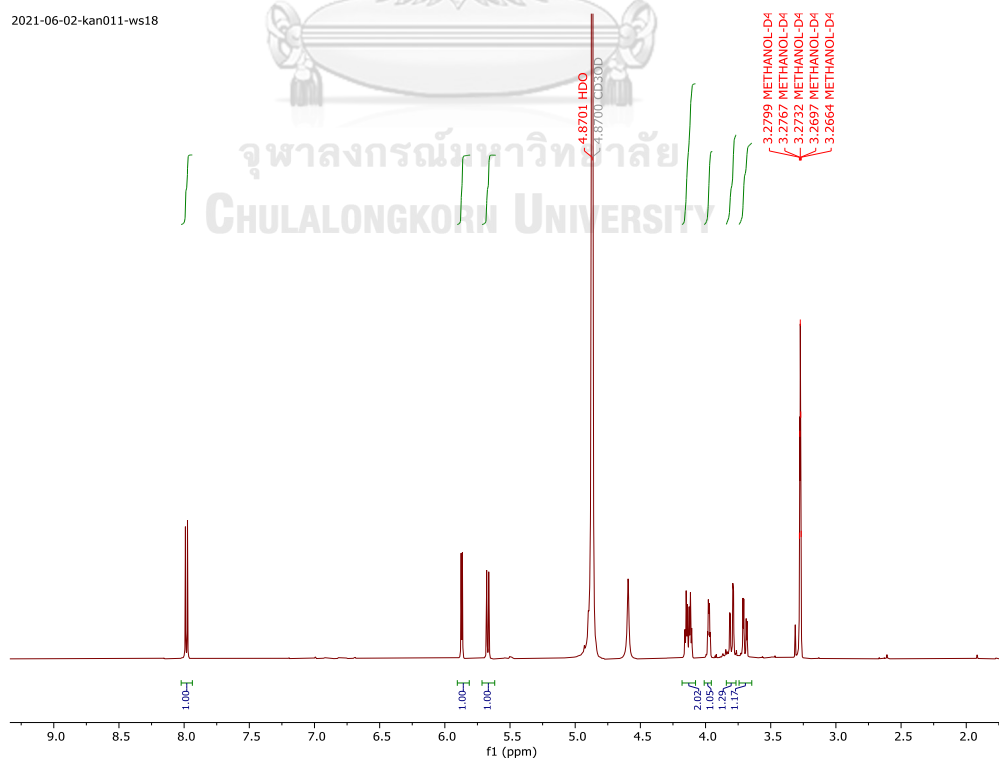


Figure S74 The ^1H -NMR spectrum of compound (19) in Methanol- d_4

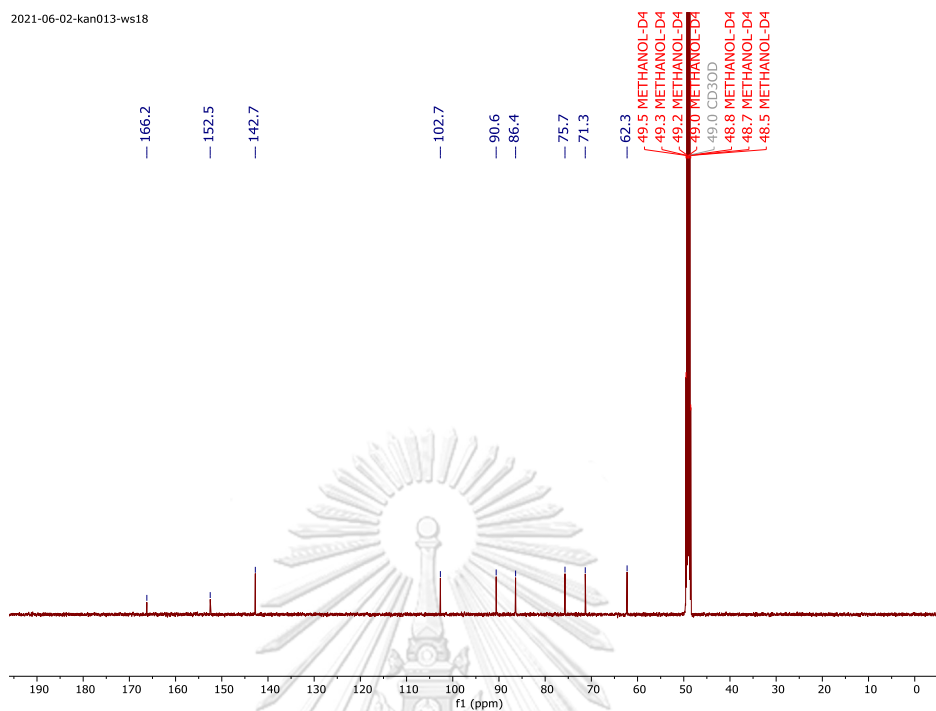


Figure S75 The ^{13}C -NMR spectrum of compound (19) in Methanol- d_4

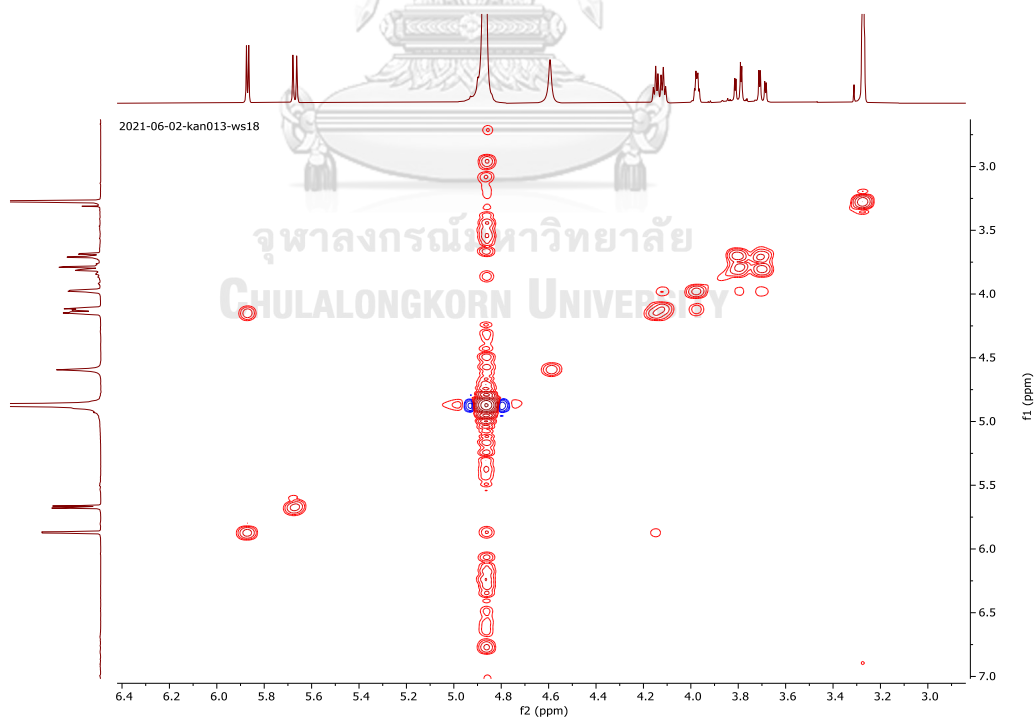


Figure S76 The COSY spectrum of compound (19) in Methanol- d_4

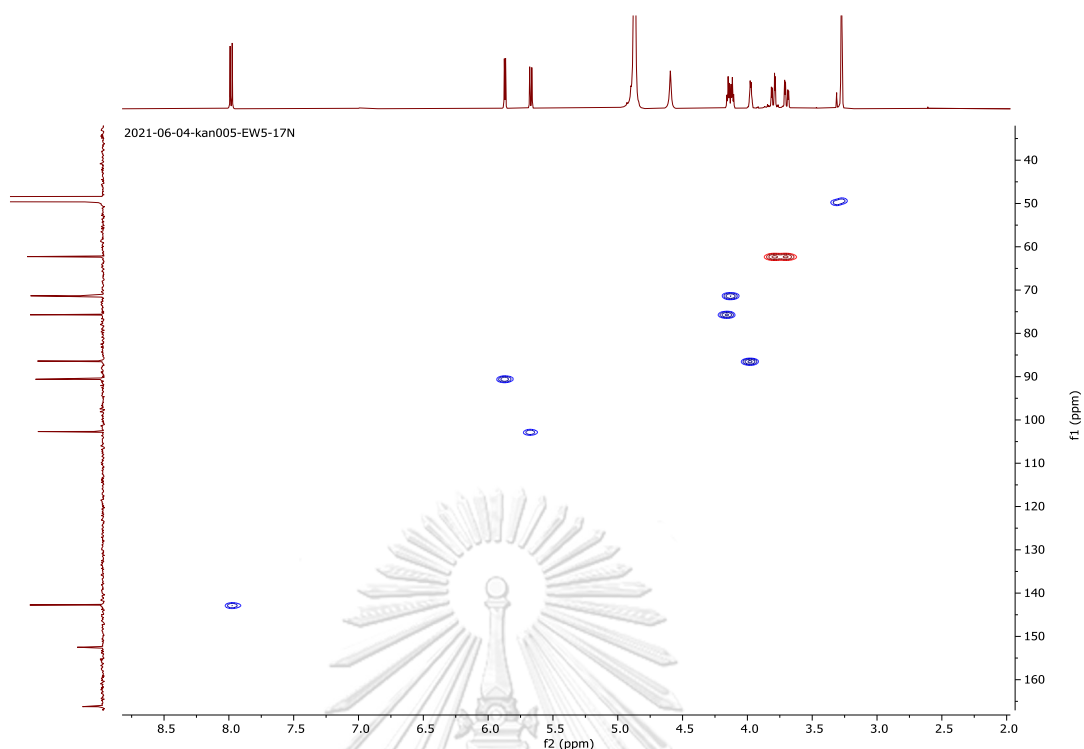


Figure S77 The HSQC spectrum of compound (19) in Methanol- d_4

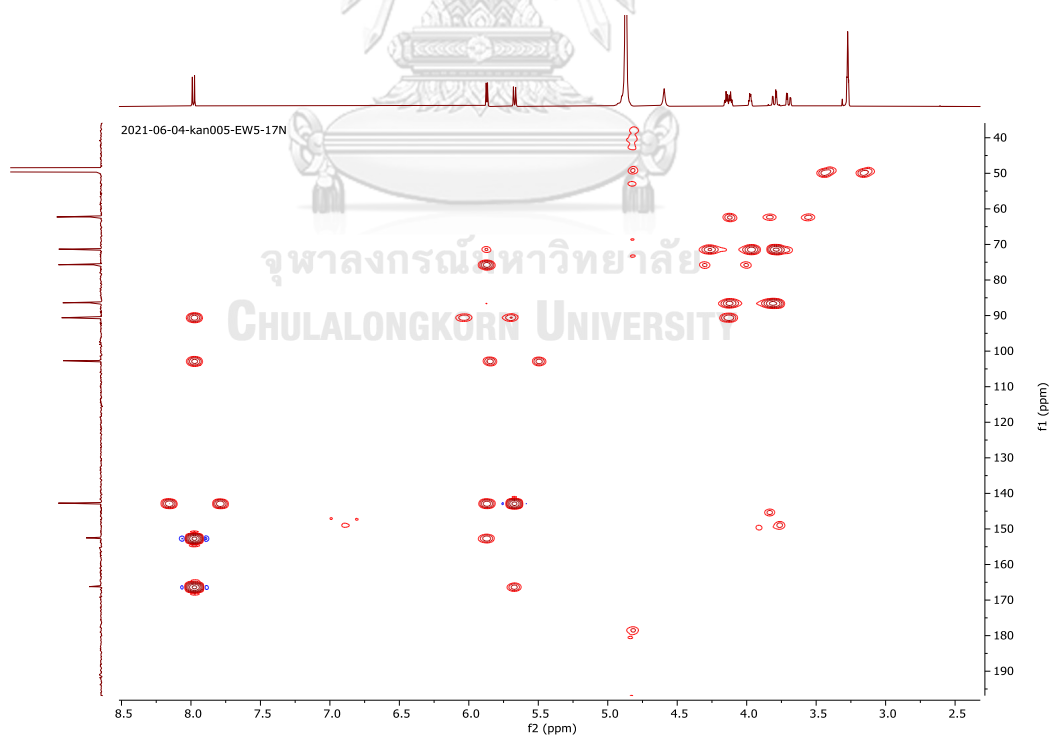


Figure S78 The HMBC spectrum of compound (19) in Methanol- d_4

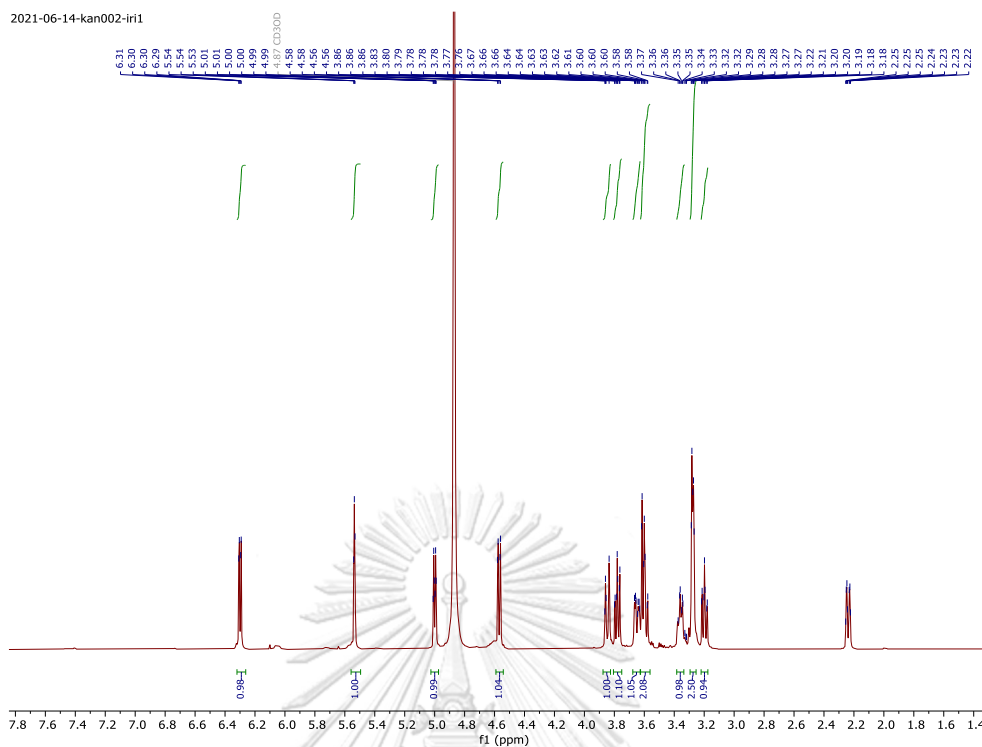


Figure S79 The $^1\text{H-NMR}$ spectrum of compound (20) in Methanol- d_4

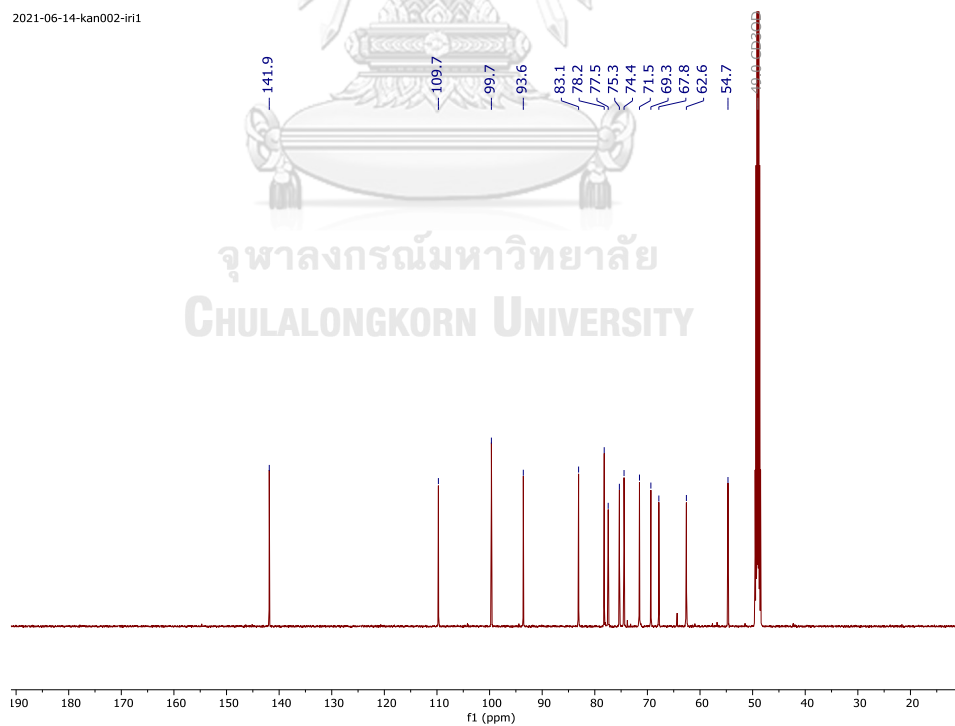


Figure S80 The $^{13}\text{C-NMR}$ spectrum of compound (20) in Methanol- d_4

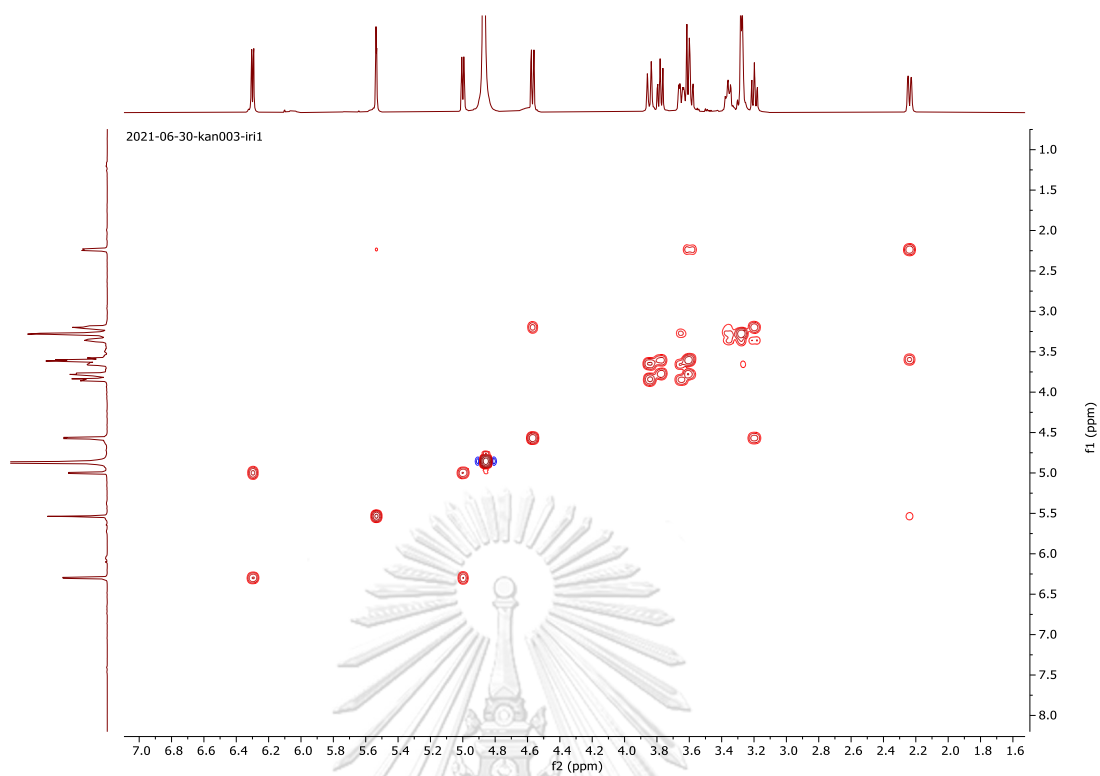


Figure S81 The COSY spectrum of compound (20) in Methanol- d_4

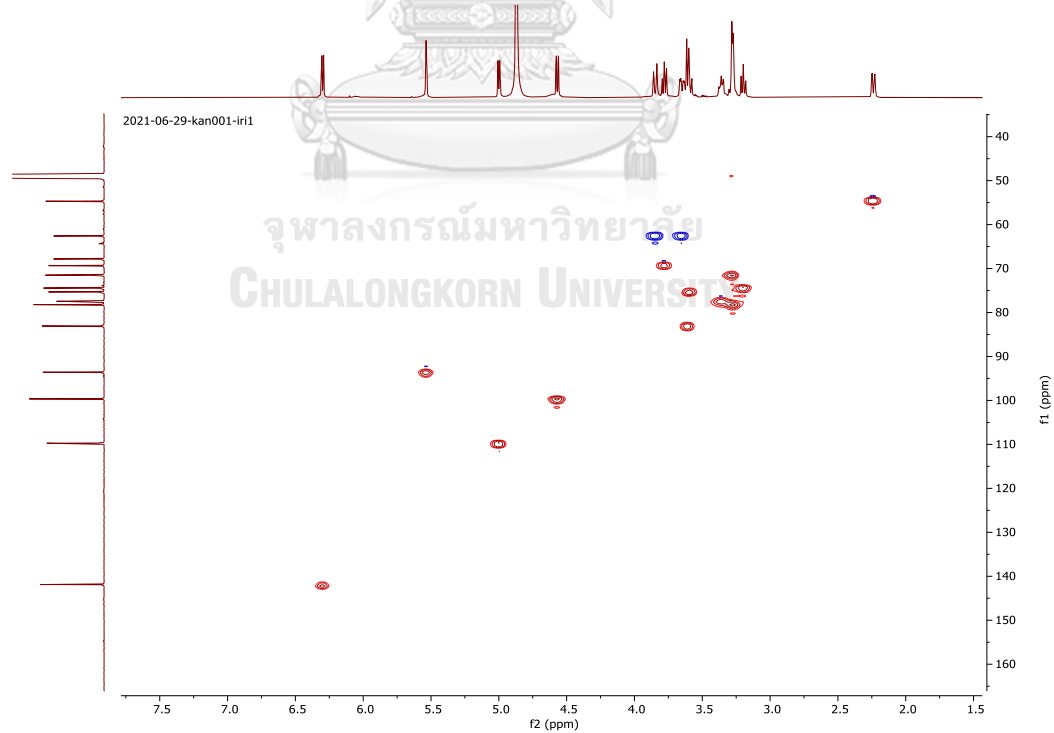


Figure S82 The HSQC spectrum of compound (20) in Methanol- d_4

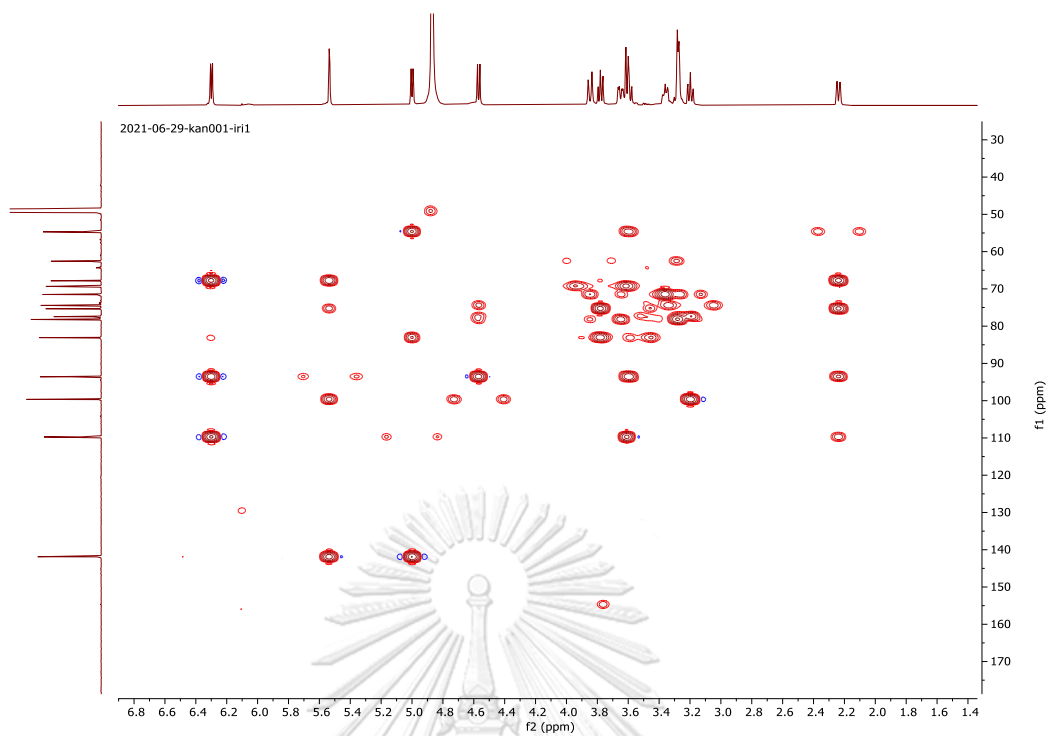


Figure S83 The HMBC spectrum of compound (20) in Methanol- d_4

REFERENCES

1. Mellitus, D., *Diagnosis and classification of diabetes mellitus*. Diabetes care, 2005. **28**(S37): p. S5-S10.
2. van de Laar, F.A., *Alpha-glucosidase inhibitors in the early treatment of type 2 diabetes*. Vascular health and risk management, 2008. **4**(6): p. 1189.
3. Wongnawa, M., et al., *Alpha-glucosidase inhibitory effect and inorganic constituents of Phyllanthus amarus Schum. & Thonn. ash*. Songklanakarin Journal of Science and Technology, 2014. **36**(5): p. 541-546.
4. Yin, Z., et al., *α -Glucosidase inhibitors isolated from medicinal plants*. Food Science and Human Wellness, 2014. **3**(3-4): p. 136-174.
5. Singh, P., et al., *Potential dual role of eugenol in inhibiting advanced glycation end products in diabetes: proteomic and mechanistic insights*. Scientific reports, 2016. **6**(1): p. 1-13.
6. Hossain, U., et al., *An overview on the role of bioactive α -glucosidase inhibitors in ameliorating diabetic complications*. Food and Chemical Toxicology, 2020: p. 111738.
7. Chan, E.W., et al., *Phytochemistry and pharmacological properties of Thunbergia laurifolia: a review*. Pharmacognosy Journal, 2011. **3**(24): p. 1-6.
8. Boonyarikpunchai, W., S. Sukrong, and P. Towiwat, *Antinociceptive and anti-inflammatory effects of rosmarinic acid isolated from Thunbergia laurifolia Lindl.* Pharmacology Biochemistry and Behavior, 2014. **124**: p. 67-73.
9. Tangpong, J. and S. Satarug, *Alleviation of lead poisoning in the brain with aqueous leaf extract of the Thunbergia laurifolia (Linn.)*. Toxicology letters, 2010. **198**(1): p. 83-88.
10. Morkmek, N., et al., *Detoxification of cadmium induced renal and hepatic injuries in rats by Thunbergia laurifolia Lindl. leaf extract*. Thai Journal of Toxicology, 2010. **25**(2): p. 115-115.
11. Usanawarong, S., et al., *Effect of Thunbergia laurifolia Linn. on detoxification of paraquat*. Warasan Wichai Mo-Kho, 2000.

12. Chinacarawat, N., et al., *Study on the Efficacy and Side Effects of Thunbergia laurifolia Lindl. Extract on Reducing Chemical Toxicity among Agricultural Workers Receiving Organophosphate and Carbamate Insecticide Poisoning (Clinical Trial Phase II)*. Thammasat Medical Journal, 2012. **12**(3): p. 496-505.
13. Pongphasuk, N., W. Khunkitti, and M. Chitcharoenthum. *ANTI-INFLAMMATORY AND ANALGESIC ACTIVITIES OF THE EXTRACT FROM GARCINIA MANGOSTANA LINN.* in *III WOCMAP Congress on Medicinal and Aromatic Plants-Volume 6: Traditional Medicine and Nutraceuticals 680*. 2003.
14. Wonkchalee, O., et al., *Anti-inflammatory, antioxidant and hepatoprotective effects of Thunbergia laurifolia Linn. on experimental opisthorchiasis*. Parasitology research, 2012. **111**(1): p. 353-359.
15. Suwanchaikasem, P., C. Chaichantipyuth, and S. Sukrong, *Antioxidant-guided isolation of rosmarinic acid, a major constituent from Thunbergia laurifolia, and its use as a bioactive marker for standardization*. Chiang Mai J Sci, 2014. **41**(1): p. 117-27.
16. Aritajat, S., S. Wutteeapol, and K. Saenphet, *Anti-diabetic effect of Thunbergia laurifolia Linn. aqueous extract*. Southeast Asian J Trop Med Public Health, 2004. **35**(Suppl 2): p. 53-8.
17. HONGSING, P., C. PALANUVEJ, and N. RUANGRUNGSI, *Quality assessment and in vitro anti-diabetic activity of Thunbergia laurifolia stems and leaves*. Walailak Journal of Science and Technology (WJST), 2020. **17**(8): p. 776-787.
18. Kanchanapoom, T., R. Kasai, and K. Yamasaki, *Iridoid glucosides from Thunbergia laurifolia*. Phytochemistry, 2002. **60**(8): p. 769-771.
19. Jensen, S.R. and B.J. Nielsen, *Iridoids in Thunbergia species*. Phytochemistry, 1989. **28**(11): p. 3059-3061.
20. Damtoft, S., L.B. Frederiksen, and S.R. Jensen, *Alatoside and thunaloside, two iridoid glucosides from Thunbergia alata*. Phytochemistry, 1994. **35**(5): p. 1259-1261.
21. Ismail, L.D., et al., *Iridoid glycosides from Thunbergia grandiflora*. Phytochemistry, 1996. **42**(4): p. 1223-1225.
22. Rattanangkool, E., et al., *Quercitylcinnamates, a new series of antidiabetic*

- bioconjugates possessing α -glucosidase inhibition and antioxidant*. European journal of medicinal chemistry, 2013. **66**: p. 296-304.
23. Abeygunawardena, C., et al., *Furanonaphthoquinones from two Lantana species*. Phytochemistry, 1991. **30**(3): p. 941-945.
 24. Perry, P.J., V.H. Pavlidis, and J.A. Hadfield, *Synthesis of cytotoxic furonaphthoquinones: regiospecific synthesis of diodontunzone and 2-ethylfuronaphthoquinones*. Tetrahedron, 1997. **53**(9): p. 3195-3204.
 25. Monthong, W., et al., *(+)-Syringaresinol lignan from new species Magnolia thailandica*. American Journal of Applied Sciences, 2011. **8**(12): p. 1268-1271.
 26. Worawalai, W., et al., *furofuran lignans as a new series of antidiabetic agents exerting α -glucosidase inhibition and radical scavenging: Semisynthesis, kinetic study and molecular modeling*. Bioorganic chemistry, 2019. **87**: p. 783-793.
 27. Gabaston, J., et al., *Pinus pinaster Knot: a source of polyphenols against Plasmopara viticola*. Journal of agricultural and food chemistry, 2017. **65**(40): p. 8884-8891.
 28. Kalia, N.K., B. Singh, and R.P. Sood, *A new amide from Zanthoxylum armatum*. Journal of Natural Products, 1999. **62**(2): p. 311-312.
 29. Akoury, E., *Isolation and structural elucidation of rosmarinic acid by nuclear magnetic resonance spectroscopy*. Am. Res. J. Chem, 2017. **2**: p. 17-23.
 30. Dharmaratne, H., M. Napagoda, and S. Tennakoon, *Xanthones from roots of Calophyllum thwaitesii and their bioactivity*. Natural product research, 2009. **23**(6): p. 539-545.
 31. Park, J.-S., et al., *A study on the constituents from the roots of Polygala tenuifolia*. Korean Journal of Pharmacognosy, 1999. **30**(4): p. 417-419.
 32. Gonzalez, M.J., et al., *Immunomodulatory activity of xanthones from Calophyllum teysmannii var. inuphyllode*. Planta medica, 1999. **65**(04): p. 368-371.
 33. José, M., et al., *Xanthones from Cratoxylum maingayi*. Phytochemistry, 1998. **49**(7): p. 2159-2162.
 34. Li, W., et al., *Xanthones from Polygala caudata*. Phytochemistry, 1999. **51**(7): p.

- 953-958.
35. Kozerski, L., et al., *Comparative structural analysis of cytidine, ethenocytidine and their protonated salts III. ^1H , ^{13}C and ^{15}N NMR studies at natural isotope abundance*. Nucleic acids research, 1984. **12**(4): p. 2205-2223.
 36. Adam, P., et al., *Studies of the intermediary metabolism in cultured cells of the insect *Spodoptera frugiperda* using ^{13}C -or ^{15}N -labelled tracers*. BMC biochemistry, 2005. **6**(1): p. 1-11.
 37. Wu, Q.-L., et al., *Xanthones from *Hypericum japonicum* and *H. henryi**. Phytochemistry, 1998. **49**(5): p. 1395-1402.
 38. Damtoft, S., et al., *Iridoids and verbascosides in *Retzia**. Phytochemistry, 1993. **34**(1): p. 239-243.
 39. Li, N., et al., *Bioactive lignans from *Peperomia duclouxii**. Journal of natural products, 2007. **70**(4): p. 544-548.
 40. Lin, C.-N., et al., *γ -Pyrone compounds. IV: Synthesis and antiplatelet effects of mono-and dioxygenated xanthones and xanthoxypropanolamine*. Journal of pharmaceutical sciences, 1993. **82**(1): p. 11-16.
 41. Hua, J., J. Qi, and B.-Y. Yu, *Iridoid and phenylpropanoid glycosides from *Scrophularia ningpoensis* Hemsl. and their α -glucosidase inhibitory activities*. Fitoterapia, 2014. **93**: p. 67-73.



จุฬาลงกรณ์มหาวิทยาลัย
CHULALONGKORN UNIVERSITY

VITA

NAME	Khoa Anh Nguyen
DATE OF BIRTH	21 October 1997
PLACE OF BIRTH	Tay Ninh Province, Vietnam
HOME ADDRESS	Trang Bang District, Tay Ninh Province, Viet Nam
PUBLICATION	Khoa Nguyen Anh, Preecha Phuwapraisirisan. “First identification of α -glucosidase inhibitors from the stem of <i>Thunbergia laurifolia</i> ”. Proceeding of 47th Congress on Science Technology and Technology-based Innovation” Kasetsart Univerisity Kamphaeng Saen Campus, Nakhon Pathom, Thailand, 5-7 October 2021, pp 356-363.